Gold Nanoparticle Interaction with Cell Membranes

A Major Qualifying Project report submitted to the faculty of
Worcester Polytechnic Institute
In partial fulfillment of the requirements for the Degree of Bachelor of Science

Submitted by:
Theresa Logan
Michelle Ly

Advisor: Dr. Terri Camesano

Abstract

The increasing diversity of commercial applications for nanoparticles increases the probability of environmental and human exposure. Therefore, it is essential to determine the toxicological effects of nanoparticles with respect to humans and the environment. Properties that potentially influence nanoparticle toxicity include: chemical composition, size, shape, concentration, surface charge, redox activity and chemical functionalization. The effects of chemical functionalization on the interaction between nanoparticles and cell membranes was examined using quartz crystal microbalance with dissipation (QCM-D), which detects changes in frequency and dissipation. Changes in frequency and dissipation correlate to changes in membrane mass and rigidity, which effect cell membrane integrity. Cell membrane integrity can be affected by two mechanisms at varying extents: nanoparticle adsorption to the membrane and membrane fracture. Anionic (3-mercaptopropionic acid) and cationic (2-aminoethanethiol) functionalized nanoparticles were used and both fractured the membrane, disrupting its integrity. Humic acid, which was used to predict nanoparticle behavior in the environment, significantly influenced the interaction of the nanoparticles and the cell membrane by altering the magnitude and interaction, and the mechanism of cell membrane integrity disruption. Both anionic and cationic nanoparticles are likely to interact with the environment.

Acknowledgements

We would like to thank our advisor, Dr. Terri Camesano for her support and assistance throughout this project and for giving us the opportunity to work in her lab.

We would also like to thank the graduate students in Professor Camesano's lab for their help and support throughout this project. In particular, we would like to thank Kellie Waterman for teaching us how to use the QCM-D and guidance and help during experiments and with analyzing our data.

Chapter 1: Introduction

Problem Definition

Potential commercial applications of nanoparticles have raised concern regarding their toxicological effects with respect to humans and the environment. Currently, general guidelines for determining nanoparticle toxicity have not been developed yet. Research studies examine specific kinds of nanoparticles on particular types of cell. This makes comparison between studies impractical because of the diverse properties of nanoparticles (composition, size, concentration, stabilizing coating agents, physiochemical properties, surface functionalization, incubation conditions etc.) [1].This project will contribute to the understanding of nanotechnology by proposing general relationships for nanoparticle toxicity.

There are several ways nanoparticles damage cells. These mechanisms include: membrane destabilization, damage by generation of reactive oxygen species, damage to DNA, damage to cell protein functionality, triggering inflammation, and damage to mitochondria [1-3]. Although there are several ways nanoparticles are cytotoxic to cells, this project focuses solely on cell membrane destabilization. Membrane destabilization can be observed using quartz crystal microbalance with dissipation (QCM-D) monitoring. QCM-D monitoring detects changes in frequency, which corresponds to changes in mass of the lipid bilayer (cell membrane), which indicates possible bilayer destruction by the nanoparticles. Properties of nanoparticles influence cell membrane destabilization, and thus contribute to toxicity. These properties include: size, concentration, and the nature of chemical functionalization. Our project focuses on the nature of chemical functionalization with respect to charge and hydrophobicity, and how these properties affect nanoparticle-membrane interactions.

A systematic molecular level study was conducted in an attempt to determine general relationships pertaining to functionalized nanoparticle toxicity. These relationships were determined by observing how functionalized nanoparticles interact with lipid bilayers under laboratory conditions, and in simulated environmental conditions (via incorporation of a soil polymer). The functionalized nanoparticles studied were 2-aminoethanethiol and 3-mercaptopropionic acid. Our goal was to determine general toxicity relationships pertaining to charge (anionic, cationic or nonionic) and hydrophobicity (hydrophilic or hydrophobic). Engineered nanoparticles are tailored for high surface reactivity, and this high surface reactivity is one of the reasons they are so useful in a number of applications. However, these surface properties raise the probability that nanoparticles will be modified by interaction with soil and aquatic polymers in the environment. These modifications may increase or decrease the ability of nanoparticles to interact with cell membranes. Therefore, the interaction of the functionalized nanoparticles in the presence of a soil polymer will be characterized in order to better understand the behavior of nanoparticles in the natural environment.

Hypothesis

We hypothesize that the functionalization of nanoparticles will result in cell membrane destabilization. This destabilization can be attributed to the ionic and hydrophobic characteristics of the nanoparticle that result from functionalization. It is likely that both anionic and cationic particles will disrupt cell membrane stability as they can adversely affect the functioning of cell DNA, proteins, receptors and ion channels which are essential for cell membrane vitality [4, 5].

We also hypothesize that functionalized nanoparticles will have decreased interaction with cell membranes in the environment. The polymers, poly(methacrylic acid) and humic acid, will decrease the interaction between the functionalized nanoparticles and the cell membrane, decreasing the extent of cell membrane destabilization. Both poly(methacrylic acid) and humic acid mimic the characteristics of soil as they contain natural organic matter (NOM). NOM adsorbs to microbial cell membranes which increases the negative charge of the cell membrane. Additionally, NOM adsorbs to NPs which alters the surface charge and reduces their ability to attach to the cell membrane [6]. Smaller NPs have greater surface area than larger ones, which enables them to have more interaction with cell membranes than larger NPs. This is true even though humic acid typically decreases interaction. The magnitude of interaction will be greater for smaller nanoparticles even in the presence of humic acid.

Project Objectives

1. Determine if functionalized nanoparticles result in cell membrane destabilization
    a. Examine the effects of nanoparticle charge.
    b. Examine the effects of nanoparticle hydrophobicity.
2. Determine if soil polymer (humic acid) will increase the extent of cell membrane destabilization to understand behavior of nanoparticles in the environment
    a. Examine the effects of nanoparticle charge.
    b. Examine the effects of nanoparticle hydrophobicity.
3. Determine if a mimic for humic acid, poly(methacrylic acid), will also have an effect on interactions.
    a. Examine the effects of nanoparticle size.

Contents

Chapter 2: Literature Review

Supported Lipid Bilayers

Phospholipid vesicles are one of the most commonly and widely studied bilayer model systems [7]. Supported membranes form from the spreading of vesicles in solution. Supported lipid bilayers (SLBs) which are widely used in biotechnology applications as models for cell and organelle membranes, are formed through the adsorption of lipid vesicle solution on certain surfaces. Silica and mica based surfaces are the most widely used solid supports for lipid bilayer formation [8]. This project uses silica-based surfaces for membrane formation. SLB formation can be hindered from the use of vesicles that contain membrane-bound molecules that protrude from bilayer membrane; such as membrane proteins or functionalized lipids, unless in low concentration [9]. Positively charged SLBs are formed through small vesicle spreading [10].

The assembly of lipids into unilamellar vesicles suspended in an aqueous medium can occur in a variety of ways. This includes: sonication of an aqueous dispersion of phospholipids, detergent analysis, reverse-phase evaporation, etc. Lipids are commonly associated into spherical and non-spherical vesicles, generally by detachment of bilayer fragments [11].

A study done in 2009 by Kristian Dimitrievski, *Influence of Lipid-Bilayer-Associated Molecules on Lipid-Vesicle Adsorption*, helps to clarify the circumstances that are likely to lead to SLB formation. In this study, Dimitrievski uses beads as a model for lipid bilayers with each bead representing small bilayer fragments. This representation of SLB formation can be seen in Figure 1.

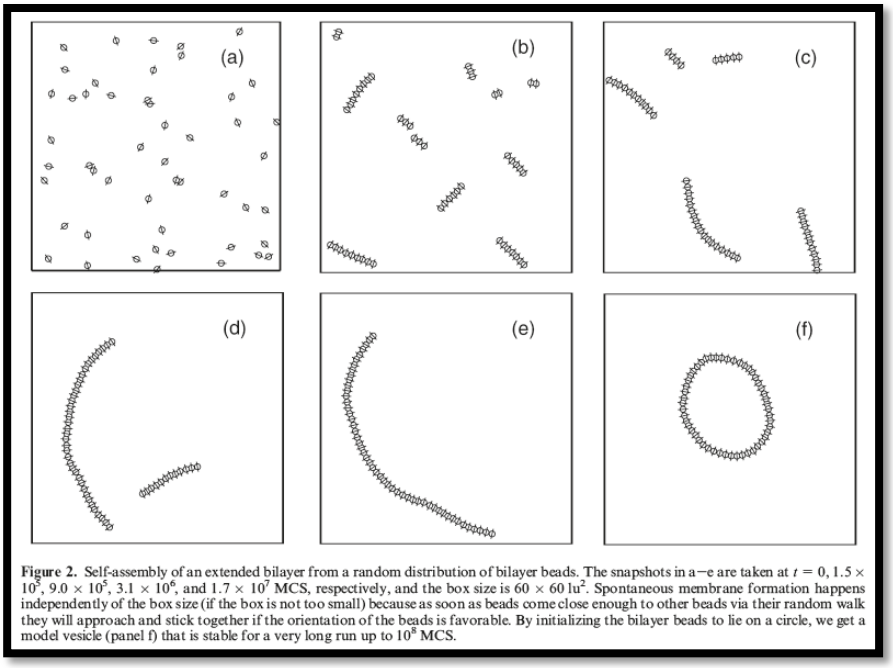

Figure 2. Self-assembly of an extended bilayer from a random distribution of bilayer beads. The snapshots in a−e are taken at $t = 0, 1.5 \times 10^5, 9.0 \times 10^5, 3.1 \times 10^6$, and 1.7×10^7 MCS, respectively, and the box size is 60×60 lu^2. Spontaneous membrane formation happens independently of the box size (if the box is not too small) because as soon as beads come close enough to other beads via their random walk they will approach and stick together if the orientation of the beads is favorable. By initializing the bilayer beads to lie on a circle, we get a model vesicle (panel f) that is stable for a very long run up to 10^8 MCS.

Figure 1: Observed SLB Formation [9]

In Figure 1, each stage of SLB formation is visualized in snapshots. In section (a), each bead (bilayer fragment) includes a vector that indicated the orientation of the bilayer fragment. This orientation is the bilayer fragment's normal orientation. There is attraction and repulsion of the beads to one another. Parallel alignment of adjacent normal vectors, section (b), is orientation-dependent. As seen in sections (c), and (d), the potential of the beads has a hydrophobic interaction that drives the system towards membrane formation. Section (e) shows the lipid-tail regions of the bilayer fragments joining to form a larger chain. Section (f) shows a final rigid bilayer fragment. One bead represents a multitude of bilayer-fragment shapes and arrangements.

By introducing a surface, such as silicon, the vesicles can adsorb onto that surface or a bilayer patch on the surface. Studies show that the adsorbed lipid vesicles can transform into bilayer patches with several mechanisms including the following three: spontaneous rupture of isolated vesicles; rupture of the vesicles induced by critical vesicular coverage; and the rupture of vesicles induced by the active edge of a bilayer patch [8].

The ability for the vesicles to adsorb onto a surface and for bilayer formation depends on the bilayer-surface interaction strength, which depends on the type of substrate used and the composition of the vesicle [9].

The two important influences of final configuration of the vesicle are: bilayer adsorption on the surface, and the diffusion of membrane-bound molecules within the bilayer. Both are timescales. Propagation of bilayer adsorption is much faster than the diffusion of membrane-bound molecules

within the bilayer. This causes the final vesicle configuration to be diverse for intermediate concentration vesicle solutions. Higher concentration vesicle solutions results in fewer bilayer bead adsorption into the final vesicle configuration. In some instances, the use of high concentration vesicle solution results in the adsorption of the molecules as opposed to the bilayer formation [9].

There are many different techniques to study the supported membrane formation process, but the one in particular that this project will utilize is the quartz-crystal microbalance with dissipation monitoring (QCM-D). QCM-D is favorable because is not only provides the hydrated mass of the membrane, but also the dissipation to distinguish between surface-bound vesicles or bilayer patches. Commonly, QCM-D and SPR are paired together to establish the concept of local critical vesicular coverage [8].

Formation of the Membrane Using Vesicles

Lipid bilayers are supported membranes on a solid substrate. They serve as model membranes in studying biosensors and cellular processes. In biosensing, lipid bilayers allow immobilization of receptors at an adsorption resistant interface by providing high sensitivity [12]. As described in the study, *Formation of Supported Membranes from Vesicles*, done by Keller et al, small unilamellar vesicles are prepared in a buffer solution and adsorbed onto a clean SiO_2 surface evaporated onto a quartz crystal membrane (QCM). This is currently the most common way of forming high quality supported lipid bilayers. In Figure 1, taken directly from the study shows the adsorption of lipid vesicles on a SiO_2 surface:

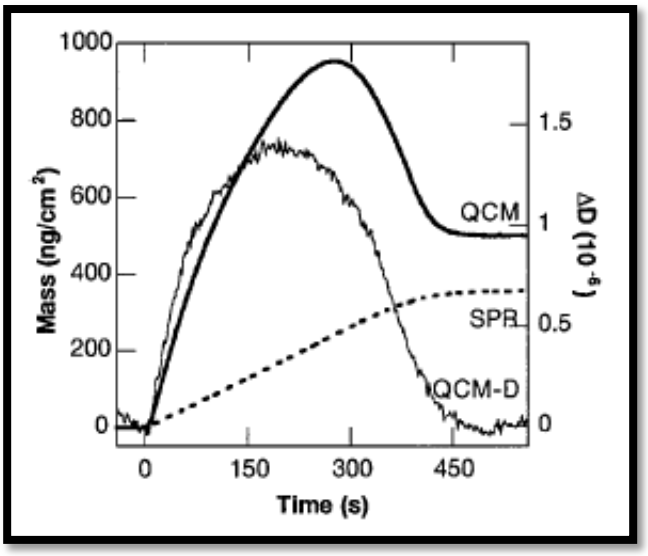

Figure 2: QCM and SPR data for the adsorption of lipid vesicles on a SiO2 surface [12]

From Figure 2, there is a difference in the mass uptake (heavy lines) measured with QCM and SPR due to the difference in sensitivity to trapped water. Adsorbed liquid, water trapped inside and between adsorbed vesicles, and a small amount of water adjacent to adsorbed vesicles couple together to the surface of the QCM, causing the resonant frequency (f) of this mode to decrease (QCM oscillates in a shear mode). The SPR measures the index of refraction near the surface as water is replaced by adsorbed lipid. As the adsorption continues, the number of vesicles increases on the crystal surface and the amount of water trapped decreases. This continues until the amount of water trapped decreases to zero [12].

Figure 3 below, taken directly from the study, shows the completion of the supported membrane. The difference between adsorbed mass is measured with QCM and SPR.

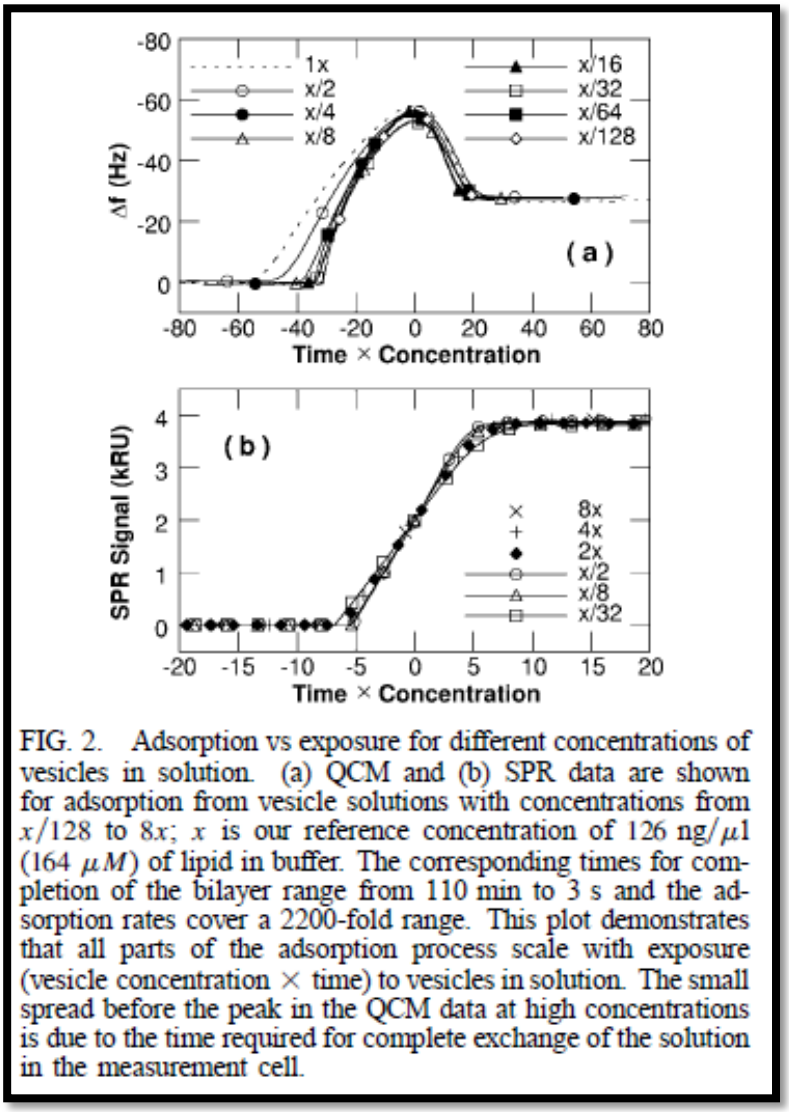

FIG. 2. Adsorption vs exposure for different concentrations of vesicles in solution. (a) QCM and (b) SPR data are shown for adsorption from vesicle solutions with concentrations from $x/128$ to $8x$; x is our reference concentration of 126 ng/μl (164 μM) of lipid in buffer. The corresponding times for completion of the bilayer range from 110 min to 3 s and the adsorption rates cover a 2200-fold range. This plot demonstrates that all parts of the adsorption process scale with exposure (vesicle concentration × time) to vesicles in solution. The small spread before the peak in the QCM data at high concentrations is due to the time required for complete exchange of the solution in the measurement cell.

Figure 3: Measuring Lipid Bilayer Formation [12]

This particular example shows that there is still a significant amount of water associated with the membrane. As seen in Figure 3, there are two parts to the supported membrane formation. The first part is the vesicle adsorption and the second is the rupture and fusion of the membrane.

Biological and Biomedical Applications of GNPs

Biological Applications

Gold nanoparticles (GNPs) have several promising applications in the biological field. These applications are divided into 4 categories: "labeling, delivering, sensing, and heating" [13]. GNPs are particularly promising in biological applications because of their unique properties including: their optic, conductivity and catalytic properties and their biocompatibility, high surface to volume ratio, and density [13] [14]. Compared to colloidal NPs traditionally used for biological applications, GNPs have the advantages of: ease of synthesis, colloidal stability, and the ability to be easily conjugated with biological molecules. In addition, the optical properties of GNPs allow them to be visualized using several methods, and there is little evidence of GNP corrosion. Lastly, GNPs are inert, which enhances their biocompatibility, which is vital in most biological applications [13].

Labeling

The optic properties of GNPs make them extremely useful in labeling applications. GNPs are often used as contrast agents and can be visualized with several different techniques. Most of the techniques utilize GNPs ability to absorb and scatter light. These techniques include optical microscopy (phase contrast and differential interference contrast), dark field microscopy and fluorescence microscopy. Transmission electron microscopy (TEM) can also be used but utilizes the high atomic weight of GNPs as opposed their interactions with light to provide contrast. X-ray imaging and gamma radiation can also be utilized to visualize GNPs. GNPs conjugated with antibodies can bind to specific animal organs and enhance the contrast of x-ray images [13].

GNPs are extremely useful in immunostaining which is used to visualize molecular components of biological cells. The most commonly used visualization technique in immunostaining is TEM. Typically immunostaining is done using fluorescence labeling however using GNPs for labeling instead has several advantages. GNPs are more stable, eliminate photobleaching, and provide better lateral resolution and higher contrast [13].

GNPs have also shown promise in single particle tracking, which is used to visualize the movement of molecules and molecular structures. Single particle tracking labels the desired structure or molecule with antibody-conjugated NPs allowing for visualization via optical microscopy. It is most frequently used to investigate the trajectory and diffusion of a membrane-bound receptor molecules within a cell. Traditionally, organic fluorphores and quantum dots are used for labeling. However, both have limitations as they are affected by photobleaching and the

time limitations of fluorescence. GNPs are advantageous in single particle tracking as they are not hindered by photobleaching and have no limitations on observation time [13].

Additionally, GNPs can be used to image the movement of cells adhering to substrates. When the surface of the substrate is coated with a layer of colloidal GNPs, cells moving along the substrate leave behind a "phagokinetic track." Using TEM, the "phagokinetic track" can be seen and the movement of cells along the substrate is reveled [13].

Delivery

GNPs are also useful for delivery of molecules into cells as molecules can be absorbed onto the surface of GNPs and detach themselves once inside the cell. Typically delivery of GNPs into cells is achieved using gene guns or by cells ingesting NPs. The goal of both particle ingestion and gene guns is to absorb molecules onto the surface of GNPs to facilitate their entry into cells.

Entry occurs naturally during particle ingestion while gene guns forcefully shoot desired particles into cells. Gene guns are most commonly used to introduce plasmid DNA into cells while particle ingestion is used for gene therapy and drug targeting. Gene therapy and drug targeting research is promising and both are likely to advance the treatment of certain diseases in the future [13].

Sensing

GNPs are useful "...in interfacing biological recognition events with signal transduction and in designing biosensors..." [14]. Sensors are "a class of devices that produce measurable responses to changes in physical conditions or chemical concentrations"[14]. Biosensors are simply sensors that contain biological recognition elements called bioreceptors or transducers. Biosensors typically measure biological processes. Although GNP biosensors are not currently used in industry, research has shown that they are more reliable and sensitive than the biosensors currently in use [14].

GNPs' high surface energy is particularly important as it allows for the immobilization of biomolecules without destroying their bioactivity. There are three types of GNP-based biosensors: optical biosensors, which detect changes in optical properties, electrochemical biosensors which detect changes in electrical characteristics; and piezo-electric biosensors, which detect changes in mass [14].

Optical based biosensors measure changes in light or photon output often, using surface plasmon resonance (SRP) and surface enhanced Raman scattering (SERS) in sensing. Using SPR and SERS in sensing is particularly reliable when GNPs are utilized in optical based biosensing [14] [13]. When SRP sensing is used, GNPs are capable of amplifying SRP signals and detecting physiochemical changes on films [14].When SERS is used, complex molecules can be detected, identified as incident light, and is scattered to produce Raman spectras. Most molecules have a characteristic Raman spectrum and can therefore easily be identified. GNPs enhance the light scattering and therefore improve the sensitivity of optical based biosensors using SERS as sensing method [13].

Piezo-electric biosensors measures mass changes resulting from biological recognition processes. Measurements are based on the piezoelectric effect which states that when "mechanical stress is applied it produces an electrical voltage that is proportional to the stress" [14]. The most commonly used technique based on this effect is quartz crystal microbalance (QCM). Researchers are attempting to enhance the sensitivity of this technique to allow for detection of even smaller molecules. They have discovered that incorporating GNPs into the QCM sensing process can amplify the mass change during analysis and increase sensitivity. GNPs also have the potential to amplify sensing surface area and improve the stability and quality of biological recognition [14].

Biomedical Applications

GNPs are particularly useful in the following biomedical areas: disease diagnosis, targeted drug delivery and regenerative medicine. Research suggests that GNPs promote early disease detection as they assist in determination of pathologies of individual cells. Additionally GNPs make it "possible to identify proteins in blood serum, distinguish different bacterial strains and differentiate healthy and cancerous cells" [15]. Gold nanoparticles also enhance the "imaging, tracking and recognition" or tumor cells and allow for the detection of smaller proteins than methods currently used [16].

In addition, GNPs show promise in regenerative medicine, which is used to treat conditions such as diabetes and osteoarthritis and injuries of the cardiac muscle and central nervous system. "The fundamental principle of regenerative medicine is that the biocompatible materials and the signal drug molecules capable of initiating regenerative processes at the cell level can be delivered to the affected region" [15]. Additionally, GNPs can increase the efficiency of certain drugs as they can be conjugated with antibodies that promote selective binding to injured cells.

GNPs can be utilized in targeted drug delivery as well, as they facilitate "reduction of drug doses, enhancement of their therapeutic effects and increase in their safety" [15]. For example, NPs have shown potential in chemotherapeutic cancer treatment and tumor specific drug delivery. "Owing to their small-size, ligand coated NP's can be efficiently directed toward, and subsequently internalized by tumor cells through ligand-receptor recognition and interaction, thereby offering an effective approach for specific targeting of tumor cells" [16].

Endocytosis of Nanoparticles

In order to effectively utilize NPs for the biomedical applications discussed above "it is essential to understand the underlying mechanisms that govern the transmembrane transport and invagination of the NPs in biological cells" [16]. Researchers are particularly interested in the rate at which NPs can be endocytosed into a cell as this rate is important in several biological and medical applications. For example, the rate at which NPs are endocytosed determines the "maximum drug-delivery capability when NPs are used to internalize drug molecules" [16]. Endocytosis consists of a cell wrapping a particle. NP can be wrapped by cell membranes with varying degrees as illustrated by Figure 4 below.

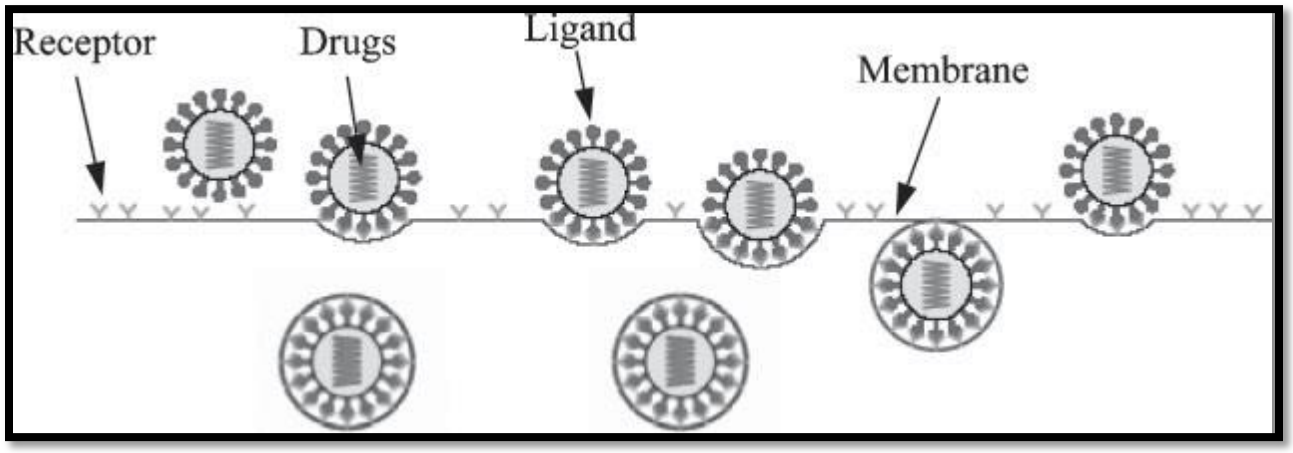

Figure 4: Schematics of adhering NPs wrapped by cell membrane with different degrees of wrapping [16]

According to Zhang et al., the cellular uptake is controlled by two factors: surface tension and particle size. Particle size has the greatest influence on cellular uptake. Figure 5 below illustrates the relationship between cellular uptake and particle size. It highlights that the optimal radius for nanoparticles endocytosis is between 25-30 nm.

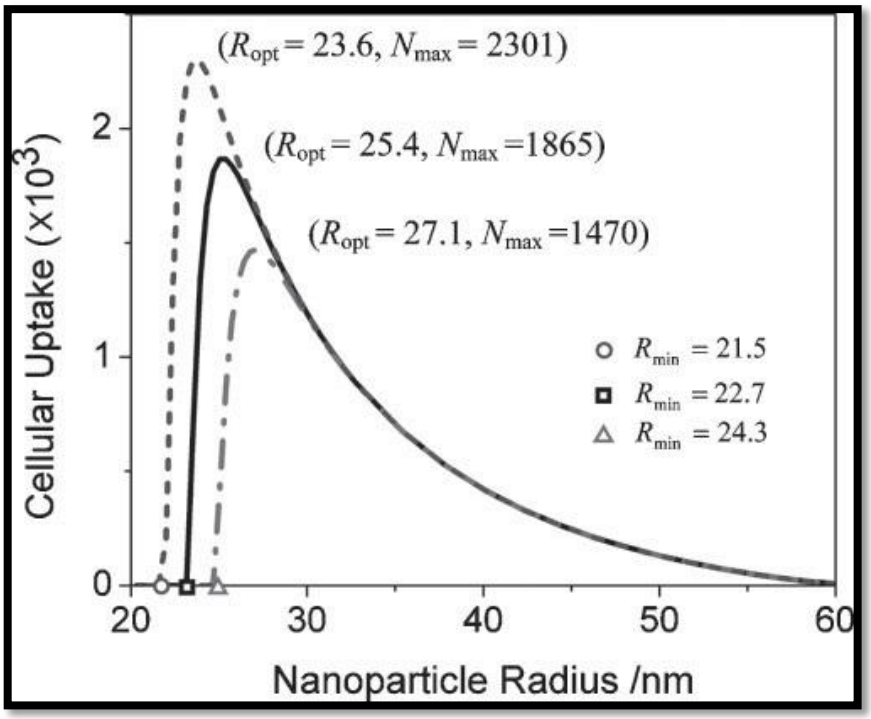

Figure 5: Size-dependent cellular uptake of NPs characterized by two typical radii: R_{min} and R_{max} [16]

In general, cellular uptake increases with increasing membrane tension. Although cellular uptake is controlled by particle size and membrane surface tension, it is also influenced by the surface concentration of adhering NPs. Endocytosis is receptor-limited. At low concentrations, there are sufficient receptors available to fully wrap all NPs present on the cell membrane. As a result, a linear relationship between cellular uptake and surface concentration can be seen. As the concentration increases and receptors become saturated, cellular uptake decreases [16]. The relationships between cellular uptake and membrane tension and surface concentration are highlighted in Figure 6 below.

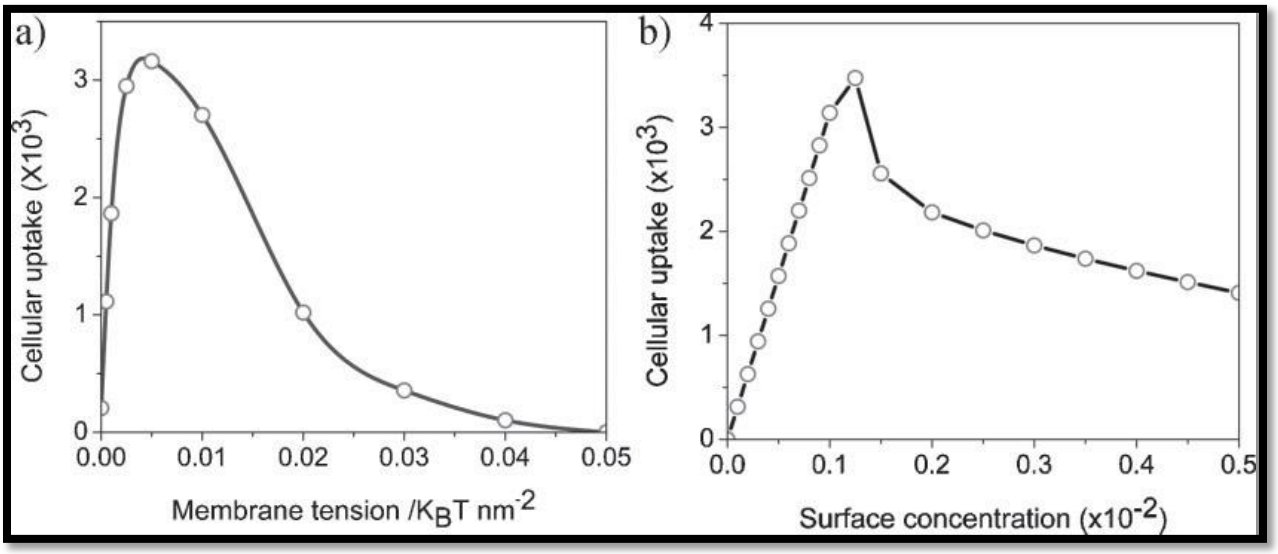

Figure 6: The effects of membrane tension and surface concentration on the cellular uptake [16]

"When binding occurs between a ligand-receptor pair, the released chemical energy, μ, drives the local wrapping of the membrane around the NP at the cost of elastic deformation energy of the membrane" [16]. The elastic deformation energy is composed of the bending energy resulting in curvature formation and the stretching energy that results from the lateral membrane tension. The elastic deformation energy can be calculated using the Helfrich equation, Equation 1 below, where σ is the lateral tension, κ is the bending modulus and C_1 and C_2 are the local principles of curvature [17].

$$e_H = \sigma + \frac{\kappa}{2}(C_1 + C_2)^2 \qquad \text{[Equation 1]}$$

Membrane wrapping of NPs less than 64 nm is mainly influenced by bending energy while wrapping of larger particles is controlled by tension [17].

Environmental Effects of Gold Nanoparticles

GNPs in Water

NPs have been detected in sewage sludge, wastewater treatment plant influent and natural waterways [18]. The increasing use of NPs in both industry and research has facilitated their intentional and unintentional introduction into waste streams in water treatment facilities. The impact of NPs on water treatment plants and the environment is still unclear. The majority of current studies concerning nanoparticles are focused on NP synthesis as opposed to environmental concerns and toxicity [19].

Recent research suggests that NPs can adversely affect the environment as they frequently escape treatment plants and are discharged into natural waterways. Discharged NPs can potentially be toxic to aquatic life [19]. A recent study done by Garcia et al. evaluated the effect of four different metal oxides and zero-valent metal nanoparticles on the activity of microbial communities in a wastewater treatment plant. It was found GNPs and titanium oxide NPs presented zero or low toxicity towards ordinary heterotrophic organisms (OHO), ammonia-oxidating bacteria (AOB), and anaerobic biomass, while GNPs presented intermediate toxicity [18]. As a result of certain NPs being toxic to bacteria during the water treatment processes, more research is needed to understand their toxicity in drinking water [20]. The toxicity of NPs themselves is not the only thing to consider when using them in waterways. The effect of nanoparticles on other toxins already in the waterways must also be taken into account [19].

Additionally, NPs are able to bind to organic matter, metals, and other contaminants in the water treatment process. This could lead to undesired consequences such as undesired NP accumulation in wastewater sludge after settling organic matter for removal. As a result, when the removed sludge is sent to landfills, there is possible NP contamination of the soil [19].

GNPs in Soil

Generally, NPs are present in soil through passive and active mechanisms with groundwater. The addition of NPs in water treatment can also result in leakage of NPs into soil. NPs in the soil can help to decrease sequestration of hydrophobic contaminants, such as polycyclic aromatic hydrocarbons and be helpful in remediating soil [19].

NPs bound to soil can render that soil immobile. This can have a negative impact on the respiration rate and biomass of the surrounding environment. NP contamination of soil can also lead to the disturbance of soil protozoan growth and also impact the growth of fast-growing bacteria. Disrupting the balance of interactions between soil and microorganism can affect the overall health and function of the soil [19]. These affects have the potential to adversely affect plant growth and increase human exposure to NPs.

Recent studies showed that GNPs functionalized with citrate could attract certain types of microorganisms in soil. Additionally, these studies showed that interactions with these bacteria

allowed the GNPs to undergo redox reactions [19]. This can either help or hinder the availability of oxygen in soil for aerobic bacteria. Too much oxygen can lead to an exponential growth of bacteria that can lead to a disruption of soil functioning that is potentially difficult to contain and likely to contaminate groundwater and aquifers. Too little oxygen can lead to a microbial population decay, which can lead to lack of oxygen in the soil, making it useless for plant growth.

Humic Acid

Humic acid is frequently used as a model system to mimic the characteristics of soil in the environment. It is often used to study the interaction between nanoparticles and the environment. Humic substances (HS) are composed of amorphous, chemically complex and internally structured molecules or molecular aggregates. These molecules are classified as soft-colloidal matter as they have a polyelectrolyte nature[21]. As the HS imitate the conditions of soil, interaction between nanoparticles and humic acid will reflect the interaction between nanoparticles and the environment. In a study done by Stankus et al 2011, humic acid altered the aggregation mechanism of NPs.

Humic acid is considered the most abundant organic macromolecule (OM) in many types of groundwater. In laboratory column studies, retention of bacteria decreased on humic-acid coated substrates. This is partly due to the sorption of humic acid onto bacterial cell walls which increases the negative surface charge of the cell wall or hinders the sorption of OM and bacteria onto the surface [6]. Humic substrates, mainly present as fulvic acid (FA), are water-soluble at acidic pH [22]. In most natural waters, HS are negatively charged [21]. Humic acids adsorb to or interact with nanoparticles regardless of the type or capping agent under environmentally relevant conditions [23].

The adsorption of NOM to the surfaces of natural colloids and NPs influences surface properties and colloidal stability [24]. The main effect of NOM sorption on the surface characteristics is alteration of surface charge [25]. Much of this alteration is due in part to the organic matter masking the positive charges of NPs, reducing attraction [26]. Studies have also shown that sorbed humic acid interferes with bacterial interaction with clay [27]. HS are a good model for NOM when observing the behavior of NPs in the environment.

The effects of mono- and divalent ions and pH on the stability of NPs are observed to follow Derjaguin-Landau-Verwey-Overbeek (DLVO) theory [24]. The pH affects both the charge density and the hydrodynamic radius of the humic particles [21]. In DLVO, particle stability is controlled by total interaction energy. This includes repulsive electrostatic interactions between like charged particles and attractive van der Waals forces. In the presence of NOM and other stabilizing agents, non-DLVO forces including: hydrogen bonding, hydration pressure, Lewis acid base interactions, and steric interaction are present [24].

Studies also show that low concentrations of NOM can increase the stability of some NPs through surface-coating [23]. In other words, low concentrations of NOM coating NPs and cell walls alter the surface charges of them, stabilizing them through surface coating [23]. If high interaction with cells is preferred, it is advised to not include the use of humic acids [27]. In summary, humic acid (NOM models) can reduce the interaction between GNPs and cell membranes, as the polymer alters surface charge of the NPs in a way that reduces the NPs' ability to repel or attract. While this occurs, the stability of the NPs is increased. This relationship will be studied through experimental data analysis.

Plants

Recent studies also show that TiO_2 nanoparticles can promote photosynthesis and nitrogen metabolism to improve plant growth. However, further research showed that some NPs (Al_2O_3) could hinder root elongation of corn, cucumbers, soybeans, cabbages, and carrots. Effects of NPs on plants are specific depending upon the type of NPs and the type of plant. For example, nano-scale zinc can hinder the seed germination of ryegrass while it does not affect the seed germination of radish, lettuce, corn, or cucumbers. Another factor that influences NPs effect on plants is the functionalization of the NPs. It was discovered that non-functionalized carbon nanotubes inhibited root length more than functionalized ones [19]. As a result of the complications of using NPs on plants, further research needs to be done. Thus, it is important to study the effect and mobility of nanoparticles in soil and water as they directly affect plants.

GNPs in Air

Airborne NPs are important to study since one of the largest concerns surrounding NPs is human exposure through skin absorption. Skin is an excellent absorptive material due to its rich supply of blood and tissue macrophages, lymph vessels, dendrites, and nerve endings. Exposure through skin absorption is especially concerning in textiles as the likelihood of skin contact and contact with babies and small children is high [20].

NPs are mostly present in the air through aerosols (in solid or liquid phase). It is also possible for nanoparticles to become airborne when bound to dried sludge. This is because some dried sludge is incinerated, which allows nanoparticles to further leach into the atmosphere. Unfortunately there is currently a lack of research that evaluates the potential environmental consequences of airborne NPs [19]. It would be beneficial to society to study this further as human exposure concerns and the lack of solidity in the toxicity and cytotoxicity of NPs and GNPs hindered advancement of GNPs in both biomedical and environmental applications.

Environmental Toxicity of Engineered Nanoparticles

In order to understand the environmental toxicity of engineered nanoparticles (ENPs) it is important to consider the factors controlling the interaction between natural organic matter (NOM) and nanoparticles. Literature indicates that interactions between NOM and ENPs influence surface chemistry and stability, thus influencing environmental toxicity. However, much

remains unknown about "(1)what characteristics of NOM influence their interactions with engineered nanoparticles; (2) the influence of NOM concentration; and (3) the mechanism by which NOM interacts with ENPs (coated and uncoated) and what implications those interactions have for ENP colloidal stability in aquatic systems"[24].

When engineered nanoparticles are released into aquatic environments, their aggregation state significantly influences their cytotoxicity as it influences environmental transport and transformations. Research has suggested that interaction between ENPs and natural organic matter influences ENPs colloidal stability in aquatic environments. Additionally, the absorption of NOM onto the surface of ENPs controls surface properties and colloidal stability of the ENPs. NOM influences nanoparticle solubility, chemical reactivity, surface chemistry, binding affinity and colloidal stability in similar ways as capping agents such as charged species, organic ligands and polymer would [24].

Several factors influence NOMs ability to influence stability. Both the type and concentration of NOM influence colloidal stability. Additionally, "the extent of NOM absorption, the conformation of the NP surface, and the interaction between NOM molecules on adjacent particles" also influence stability and NOM with larger molecular weights provides greater stability[24]. Since it is difficult to examine interactions between NOM and ENPs, soil polymer (humic acid), a single NOM isolate is often used to represent NOM.

Toxicity and Cytotoxicity

As previously mentioned the growing interest and potential commercial applications of nanoparticles (NP) have created discussions surrounding their toxicological effects with respect to both human and environmental toxicity. "The assessment of NP safety has been complicated due to a great variety in: (1) types of NPs, (2) stabilizing coating agents, (3) physicochemical parameters of the NPs (diameter, surface charge, surface topography, surface area), (4) incubation conditions (time and concentration) (5) type of cell used, (6) type of assay used, or (7) possible interference of the NPs with the assay readout"[1]. Currently, most research studies examine the effect of a specific kind of NP on a particular cell type. This makes comparisons between different studies difficult and determining guidelines pertaining to the safety of nanoparticles nearly impossible [1].

Gold nanoparticles (GNPs) toxicological effects are the center of many debates as they are commonly used for biological and medical purposes. Although many believe that GNPs are potentially non-cytotoxic, the cytotoxicity of GNPs is still controversial as recent literature contains conflicting data regarding GNP cytotoxicity. Researchers agree that the toxicity of gold nanoparticles is directly related to the five following factors: "surface chemistry, coating materials, size, shape, and biological target tested" [28]. Pan et al. highlighted the role that size plays in toxicity after conducting several experiments that showed that 15 nm GNPs are nontoxic

at all concentrations while 1-2 nm GNP cause rapid cell death by necrosis at low concentrations. Chithrani et al. also demonstrated the importance of size showing that size and shape directly affect the "kinetics for GNP alteration and saturation within mammalian cells" [28].

Particular concerns center on the effects of nanoparticles used in the biological and medical fields. "As these nanoparticles are intentionally engineered to interact with cells, it is important to ensure that these enhancements are not causing any adverse effects" [29]. Toxicological classification of nanoparticles used for *in vivo* applications is not as complicated as the classification of nanoparticles used for *in vitro* applications. Classifying nanoparticles used for *in vivo* applications simply involves understanding the kinetics and toxicology of the particle. Classification of particles used for *in vitro* applications requires cytotoxicity studies of "nanoparticles using different cell lines, incubation times and colorimetric assays" [29]. The lack of standardization in concentration and exposure times makes it difficult to make general conclusions about whether or not nanoparticles are cytotoxic. Additionally, the wide range of concentrations and exposure times makes is difficult to determine if "cytotoxicity observed is physiologically relevant" [29].

Mechanisms of Cytotoxicity

Cytotoxicity is dependent upon direct contact with the cell membrane [30]. Current hypothesized cytotoxicity mechanisms include: disruption of intracellular metabolic pathways, oxidative stress, and physical membrane damage [2]. Additional cytotoxicity mechanisms include: disruption of cell DNA, damage to the functionality proteins and enzymes, triggering of inflammation, and damage by generation of reactive oxygen species (ROS). Of the mechanisms, cell membrane disruption is the only one that requires nanoparticulate nature of the material. All other cytotoxicity mechanisms can be caused by the molecular, atomic, or ionic species constituting the nanoparticle. Nanoparticulate nature is not essential as it is in membrane destabilization.

In the case of quantum dots showed that toxicity is known to occur at low concentrations of the core metals such as cadmium, lead, and arsenic. When exposed to an oxidative environment, toxicity is directly related to the release of free ions. Quantum dots with a cadmium core can induce mitochondrial damage and oxidative stress from free-radical Cd^{+2} formations [31]. Mitochondrial damage is therefore not dependent on nanoparticulate nature.

In the pharmaceutical industry, engineered nanoparticles are used for drug delivery. These nanoparticles can help or hinder immune responses by binding to proteins in the blood. They may even be able to decrease the immune-toxicity of drugs by improving drug solubility in the body. However, there are indications that nanoparticles are not anymore immune-toxic than conventional small molecule pharmaceuticals. Therefore, molecular scale actions can lead to inflammation and this mechanism of cytotoxicity is not dependent on nanoparticulate nature [3].

A study by Limbach et al illustrates that the generation of ROS occurs readily from molecular solutions, such as Fe_2O_3, Co_3O_4, Mn_3O_4, and TiO_2 [32]. ROS can also be generated from

nanoparticles. The amount of ROS generated from nanoparticles and the amount generated from molecular solutions varies, but cytotoxicity occurs on both the molecular and naoparticulate level. Therefore, the generation of ROS does not require nanoparticulate nature of material to be cytotoxic.

When comparing the effects of different nanoparticles (such as metallic silver, semiconductor CdO, and MoO_3) to the effect of different corresponding salt solutions (silver carbonate, cadmium chloride, and sodium molybdate) on plasma membrane integrity, soluble salts had no effect in all cases [33]. However, all of the nanoparticles examined adversely affected cell membrane integrity. Therefore, cytotoxicity in the form of membrane destabilization is not caused by the molecular scale action of constituent molecules, but rather the nanoparticulate nature of the nanoparticles.

Nanoparticulate Nature

It is still unclear whether nanomaterials can enter and cause harm to humans. Several research papers suggest that nanoparticles can enter organisms' lungs and intestines through inhalation and ingestion. A study done by Li et al. highlights the danger of nanoparticles entering the lungs indicating that when GNPs enter the lungs they cause oxidative stress in the lung's fibroblasts [1]. Qui et al. confirmed these findings demonstrating that the accumulation of Au NPs in human breast adenocarcinoma (MCF-7) cells resulted in mitochondrial damage [1]. Li and Qui's research illustrates the potential adverse effects nanoparticles could have on human cells if used for certain biological and medical applications. Additionally, many believe it is possible for nanoparticles to penetrate the human skin. However, there is less evidence to support this. Research has shown that a nanoparticles' likelihood of entering an organism is based on the nanoparticle's size, surface properties, and functionalization. Furthermore, once a nanoparticle is in the body, its distribution depends mostly on its surface characteristics [34].

Size

Researchers are particularly concerned about the adverse cellular effects of GNPs less than 5 nm in diameter. Research has suggested that GNPs less than 4-5 nm in diameter may be toxic as they are capable of "penetrating the nuclear compartment and binding to DNA" [1]. Scientists believe that GNPs are attracted to DNA grooves because of their electronegativity and DNA's negative environment.

Additionally extremely small NPs, 1.4 nm or less in diameter, fit perfectly in DNA's grooves. Researchers are concerned that these NPs are similar to the size of natural proteins and will therefore be able to enter places such as the nucleus that larger particles cannot. This is alarming because when cells recognize NPs as foreign materials they produce reactive oxygen species (ROS), chemically active oxygen-containing molecules, as a defense mechanism. Cells are capable of buffering certain levels of ROS species however when the level reaches a certain point cell functioning is adversely affected. GNPs could promote the generation of ROS species as a result of their oxidizing capabilities. Although the possible generation of ROS species is viewed

as a potential safety concern for certain GNP application the connection between ROS levels and cytotoxic effects needs to be researched further [1].

Functionality and Surface Properties

Surface modifiers such as anionic and cationic groups and surface charge are among the important factors that influence a particle surface chemistry. Goldman et al. demonstrated the influence of surface modifiers illustrating that cationic GNPs are more cytotoxic than anionic GNPs. His research team attributed these finding to the fact that the cationic particles more closely resembled the negatively charged cell membrane [28].

Charge of Nanoparticles

Repulsion between nanoparticles is needed for stability [35]. The stability of magnetic nanoparticles in colloidal aqueous suspension therefore requires Van der Waals and dipole-dipole interactions [35]. Once a stable aqueous dispersion of nanoparticles is obtained, the positive surface charge of particles can be increased or decreased by changing the ratio of oppositely charged components [36].

A nanoparticle's charge is essential in its ability to induce DNA structural damage. The electrostatic interaction between DNA and a nanoparticle depends upon many factors; a significant factor being the averaged contribution from micro-ions surrounding the DNA and nanoparticle, such as salt ions and their counter-ions [37]. "Highly charged macromolecules form large complexes with dextran-coated nanoparticles, adsorb to the cell membrane via electrostatic interactions and induce membrane bending that triggers endocytosis." [37]

Cationic nanoparticles are capable of binding to DNA as they are positively charged and are attracted to negatively charged DNA. When DNA binds to highly positive nanoparticles, it wraps around the nanoparticle and bends. This bending causes damage to the DNA. If a nanoparticle is too weakly charged, then it does not damage the DNA as the DNA will not wrap around the nanoparticle and bend. The chemical nature of the nanoparticle determines whether DNA is damaged from being bent or compacted. Usually, hydrophobic ligands bind to the minor grooves and charged ligands can bind to minor and major grooves. Major groove binding requires high electrostatic and van der Waals interactions [5].

A study done by Railsback et al confirms that the binding of charged gold nanoparticles causes significant DNA bending. Gold nanoparticles bind to the major grooves of DNA due to the large electrostatic interactions between the charged ligands of the nanoparticles and the phosphate backbone of the DNA strand. Gold nanoparticles can also bind to minor grooves. Gold nanoparticles with alkane-terminated ligands bind to minor grooves and penetrate the DNS helix, flattening it [5]. Positively charged nanoparticles with high enough surface charge densities may attach to DNA irreversibly [37]. Upon attachment, each nanoparticle acquires a dipole moment due to the different in ionic strength between the water medium and the bilayer [38].

Anionic nanoparticles can be internalized within a cell through endocytotic pathways. Nanoparticle endocytotic uptake in localized cell lysosomes is triggered by adsorption on the cells outer membrane. Under cold conditions (4 Celsius), nanoparticles cluster on the cell outer membrane because dynamic endocytotic events cease. Under water conditions (37 Celsius), nanoparticles being to accumulate in intracellular compartments [4].

Hydrophobicity

Hydrophobic nanoparticles can strongly partition into lipid-rich environments such as cell membranes. The hydrophobicity of a nanoparticle influences its cellular uptake and cytotoxicity. Current methods for characterizing hydrophobicity can be divided into three categories: measurements of surface tension, the relative partitioning of a compound for reference phases and measurements of the surface adsorption of hydrophobic or hydrophillic probe molecules,. Surface tension is typically obtained by measuring of contact angles. The relative partioning is measured by testing two immiscible liquid phases, typically water and one organic solvent, and measuring the distribution. The measurement of surface adsorption evaluates the affinity of tested substances to standard hydrophobic material and is most suitable for measurements at the nano scale as it is applicable to all sizes [39].

The physiochemical characteristics of nanocarriers (nanoparticles designed for drug delivery) are determined by their surface properties. The surface hydrophobicity of nanocarriers determines if they bind to proteins in the blood. The stability of cationic solid lipid nanoparticles (SLNs) depends on their extent on electrostatic stabilization [40]. Hydrophilic nanoparticles are more colloidally stable than their hydrophobic counterparts [41]. Surface hydrophobicity strongly influences a nanocarrier's interaction with a cell membrane. A decrease in particle hydrophobicity hinders protein adsorption into a membrane [42].

The surface hydrophobicity of polystyrene-nanoparticle composites is dependent upon the dispersion of nanoparticles in the polymer matrix. In the case of well-dispersed nanoparticles, the cosine of the angle of water contact decreases linearly with the increasing mass percentage of nanoparticles as modeled by the Cassie-Baxter equation [43]. This is represented in Equation 2 below:

$$cos\theta^r = f_1 \cos\theta^s - f_2 \qquad \text{[Equation 2]}$$

In which, f_1 is the fraction of surface area of solid and f_2 is the fraction of surface area of air. The Cassie-Baxter model shows that for a completely wet-table solid, a contact angle of 90 degrees is expected if the fraction of surface area of solid is equal to the fraction of surface area of air [43]. This is illustrated in Figure 7 below:

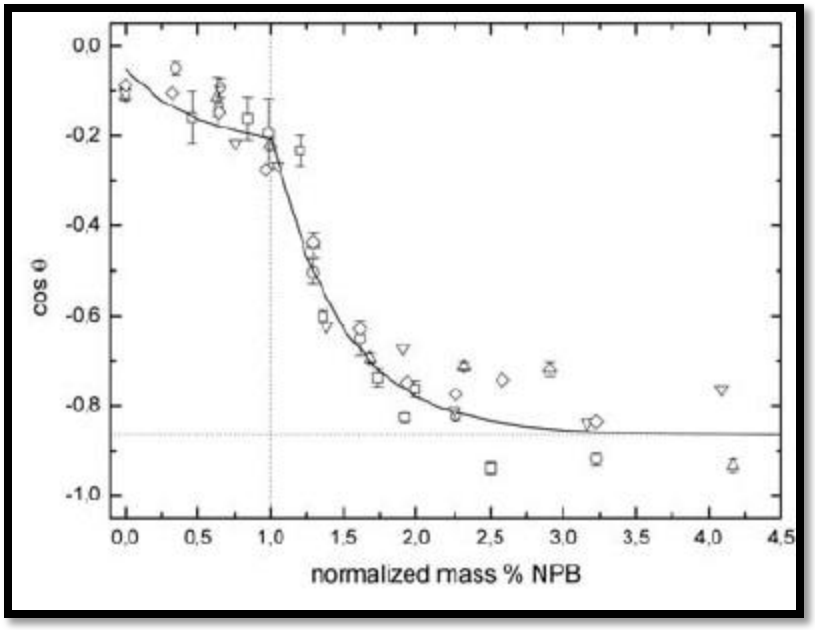

Figure 7: The cosine contact of a water droplet on the polystyrene-nanoparticle composite surface [43]

Measuring Cytotoxicity

Standardized methods to measure cytotoxicity are desperately needed as NPs have several promising application in the biological and medical fields. Reliable data on the cytotoxicity of NPs is needed as researchers need to determine if NPs are safe for these applications. Standardization of protocols and assays used to measure cytotoxicity is necessary so cytotoxicity data from different labs can be compared and more definite conclusion of the cytotoxicity of NPs can be made. Figure 8 below, created by Soenen et al., outlines ways to increase reliability and comparability of measuring cytotoxicity of NPs.

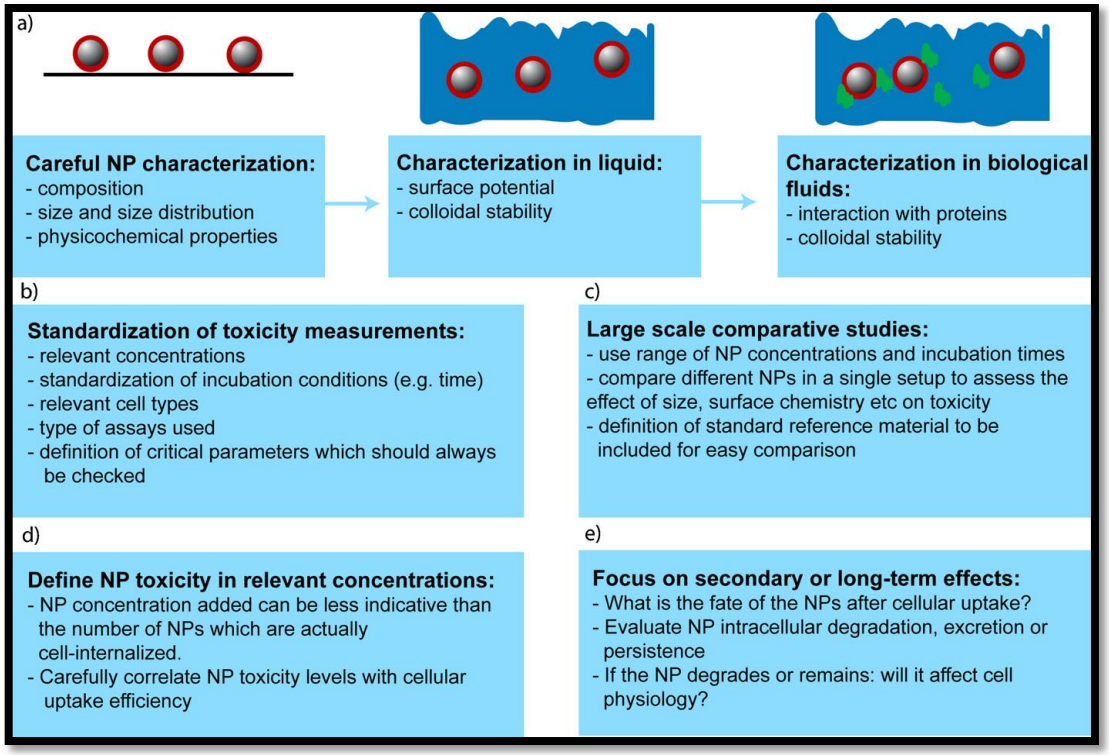

Figure 8: Schematic overview of the key parameters involved in evaluating NP toxicity [1]

With the guidelines illustrated in Figure 8, procedures can be developed to increase the effectiveness of future GNP cytotoxicity research. These procedures can test and compare the effects of concentration and size and help researchers characterize GNPs. Characterization is essential as once extensive research is conducted it will allow researchers to make generalizations about NP toxicity. In order to effectively understand and efficiently research the cytotoxicity of GNPs the functionality of GNPs must be studied first.

Functionality

The functionality of GNPs is dependent upon the ligands that bond to them. To describe the functionality of GNPs the synthesis process, which is defined as the stabilization of NPs with the addition of ligands, must be understood.

Synthesis

NPs have recently received much attention as they have been used to form super molecule structures for molecular, electronic and sensor applications. The usage of NPs and their functionality is limited as a result of the synthesis process because only during the synthesis process can a ligand can be added, which determines a nanoparticle's functionality [44]. Factors that typically influence the practicality and applicability of NPs in industry include: core size,

shape and dispersity and the nature of the ligand shell. Many of these factors are directly influenced by the synthesis process particularly the binding of ligands to NPs [45]. Researchers are still attempting to control these factors while developing a "simple and widely applicable preparation method" for synthesizing GNPs [45].

There are several methods for synthesizing GNPs. GNPs are most commonly synthesized by chemical reduction of $HAuCl_4$ [46]. Chemical reduction in solution is currently the most popular method for synthesizing metal NPs such as GNPs [15]. Several different reducing agents are utilized in synthesis processes. Currently two-phase and one-phase synthesis processes are the most commonly used. After synthesis functionalization must be achieved. "Functionalization is the process by which organic/surfactant molecules are attached to the nanoparticles to keep them in dispersed state" [19].

In the solution synthesis of GNPs, two principal concepts can be distinguished. The first and older distinction employs reducing agents such as sodium citrate or sodium borohydride. This reduces the tetrachloroaurate ions in aqueous media. The NPs in the resulting hydrosols are stabilized electrostatically. Therefore, this first distinction can be done with or without the presence of additional ligands. Through this step, functionalization of the GNPs can be achieved, but is restricted to water-soluble ligands. The disadvantage of this first distinction is that there is poor control over particle size and monodispersity [45].

The second distinction of solution synthesis of GNPs involves synthesis in organic solvents. The most popular method is the two-phase synthesis which involves the transfer of tetrachloroaurate ions into toluene with the use of tetraalkylammonium bromide. Then, there is the subsequent reduction with sodium borohydride in the presence of thiols. The achieved core sizes range from 1-4 nm depending upon reaction conditions [45].

A simpler alternative to two-phase synthesis is the single-phase synthesis. Single phase synthesis usually employs reduction with borohydrides that are soluble in the organic solvent in the presence of the capping ligand. If nonpolar solvents are used additional surfactants have to be added to render gold salt soluble" [45]. Advantages of single-phase synthesis include: "(1) good control over particle size and dispersity by tuning the gold-to-salt ligand ratio and reaction condition; (2) the possibility of introducing a variety of functionalized ligands; and (3) simple isolation, cleaning, and redispersion of particles in different solvents" [45]. Disadvantages include: "impurities introduced by using surfactants; the restriction of carrying out the reduction in the presence of the capping ligand; and achieving complete ligand exchange" [45].

Studies show a new method of producing GNPs can combined the advantages of both concepts, as described by Schulz-Dobrick et al in their study, *Surfactant-Free Synthesis and Functionalization of Gold Nanoparticles*. They found that GNPs can be formed by reducing a solution of hydrogen tetrachloroaurate in diethylene ether (diglyme) through the use of sodium napthalenide in diglyme as the reduction agent. Even though sodium naphthalenide can be considered a harsh reducing

agent, the reaction does not require any further stabilization surfactant. To the yellow aurate solution, a dropwise addition of sodium naphthalenide turns the solution slightly green and then deep brown to indicate the formation of GNPs. These GNPs are weakly protected and can be stabilized and functionalize by the addition of various ligands [45].

The disadvantage to this new method is the over addition of the reducing agent. Upon further addition of the reducing agent the solution turns dark purple, which implies an increase in particle size of about 2nm attributed to the surface plasmon resonance. Even though the particle growth is slow in the diglyme, they tend to agglomerate and form a loose purple precipitate and the diglyme-protected NPs are difficult to isolate or clean even with the use of a stand centrifuge and redispersion procedure [45].

Stabilization

If the procedure is done correctly, NPs can be presumed to be stabilized only by solvent molecules after the particles have been reduced. These solvent molecules can easily be replaced by ligands that offer strong bonding groups. These ligands give the particles' functionality. Strong binding groups include thiols and amines. The ligands also offer enduring stabilization of the NPs. Ligand binding is usually quick. Another advantage of using the new synthesis method mentioned above is that within the diglyme solution, non-polar nanoparticles readily participate. After the addition of ligands, the NPs can be isolated with the use of a centrifuge. The NPs can be washed with ethanol to clean them from excess unbound ligands and remove the diglyme naphthalene. The size of the dodecanethiol-capped nanoparticles ranged 1.9 to 5.2 nm. The addition of excess reduction solution does not result in larger particles [45].

Ligands

As earlier stated, the functionality of GNPs is dependent upon the ligands that have been bonded to them. For example, ligands with thiol or amine binding groups can enhance the solubility of GNPs in organic solvents. To produce water-soluble gold nanoparticles, 2-(dimethylamino)ethanethiol hydrochloride can be used as a ligand in CH_2Cl_2 [45].

Other methods to prepare NPs use functionalities of metal capping agents such as thiols, amines, phosphines, isocyanides, and citrate. These capping agents also prevent agglomeration of the particles, but some are difficult to displace due to coulombic repulsion. This coulombic repulsion also impedes packing in NP films [44].

The binding of proteins and other biomolecules on a NP's surface is possible because of the electrostatic effects of citrate adsorption. Past research has shown that GNPs reduced and stabilized by citrate have a negatively charged surface and tend to bind to thiol, amine, cyanide, diphenolyphosphine functional groups, and other molecules. Using surface plasmon resonance (SPR) spectroscopy, gold surfaces are also used to study peptide-peptide or peptide-protein

interactions. For preparation of GNPs, parallel with the change of Gold-to-Citrate ratio, the size of the particles is controllable [45].

Characterization

Before NPs can be applied in accordance to their ligand-given functionality (sensory, optical, etc.), they need to be characterized. NPs are commonly characterized with UV-vis spectroscopy, TEM microscopy, and particle-size distribution [46]. An illustration of characteristic surface plasmon resonance (SPR) in the absorption spectra can was taken from the case study done by Schulz-Dobrick et al can be seen below in Figure 7.

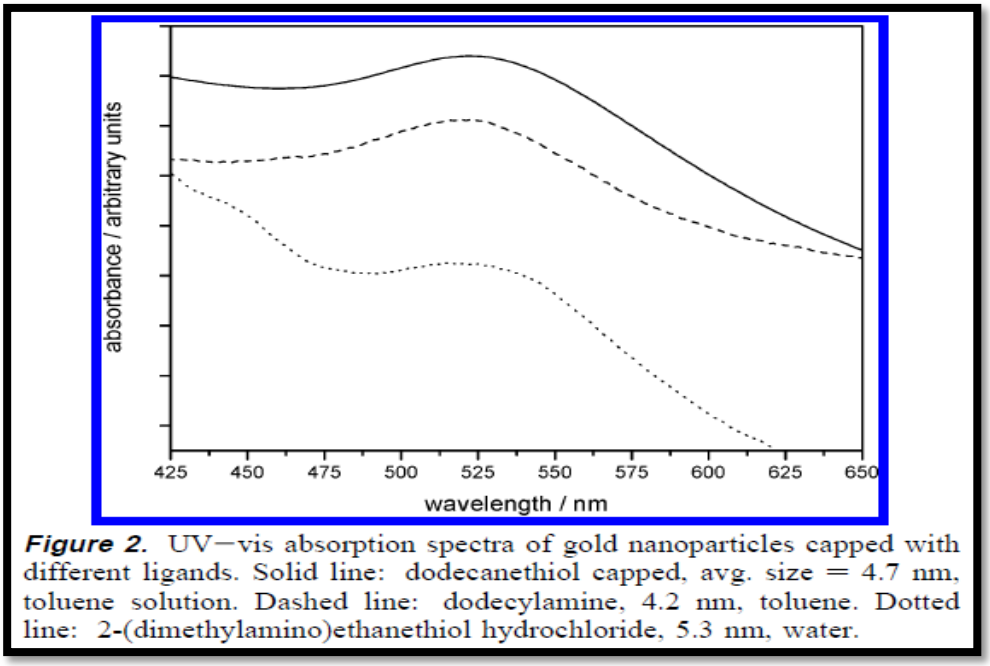

Figure 9: Characteristic SPR in the absorption spectra [45]

As seen in Figure 9, detection, characterization, and functionality heavily depend on the type of ligand used to bind to the NPs. GNPs (with a diameter of ~10-20 nm) observe absorbance maximum in the visible spectrum of about 525 nm. Metal NPs emit surface plasmon oscillations in the visible wavelength range and have optical properties. In most biological studies, GNPs are based on citrate adsorption [45].

Surface Functionalization

Surface functionalization of GNPs is essential to their biomedical applications. This is because the GNPs need to target specific diseased areas and allow for selective interaction with cells and biomolecules. By adsorption of the ligands to the surface of the GNPs, conjugating antibodies and

other targeting moieties can be achieved. Unfortunately, surface adsorption can denature proteins or limit the ligand-to-target interaction on the cell surface because surface adsorption can hinder sterility [47]. Similar to the functionality of GNPs, the size of GNPs can often be controlled during synthesis. Both size and functionality are important in many GNPs applications and in determining the toxicity and cytotoxicity which was previously discussed.

Functionalization of Gold Surfaces

The self-assembly of alkanethiols on gold is an effective way to functionalize gold surfaces. Research has demonstrated that gold surfaces are ideal for self-organized assemblies. Long-chain alkanethiols, $HS(CH_2)_nX$, adsorb onto gold surfaces forming self-assembled oriented monolayer films. The structure of the terminal group, X, can be varied resulting in a great range of possible functional groups on the surface [48]. Chemical functionality on the surface of a nanoparticle can be controlled by the terminal tail group, X. This makes it possible to research the effects of the properties such as hydrophobicity and charge that functional groups impart on nanoparticles. The absorption of n-alkanethiols onto a gold surface results in a hydrophobic surface. In contrast, the absorption of alcohol and carboxylic acid terminated thiols such as 2-mercaptoethanol and 3-mercaptopropionic acid result in hydrophilic surfaces [48].

Short thiol molecules such as 2-mercaptoethanol, 2-aminoethanethiol and 3-mercaptopropionic acid are advantageous as they allow for the functionalization of very small nanoparticles. Research suggests that these thiol molecules will form a monolayer film that is a few Å thick. However, the disadvantage of using shorter thiol molecules is that the functionalization process takes much longer than that of longer chain molecules [48]. Functionalization of a gold surface can occur within 2 seconds of contact for longer chain molecules. In contrast, functionalization can take up to 24 hours for short thiol molecules [49]. Additionally, longer chain thiol monolayer films are more thermally stable than shorter chain thiol films. Both short and long chain thiol films are stable at room temperature [48].

There are two primary methods for preparing monolayer films: "Langmuir-Blodgett techniques involving the transfer of a film assembled at an air-water interface to a solid substrate, and self-assembly, based on the spontaneous adsorption of the film components from a solution directly onto the substrate"[48]. This project will utilize the self- assembly method. Self-assembled monolayers are utilized for the absorption of organosulfer compounds on gold. There are several advantages of monolayer systems where thiols are absorbed on gold. For one, gold interacts strongly with sulfur, which allows for the formation of monolayers in the presence of functional groups. Additionally, gold is an inert metal and is not easily contaminated by the atmosphere as it does not form a stable oxide surface [48].

Monolayers are used to study the effects of functionalization as they have high structural order, flexibility in the structure of the functional group, and are easy to prepare and analyze [48]. This project will focus on the following molecules: 2-aminoethanethiol, and 3-mercaptopropionic acid.

The molecules will be used to functionalize gold nanoparticles. The properties that will result from each functionalization are summarized in Table 1 below.

Table 1: Molecules Used to Functionalize Gold Nanoparticles and Resulting Properties

Molecule	Structure	Property
2-aminoethanethiol	H-S-CH_2-CH_2- NH_2	Hydrophilic and Cationic
3-mercaptopropionic acid	H-S-CH_2-CH_2-COOH	Hydrophilic and Anionic

With the utilization of these molecules, this project will be able to study the effect of charge and hydrophobicity on the interaction between nanoparticle and cell membrane.

Chapter 3: Methodology

Vesicle Preparation (PC Lipid Solution)

PC was purchased from Sigma Aldrich (St. Louis, MO). To obtain a concentrated solution, PC were dissolved in chloroform to form a 100 mg/ml LPG concentrate to form a lipid solution. The lipid solution was dried with nitrogen to evaporate the chloroform and the dried lipids were placed in a vacuum desiccator overnight to evaporate any residual liquid. A Tris NaCl buffer of 100 mM sodium chloride and 100 mM Tris (2-Amino-2-(hydroxymethyl)-1,3 propanediol) (Sigma Aldrich, St. Louis, MO) was prepared in ultrapure water at a pH of 7.8.

The dried lipids were then suspended in buffer to form a lipid solution. The lipid solution was then vortexed and went through 5 freeze-thaw cycles while being vortexed in between each cycle.

Afterwards, the lipid solution was sonicated with an ultrasonic dismembrator (model 150T Fisher Scientific Waltham, MA) for 30 minutes. A pulse mode with a 30% duty cycle (3 second pulse at an amplitude of 60 followed by a 7 seconds break) at 0°C was used.

The lipid solution was centrifuged (Sorvall Discovery 100SE, Kendro, Newtown, 0CT) for 10 minutes at 15000 rpm to remove any probe particles. The supernatant was transferred into a clean test tube and dried with nitrogen at 4 °C. The stock solution was stored in the refrigerator for several months. It was diluted to 0.1 mg/ml for all experimentation.

The PC vesicle solution was used for all experiments.

Nanoparticle Preparation

Gold nanoparticles were purchased from Nanopartz (Loveland, CO) and refrigerated at 7 °C. The nanoparticles were stored in darkness to prevent degradation. The gold nanoparticles were diluted to the desired concentration using ultrapure water or humic acid solution. All nanoparticle solutions were vortexed within minutes prior to use.

Humic Acid Solution Preparation

Humic acid was purchased from Sigma Aldrich (St. Louis, MO). The humic acid was diluted to 100 mg/L using ultrapure water. The solution was stirred and then sonicated with a bath sonicator dismembrator (model 2510 Branson Danbury, CT) for 1 hour. The solution was stored in the refrigerator at 7 °C. The solution was stored in darkness to prevent degradation. Prior to experimental use, the humic acid was filtered twice using first a 0.8 um filter and then a 0.2 um filter. New filters where used for each experiment.

Quartz Crystal Microbalance with Dissipation Monitoring (QCM-D)

Quartz crystal microbalance with dissipation (QCM-D) monitoring technology was used in all experiments. QCM-D monitoring can quantitatively monitor changes in film thickness and mass without the addition of external labels. QCM-D measures the mass and energy dissipation properties of SLB's. This is especially useful in monitoring viscoelastic properties during film formation. QCM-D can measure the real time kinetics of the vesicle fusion process and characterize the mass and viscoelastic properties. Most importantly, QCM-D can monitor SLB interaction with other biomacromolecules such as proteins and drugs (Cho et al 2010). This includes polymers and nanoparticles. The mass change on rigid surfaces is represented using the Sauerbrey relationship in Equation 3.

$$\Delta m = \frac{-C * \Delta f}{n} \qquad \text{[Equation 3]}$$

In which Δm is the change in mass, C is the quartz crystal constant, n is the overtone number, and Δf is the change in frequency.

QCM-D can detect both mass and structural changes by monitoring both frequency and energy dissipation. QCM-D can analyze soft films as represented by the relation in Equation 4 below.

$$D = \frac{E_{lost}}{2 * \pi * E_{stored}} \qquad \text{[Equation 4]}$$

In which, D is the dissipation, E_{lost} is the energy lost, and E_{stored} is the energy stored. Equation 2 encompasses the dissipation parameter in addition to mass.

QCM-D measures cell-surface interaction in frequency and dissipation at the fundamental frequency (5 MHz) and three successive odd overtones (15, 25, and 35 MHz) (Lord et al, 2006).

QCM-D monitoring was performed using the Q-SENSE E4 system (Biolin Scientific, Sweden). The Q-SENSE E4 system allowed for monitoring of resonance frequency and energy dissipation at different overtones.

QCM-D along with its software package, Q-sense, soft films can be characterized in terms of viscosity, elasticity and correct thickness. Absorbed films with uniform thickness and density can be described as functions of overtone number, density, viscosity and elasticity (qsense).

QCM-D Crystal and Sensor Preparation

Silica-coated crystals were placed in each of the four QCM-D chambers and cleaned by running ultrapure water, ethanol and 2% sodium dodecyl sulfate solution (Sigma Aldrich, St. Louis, MO) through the system. A Plasma Prep II oxygen plasma cleaner (SPI Suppliers, West Chester, PA) was used to etch the outer surface of each silica-coated crystal. This was necessary for bilayer formation as it made the surface of the crystals more hydrophilic.

Bilayer Formation and Nanoparticle Introduction

Lipid bilayers were formed by running buffer through the QCM-D system at .15 ml/min for approximately 15 minutes. It was important to make sure the frequency and dissipation overtones stabilized before continuing with experimentation. The lipid solution (PC Lipid Solution) was then run through the QCM-D system for approximately 8 minutes, until a lipid bilayer formed. Bilayer formation occurred within 5 minutes. Buffer was then run through the system to remove any lipids that were not attached to the crystal.

Ultrapure water was run through the system to establish a baseline before the gold nanoparticles were introduced to the bilayer. The nanoparticle solution was then run through the QCM-D system for 10 minutes. Experiments were completed using functionalized nanoparticles with and without soil polymer (Humic Acid). When soil polymer was introduced a water and humic acid polymer solution was run through the QCM-D before and after the nanoparticles. This was necessary to differentiate the effect of nanoparticles and polymer. Ultrapure water and then buffer run through the system again. Frequency was examined to determine if interaction occurred between the nanoparticles and the lipid bilayer. Changes in frequency between before and after the nanoparticles are run through the system indicated interaction.

Chapter 4: Results and Discussion

Functionalized Gold Nanoparticles: Effect of NP Charge and Humic Acid Polymer

Frequency and dissipation changes were monitored to determine the effect of charge on the interaction between nanoparticles and cell membranes. 3-mercaptopropionic acid and 2-aminoethanethiol were used to represent anionic and cationic nanoparticles, respectively. Bare gold nanoparticles were used as a control. All nanoparticles used were 12 nm, hydrophilic, and at the same concentration (3.119×10^{12} particles/mL) to eliminate other factors that could influence interaction such as size, concentration and hydrophobicity. Table 2 summarizes the charge, hydrophobicity and zeta potential of all nanoparticles used. The magnitude of the zeta potential is typically a good indicator of the collidal stability of a nanoparticle. In general the higher in magnitude, the greater the stability. The zeta potentials were sufficently great enough in magnitude to conclude that all nanoparticles used were highly stable [50]. Therefore any interaction between the nanoparticles and SLBs was not attributed to nanoparticle instability. Both the anionic and cationic nanoparticles used had negative zeta potentials as the functionalized ligands bonded to the GNPs were very short. Short functionalized ligands do not have many contributing charge carriers and as a result the zeta potential is dominated by the GNP (which is negatively charged) as opposed to the functionalized ligand. Therefore for short functionalized ligands, such as 2-aminoethanethiol, the manufacturer's zeta potential is negative even though the capping agent is cationic.

Table 2: Properties of 12 nm Gold Nanoparticles

	Charge	Hydrophobicity	Zeta Potential (mV)
Gold	Anionic	Hydrophillic	-36
3-Mercaptopropionic Acid/Gold	Anionic	Hydrophillic	-42.75
2-Aminoethaethiol/Gold	Cationic	Hydrophillic	-36.9

The behavior of functionalized nanoparticles in the enviroment was simulated using humic acid polymer. Humic acid polymer was chosen as a laboratory model as it mimics some of the characteristics of soil in the natural enviroment. Frequency and dissipation changes of all nanoparticles in the prescence of humic acid were compared to controls without humic acid to determine the effect of humic acid on the interaction between cell mambranes and nanoparticles.

QCM-D Plots

QCM-D monitoring was used to measure changes in frequency and energy dissipation as changes correlate to changes in mass and bilayer rigidity, respectively. The relationship between frequency and mass is shown by Equation 5. Dissipation and rigidity are also indirectly proportional.

$$\Delta f \propto \frac{1}{mass} \qquad \text{[Equation 5]}$$

Frequency and dissipation changes were monitored at 6 different overtones (3^{rd}, 5^{th} 7^{th}, 9^{th} and 11^{th}) which corresponded to different depths of the membrane. The higher the overtone the closer it was to the sensor surface.

Figure 10 illustrates a typical QCM-D plot for an experiment without humic acid. Bilayer formation was monitored by observing frequency and dissipation changes as a solution of PC vesicles was introduced to a hydrophobic silicon crystal surface. As the vesicles attached to the silicon crystal mass was increased and the frequency dropped to approximately -60 Hz. Within 5 minutes, the vesicles adsorbed to the crystal surface ruptured, releasing water and forming a supported lipid bilayer. As the water was released, mass was being lost and the frequency increased to about 27 Hz and stabilized. The dissipation decreased as the bilayer became more rigid. Water was then flowed over the crystal surface to remove any unattached vesicles, which decreased the frequency as mass was lost. The frequency and dissipation remained relatively stable throughout the water rinse, the introduction of nanoparticles, and the second water rinse. Even though frequency and dissipation changes were relatively small, frequency changes ≥0.1 Hz

are important and the QCM-D is sensitive enough to detect such small changes in frequency and dissipation.

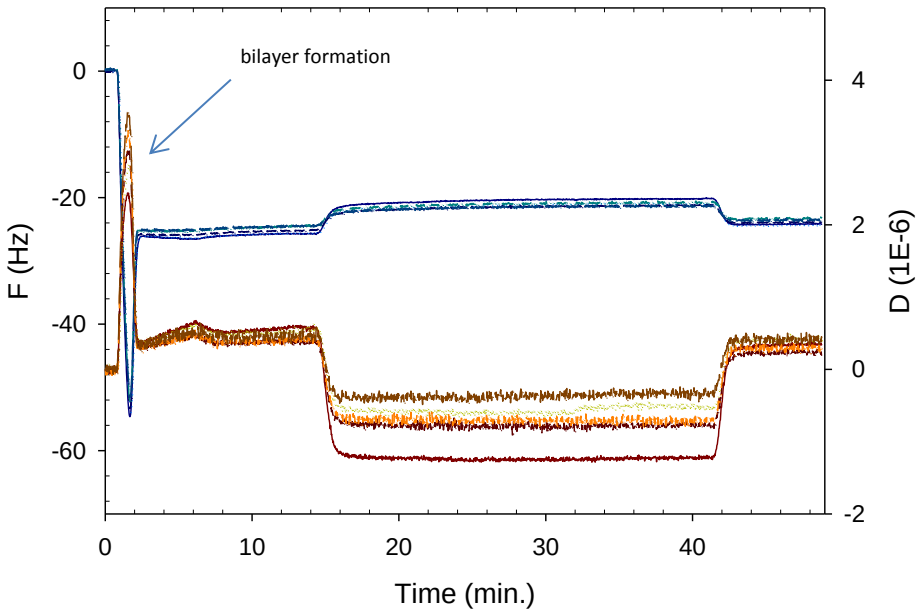

Figure 10: Formation of a PC bilayer on SiO_2 crystal. After the bilayer is formed buffer is flowed through the system to stabilize frequency and dissipation overtones. Water is then flowed through the system. Nanoparticles are introduced followed by another water rinse. Buffer is flowed through the system to complete the experiment. Blue line represents the frequency at each overtone and red lines represent the dissipation at each overtone. Overtones 3, 5, 7, 9 and 11 are shown on the plot. (Experiment conducted 1/11/2013 – Chamber 1 for bare GNP). [Buffer rinse 5:16; water rinse 13:33; NP 21:50; water rinse 32:16; buffer rinse 40:39]

Figure 11 is an example of a typical QCM-D plot for an experiment with humic acid. The QCM-D plots is similar to Figure 10, however, humic acid solution is flowed through the chambers before and after nanoparticle introduction. QCM-D plots for all experimental data can be seen in Appendix A-H.

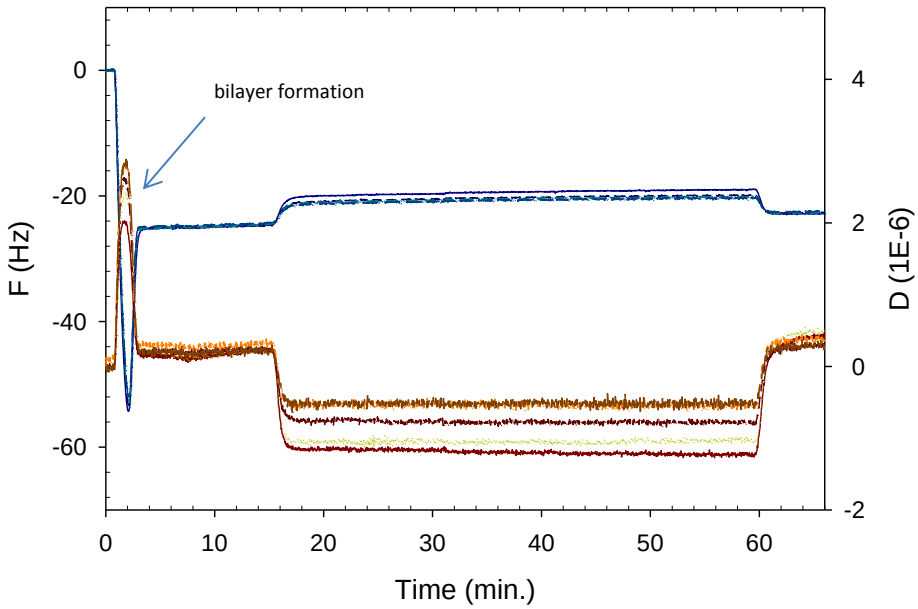

Figure 11: Formation of a PC bilayer on SiO_2 crystal. After the bilayer is formed buffer is run through the system to stabilize frequency and dissipation overtones. Water is then run through the system followed by humic acid solution. Nanoparticles diluted with humic acid are introduced followed by another humic acid solution run and water rinse. Buffer is run through the system to complete the experiment. Blue line represents the frequency at each overtone and red lines represent the dissipation at each overtone. Overtones 3, 5, 7, 9 and 11 are shown on the plot. (Experiment conducted 2/24/2012 – Chamber 4; 2-aminoethanethiol) [Buffer rinse 6:18; water rinse 14:34; polymer solution #1 22:52; polymer+NP 31:10; polymer solution #2 41:27; water rinse 49:42; buffer rinse 58:58]

12 nm Bare Nanoparticles

12 nm bare gold nanoparticles were used as a control to establish a baseline of comparison for functionalized nanoparticles. Figure 12 illustrates this baseline showing the changes in frequency for 6 replicates at several different overtones. The positive changes in frequency indicate that the bare gold nanoparticles interacted with the SLB as changes in frequency ≥ 0.1 Hz can be considered significant. Part of the SLB was likely broken but not lysed as positive changes in frequency correlate to mass loss. A more significant positive change in frequency would be necessary to conclude that membrane lyse had occurred. The QCM-D plots for all 12 nm bare gold nanoparticle replicates can be seen in Appendix A.

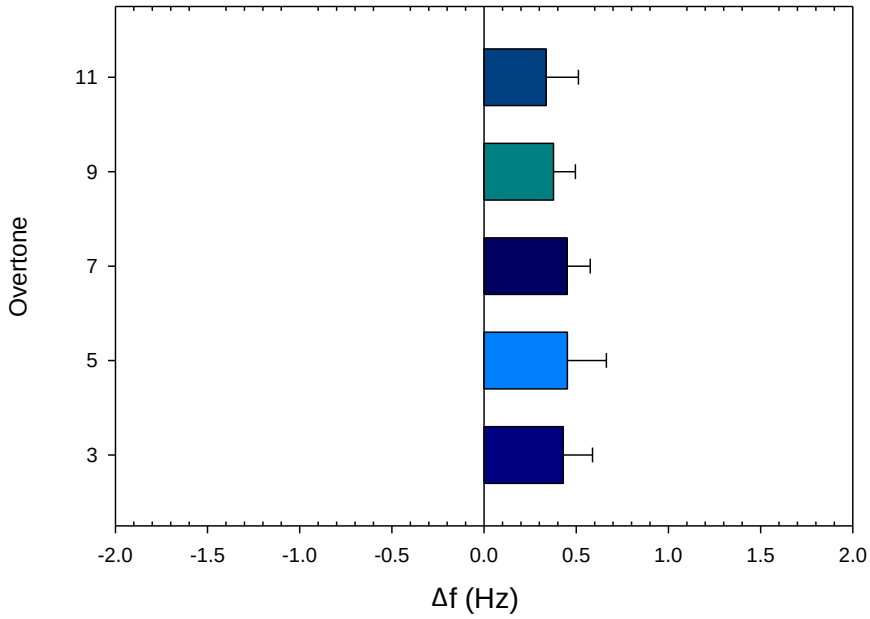

Figure 12: Analysis of the frequency change at each overtone for the interaction of 12 nm bare gold NPs with the PC lipid bilayer. Frequency change is a result of nanoparticle introduction. The plots represent the average frequency change at each overtone for 6 replicates.

3-Mercaptopropionic Acid Nanoparticles

3-mercaptopropionic acid was used to predict the interaction of anionic nanoparticles with SLBs. Figure 13 shows the interaction between 3-mercaptopropionic acid and a SLB. A positive change in frequency occurred at every overtone indicating that mass was lost and the bilayer was disrupted. When compared to the 12 nm bare gold nanoparticle control experimental data the change in frequency is approximately halved. This indicates that 3-mercaptopropionic acid did not disrupt membrane integrity to the same extent that the bare nanoparticles did. As both the bare nanoparticles and 3-mercaptopropionic acid are anionic it can be concluded that nanoparticle of anionic nature are likely to disrupt cell membrane integrity.

The extent to which different anionic functionalized nanoparticles disrupt membrane activity may be related to zeta potential. The magnitude of the zeta potential of 3-mercaptopropionic acid is greater than that of the bare gold nanoparticles and the 3-mercaptopropionic acid disrupted the SLB to a lesser extent. As increased zeta potential magnitude correlates to increased stability anionic nanoparticles with zeta potentials greater in magnitude will likely disrupt membrane integrity less. To confirm that zeta potential correlates with extent of SLB disruption additional experiments would need to be conducted with several different functionalized anionic nanoparticle with a greater range of zeta potentials. A more sensitive technique to detect charge differences could also be used. The QCM-D plots for all 3-mercaptopropionic acid replicates are located in Appendix B.

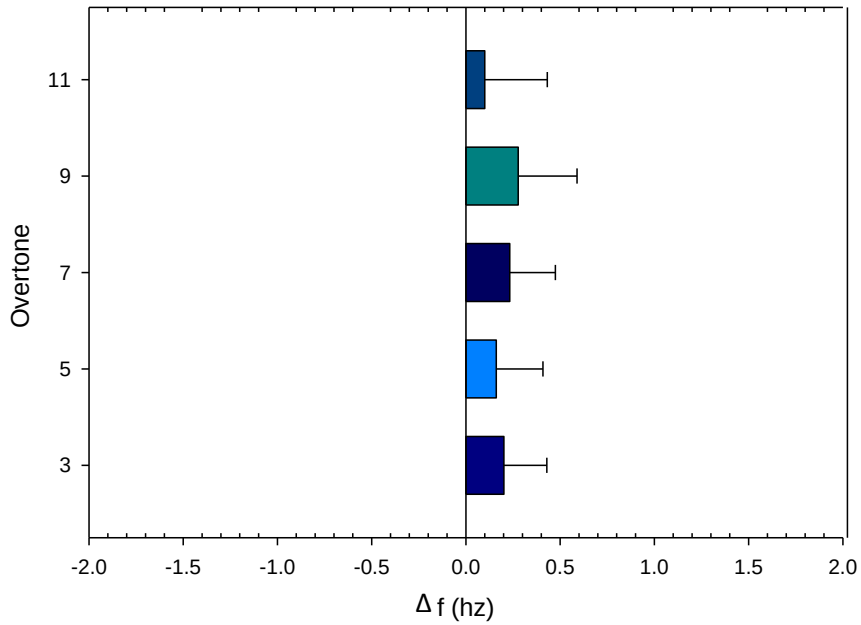

Figure 13: Analysis of the frequency change at each overtone for the interaction of 3-mercaptopropionic acid gold NPs with the PC lipid bilayer. Frequency change is a result of nanoparticle introduction. The plots represent the average frequency change at each overtone for 8 replicates.

2-Aminoethanethiol Nanoparticles

2-aminoethanethiol was used to determine how cationic nanoparticles interacted with SLBs. Figure 14 shows that a positive change in frequency occurred at every overtone. As positive changes in frequency indicate loss of mass, 2-aminoethanethiol likely broke part of the SLB and disrupted membrane integrity. The positive change in frequency for 2-aminoethanethiol was 3-fold greater than the frequency change of 3-mercaptopropionic acid, indicating that nanoparticles with cationic capping agents are more likely to disrupt cell membrane integrity than nanoparticles with anionic capping agents.

The change in frequency of 2-aminoethanethiol was similar to the change in frequency of the 12 nm bare gold nanoparticle control, indicating that 2-aminoethanethiol and bare gold nanoparticles disrupted cell membrane integrity to a similar extent. This suggests the 2-aminoethanethiol cationic capping agent did not significantly affect the interaction of the gold nanoparticle and the SLB. When compared with the bare gold nanoparticle control the frequency change of 2-aminoethanethiol was about 0.1 Hz greater and the frequency change of 3-mercaptopropionic acid was about 0.3 Hz less. This indicates that 2-aminoethanethiol, a cationic capping agent, did not affect the interaction of the GNP as significantly as 3-mercaptopropionic acid, an anionic capping agent. All 2-aminoethanethiol experimental replicate QCM-D plots can be seen in Appendix C.

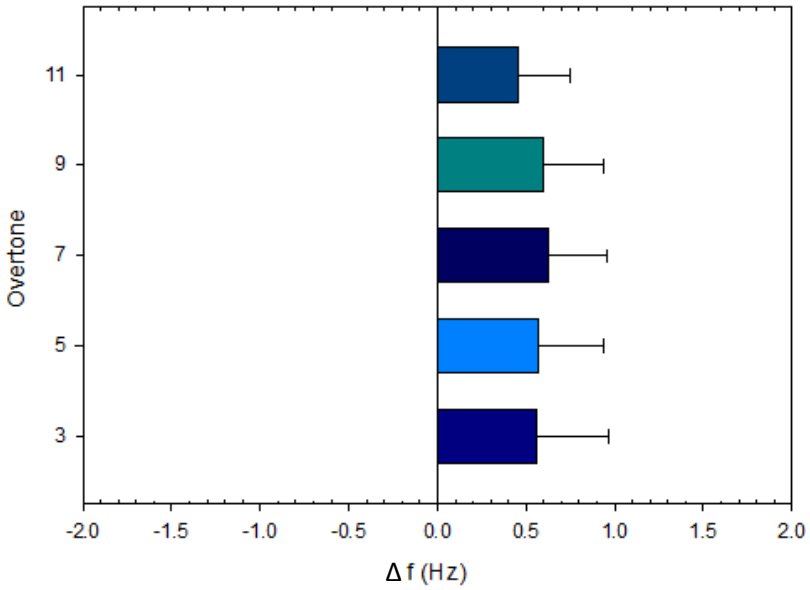

Figure 14: Analysis of the frequency change at each overtone for the interaction of 2-aminoethanethiol gold NPs with the PC lipid bilayer. Frequency change is a result of nanoparticle introduction. The plots represent the average frequency change at each overtone for 8 replicates.

Effect of Humic Acid

Humic acid affected the interaction between nanoparticles and SLBs. To determine the mechanism of this effect, frequency and dissipation changes were examined when humic acid was first introduced to the system, to determine whether humic acid was interacting with the SLB or the nanoparticles. As no significant changes in frequency and dissipation were observed it was concluded that the humic acid was not interacting with the SLB and therefore must have been interacting with the nanoparticles. The humic acid was likely binding to the nanoparticles and altering their interaction with SLBs. Figure 15 is a magnified plot of the frequency and dissipation changes when both humic acid and then 3-mercaptopropionic acid nanoparticles were introduced to the system. The frequency and dissipation remain relatively constant supporting the conclusion that the humic acid was not interacting with the SLB. In addition to this 3-mercaptopropionic acid plot, both 2-aminoethanethiol and 12 nm bare gold nanoparticle experimental plots were magnified at the introduction of humic acid and similar results were observed.

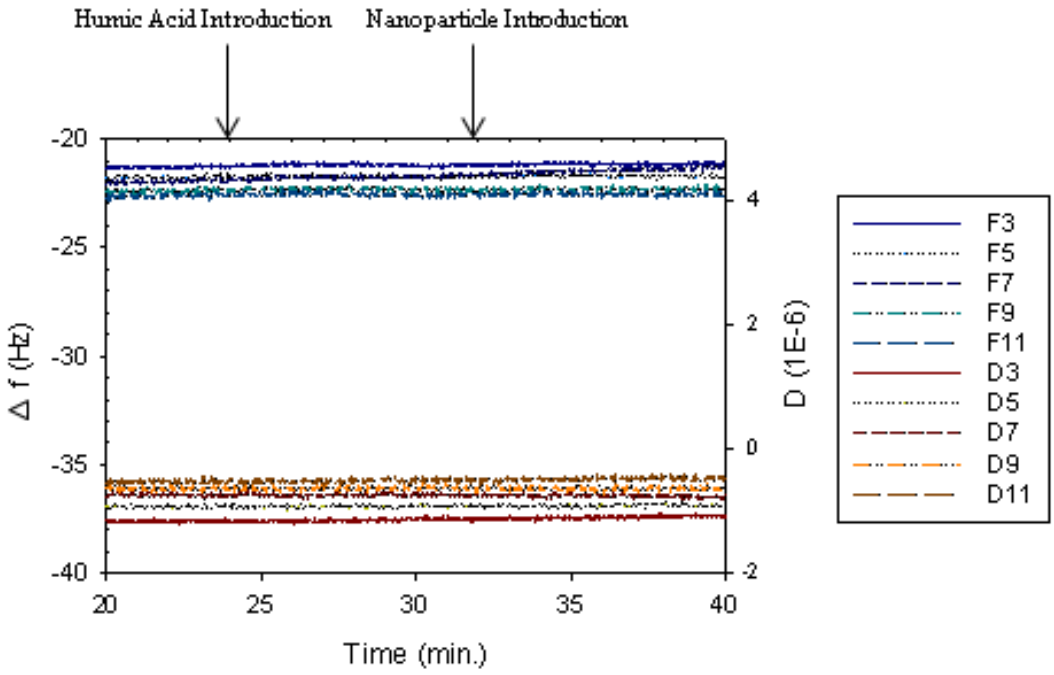

Figure 15: Magnified 3-mercaptopropionic acid experimental plot for analysis of changes in frequency and dissipation humic acid is introduced to the system. Frequency and dissipation remain relatively constant showing no significant interaction between the humic acid and the SLB. Nanoparticle introduction to the system is shown for comparison purposes.

The frequency change at all overtones was calculated when humic acid was first introduced to the system. As the frequency change was $\leq .1$ Hz at every overtone it was not considered significant. Frequency changes are illustrated in Figure 16. If the humic acid was interacting with the SLB, larger changes in frequency would have been observed when it was first introduced to the system.

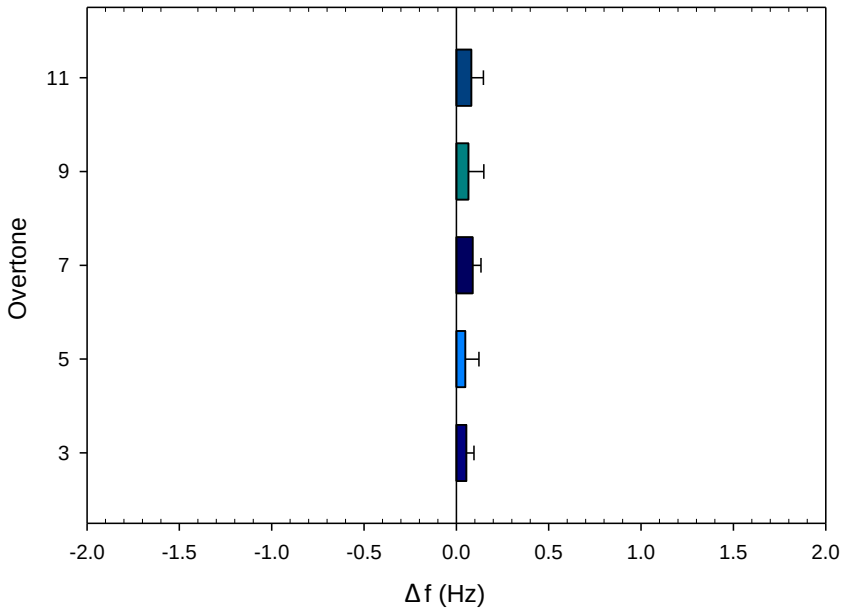

Figure 16: Analysis of the frequency change at each overtone when humic acid is first introduced to the system. Frequency change is a result of humic acid introduction. Frequency change was ≤.1 Hz at every overtone, therefore changes were not considered significant. The plots represent the average frequency change at each overtone for 4 replicates.

12 nm Bare Nanoparticles in Humic Acid Polymer

12 nm bare gold nanoparticles in humic acid were used to establish a baseline of comparison to differentiate the effects of humic acid on cationic verses anionic nanoparticle capping agents. Additionally, humic acid was used so the behavior of nanoparticles in the natural environment could be predicted. Humic acid decreased the interaction between 12 nm bare gold nanoparticles and SLBs. The changes in frequency at each overtone, which can be seen in Figure 17, are relatively close to 0 Hz indicating that the bare gold nanoparticles are not interacting with the SLB. As humic acid mimics conditions in the environment, it is not likely that 12 nm bare gold nanoparticle will interact with the environment. We suspect that humic acids ability to decrease interaction may be attributed to its ability to bind to nanoparticles and alter their surface charge consequently reducing their ability to attach to cell membranes. To confirm this hypothesis the zeta potential of a nanoparticles humic acid mixture would need to be measured to support the conclusion that surface charge was altered. The reduced probability of bare nanoparticles binding to cell membranes would significantly reduce their likelihood of interacting with the environment and being toxic to cells. Furthermore, the lack of attachment of nanoparticles to a cell membrane allows the membrane to maintain its integrity and rigidity. All 12 nm bare gold nanoparticle experimental QCM-D plots are located in Appendix D.

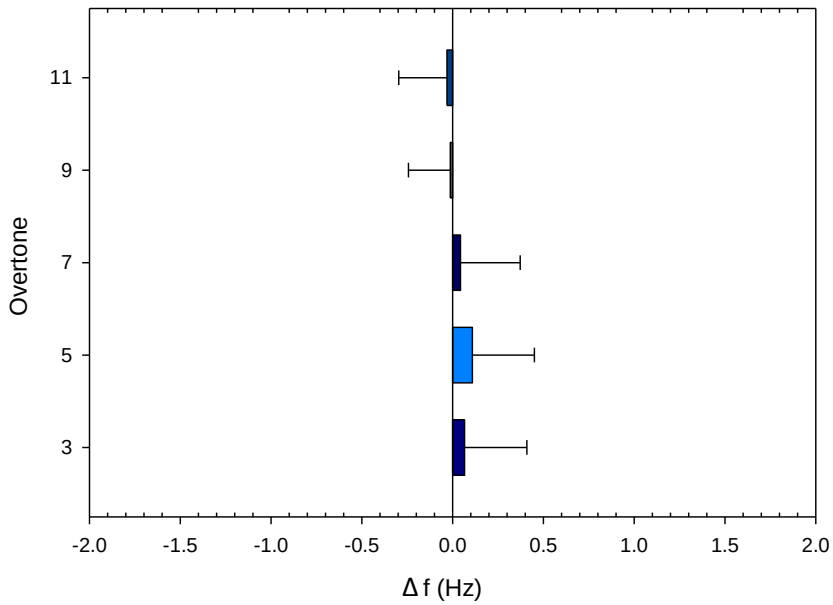

Figure 17: Analysis of the frequency change at each overtone for the interaction of bare 12 nm gold NPs in humic acid with the PC lipid bilayer. Frequency change is a result of nanoparticle introduction. The plots represent the average frequency change at each overtone for 5 replicates.

3-Mercaptopropionic Acid Nanoparticles in Humic Acid

Humic acid alters the mechanism of interaction between 3-mercaptopropionic acid and SLBs. The frequency change is negative at every overtone for 3-mercaptopropionic acid in humic acid, which can be seen in Figure 18, and positive for 3-mercaptopropionic acid in water. Negative changes in frequency correlate to increased membrane mass indicating nanoparticle adsorption to the SLB as opposed to positive changes in frequency, which correlate to decreased membrane mass and membrane fracture. As the negative changes in frequency for 3-mercaptopropionic acid in humic acid are relatively small in magnitude, the nanoparticles may be accumulating on the surface of the SLB verses adsorbing to its surface. Additional experimentation would be needed to confirm this and determine if the accumulation of nanoparticles on the surface of a SLB affects membrane integrity. The QCM-D plots for all 3-mercaptopropionic acid in humic acid replicates can be found in Appendix E.

Humic acid had a significant affect the interaction of both the anionic nanoparticles used, 3-mercaptopropionic acid and the bare gold nanoparticles, therefore it is likely that the anionic nanoparticles are interacting with the humic acid. As humic acid mimics conditions in the natural environment, it is likely that anionic nanoparticles will also interact with the environment.

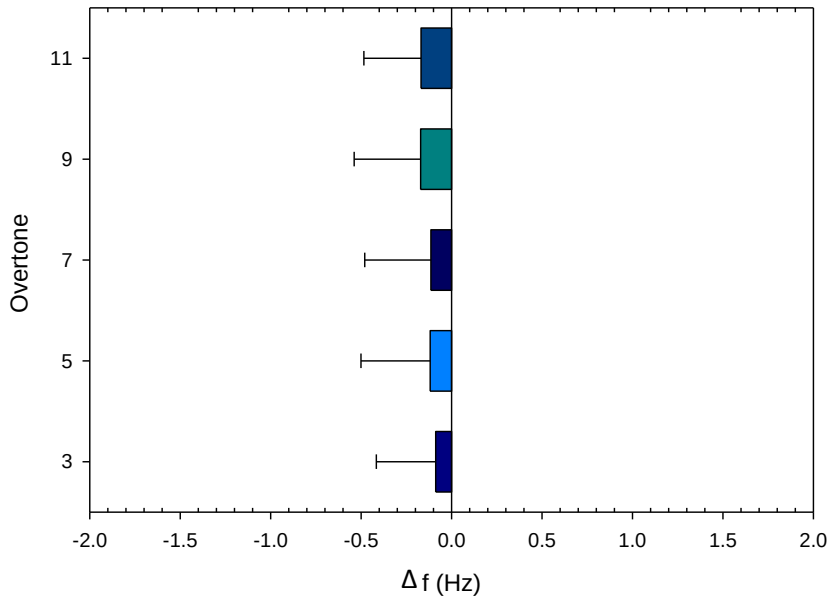

Figure 18: Analysis of the frequency change at each overtone for the interaction of 3-mercaptopropionic acid gold NPs in humic acid with the PC lipid bilayer. Frequency change is a result of nanoparticle introduction. The plots represent the average frequency change at each overtone for 14 replicates.

2-Aminoethanethiol Nanoparticles in Humic Acid

Humic acid did not affect the interaction of 2-aminoethanethiol and the SLB as significantly as it did for anionic nanoparticles. For 2 aminoethanethiol it decreased the interaction by about 0.2 Hz at every overtone. Even though interaction was decreased the frequency change was still positive (Figure 19) indicating that mebrane fracture still occurred. Membrane integrity was disrupted to a lesser extentwhen humic acid was present, however. Additionally, the realatively small decrease in frequency suggests that the humic acid did not interacting with 2-aminoethanethiol and hinder its ability to inteact with the cell membrane as it did for the 12 nm bare gold nanoparticles. Therefore, cationic nanoparticles may be more likely to disrupt cell membrane integrity in the natural enviroment than anionic nanoparticles.

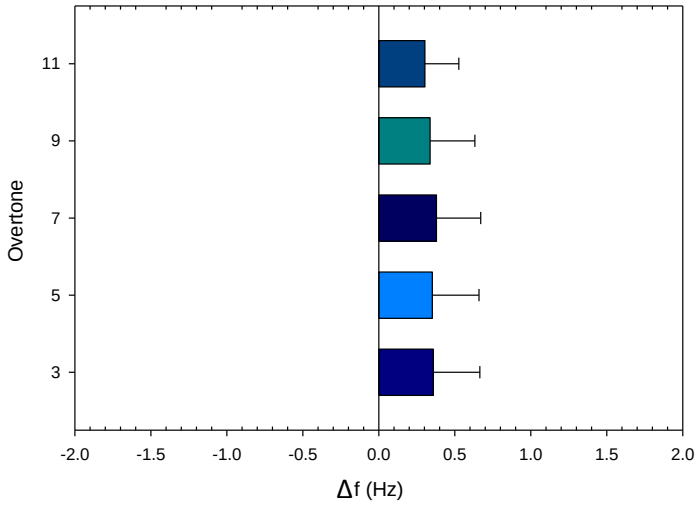

Figure 19: Analysis of the frequency change at each overtone for the interaction of 2-aminoethanethiol gold NPs in humic acid with the PC lipid bilayer. Frequency change is a result of nanoparticle introduction. The plots represent the average frequency change at each overtone for 8 replicates.

Effect of Chemical Functionality

The D/f ratio at the 7th overtone was calculated 5 minutes after nanoparticle introduction, as nanoparticle were flowed through the system for 10 minutes, for each nanoparticle used with and without humic acid to determine the nanoparticles effect on membrane rigidity. Low D/F values correspond to a fairly rigid membrane as mass is being added without a significant dissipation increase. High D/F values correspond to relatively flexible membranes as mass is being added while dissipation is also increasing. Figure 20 shows that 2-aminoethanethiol resulted in the most rigid membrane while 3-mercaptopropionic acid resulted in a more flexible membrane. In general, membrane rigidity for anionic nanoparticle was greater than the membrane rigidity for cationic nanoparticles when humic acid was not present. In addition, to affecting the interaction of nanoparticles and SLBs humic acid also altered trends in membrane rigidity. As opposed to cationic and anionic nanoparticles in water, cationic nanoparticles in humic acid had greater membrane rigidity than anionic nanoparticles in humic acid. Additionally, for anionic nanoparticles (3-mercaptopropionic acid and bare 12 nm gold nanoparticles) the presence of humic acid significantly increased the rigidity of the membrane. For cationic nanoparticles (2-aminoethanethiol) the presence of humic acid decreased the rigidity of the membrane.

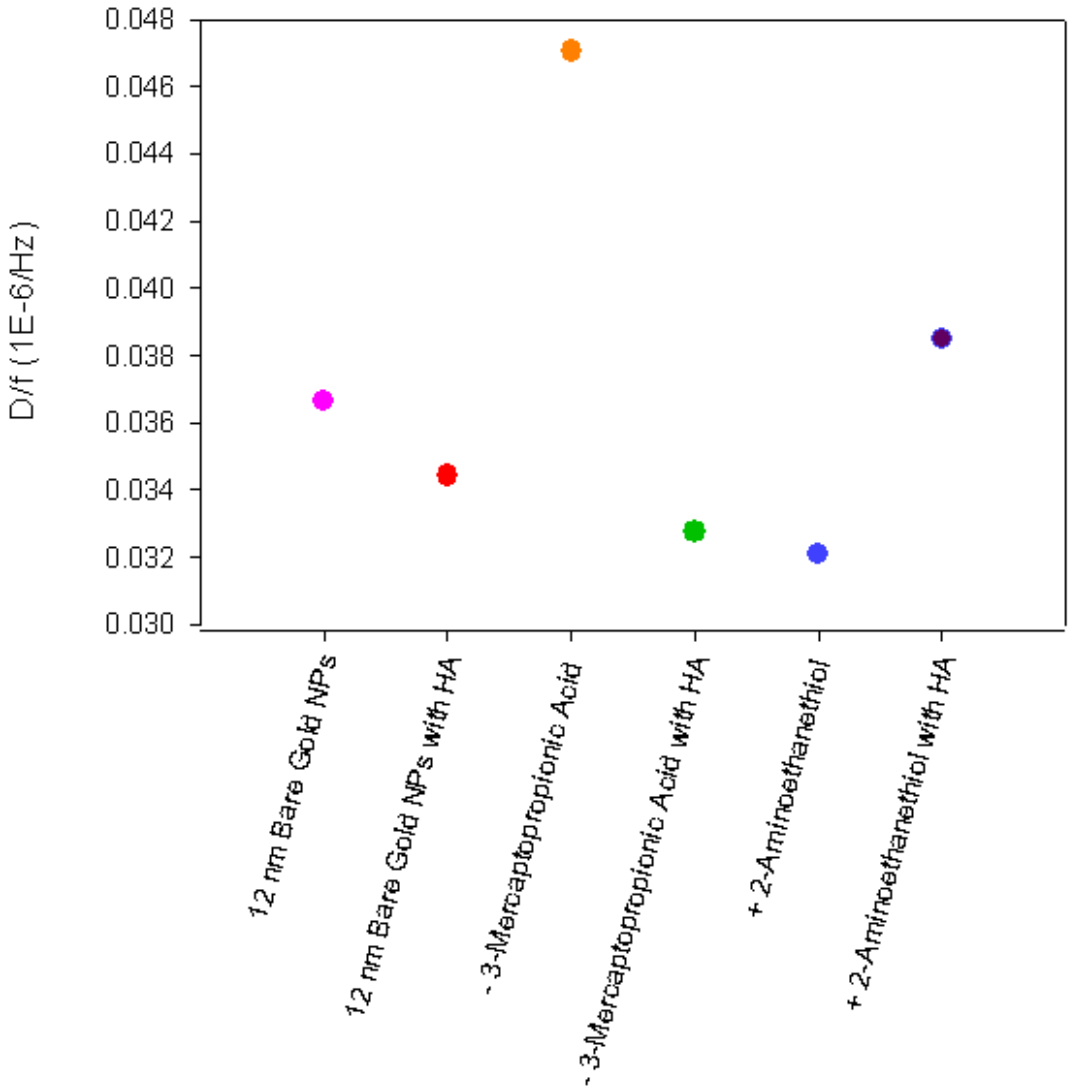

Figure 20: Comparison of D/f for 12 nm Bare Gold NPs, 3-mercaptopropionic acid and 2-aminoethanethiol with and without the presence of humic acid. D/f corresponds to membrane rigidity. D/f values were obtained 5 minutes after nanoparticle introduction. Nanoparticles were run for a total of 10 minutes.

4.7 nm Hydrophobic Ag Nanoparticles

4.7 nm hydrophobic AgNPs were used to provide insight on the frequency changes expected for cytotoxic nanoparticles. The frequency change observed for the AgNPs was approximately 10 fold greater than the 12 nm bare and functionalized gold nanoparticles used. Additionally, it was about 10 fold greater than the 5 nm bare gold nanoparticles. As these nanoparticles are similar in size, the increased frequency can be attributed to the material of the nanoparticle as opposed to its size. Silver is cytotoxic while gold is not. Therefore, gold nanoparticles, as opposed to silver, are a more appropriate experimental model when attempting to identify the influence of other factors such as size, concentration and functionality on cytotoxicity.

Figure 21 shows that the frequency change for AgNPs ranges from about -4 to -6 Hz depending on the overtone. The significant frequency decrease at all overtones indicates that mass was gained and nanoparticles adsorbed or inserted into the membrane. It is likely that this increase in mass was significant enough to result in destabilization of the SLB. This destabilization is the mechanism of AgNP cytotoxicity.

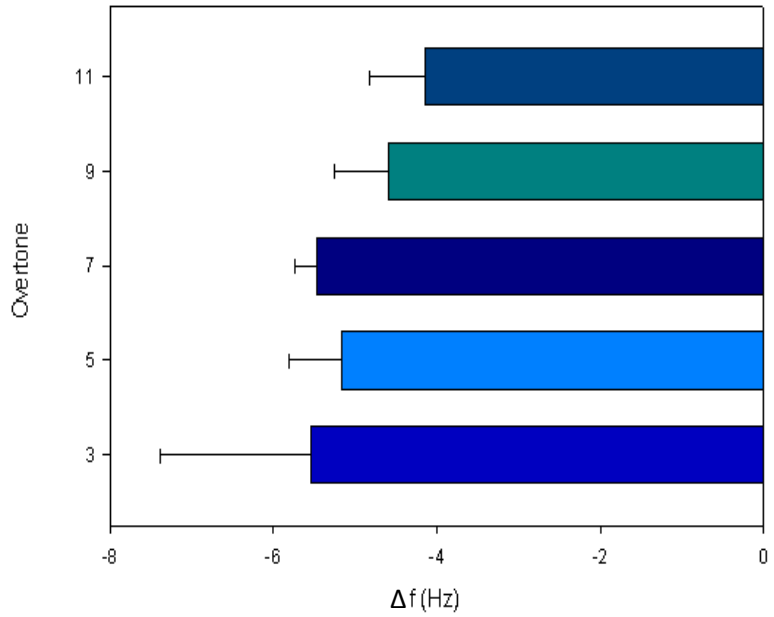

Figure 21: Analysis of the frequency change at each overtone for the interaction of 4.7 nm hydrophobic AgNPs with a 4.1PC: LPG + PG lipid bilayer. Frequency change is solely a result of nanoparticle introduction to experiments. The plots represent the average frequency change at each overtone for 4 replicates.

The AgNP experiment was also analyzed by plotting dissipation verses time at the 7th overtone (Figure 22). The dissipation increased as the nanoparticles were flowed through the system indicating that membrane rigidity was decreasing. As nanoparticles adsorbed into the membrane its stability decreased until eventually destabilization occurred. The slope of the plot provides insight on the rate at which the nanoparticles were being adsorbed into the membrane.

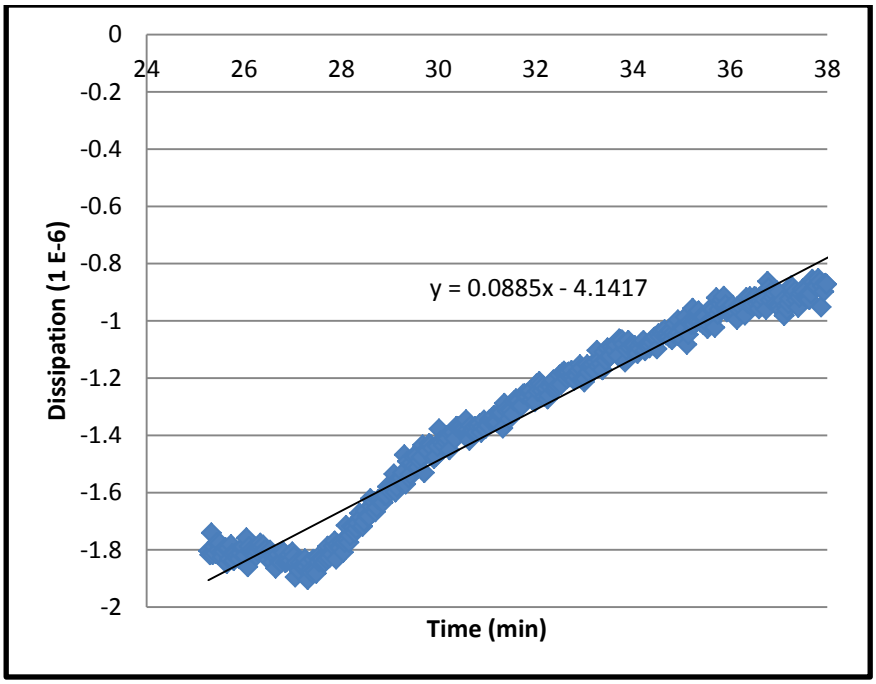

Figure 22: Dissipation versus time plot at the 7th overtone for one 4.7 nm hydrophobic AgNPs with a 4.1PC: LPG + PG lipid bilayer experiment. The graph illustrates the dissipation increase as nanoparticles are introduced and then run through the system for 10 minutes.

The D/f ratio verses time data was also analyzed to provide insight on the nanoparticle adsorption. As seen in Figure 23 the D/f ratio decreased as the nanoparticle flowed through the system, which indicates that the layer of nanoparticles adsorbing to the bilayer was not homogeneous. If the layer was homogeneous the D/f ratio would remain constant over time. The decreasing D/f ratio with time suggests that the nanoparticles adsorbed to the SLB in clusters. These clusters likely disrupted membrane integrity, and ultimately led to membrane destabilization.

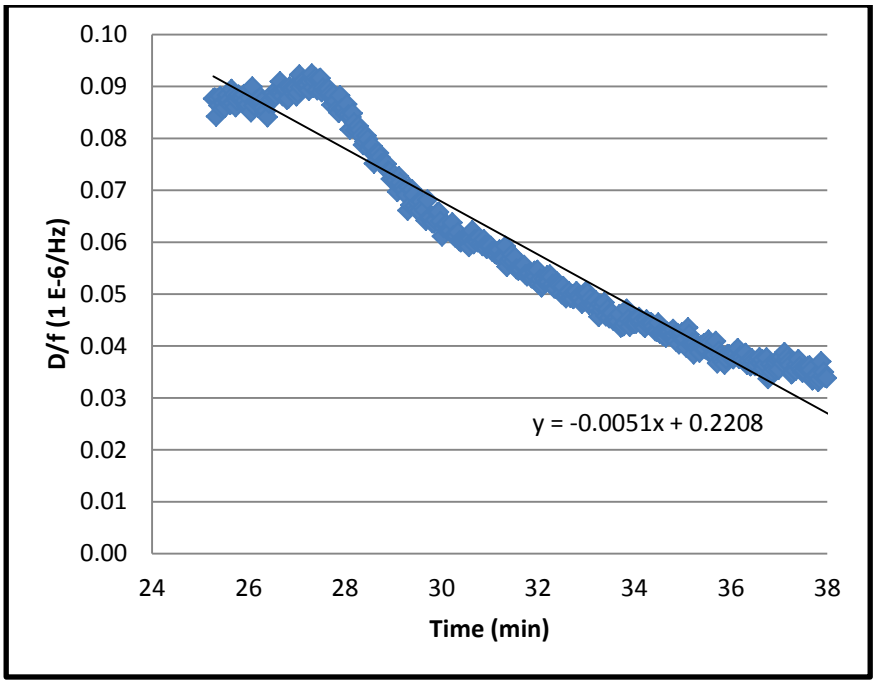

Figure 23: D/f versus time plot at the 7th overtone for one 4.7 nm hydrophobic AgNPs with a 4.1PC: LPG + PG lipid bilayer experiment. The graph illustrates the dissipation increase as nanoparticles are introduced and then run through the system for 10 minutes.

Figure 24 shows a direct comparison between the frequency and dissipation of the nanoparticle adsorption properties as opposed to the time dependency of the frequency and dissipation. It shows a decrease in frequency indicating that mass was adsorbed to the SLB. Additionally, it shows an increase in dissipation, indicating that the SLB was becoming less rigid as the mass increased as a result of nanoparticles accumulation on the membrane.

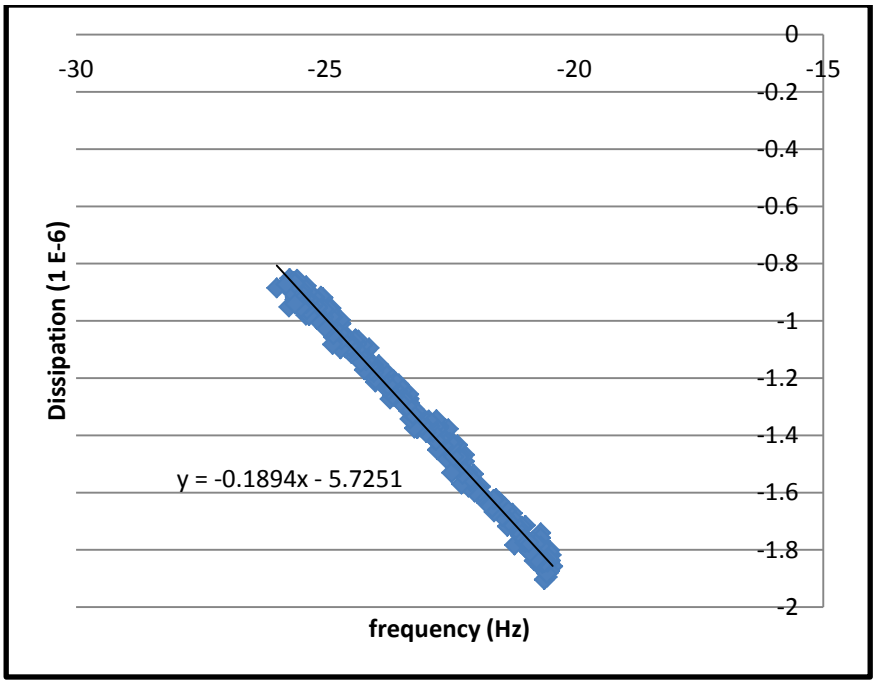

Figure 24: Dissipation versus frequency plot at the 7th overtone for one 4.7 nm hydrophobic AgNPs with a 4.1PC: LPG + PG lipid bilayer experiment. The graph illustrates the dissipation increase as nanoparticles are introduced and then run through the system for 10 minutes.

Gold nanoparticle experimental data was also analyzed by graphing frequency and dissipation versus time and dissipation verses frequency. Trends were not prevalent therefore conclusions could not be drawn for gold nanoparticles using these analytical techniques. The absence of trends can likely be attributed to magnitude of the noise resulting from QCM-D analysis being greater than the interactions between the nanoparticles and the SLBs. Plots of frequency and dissipation versus time and dissipation verses frequency for all gold nanoparticles used can be seen in Appendix J.

Bare Gold Nanoparticles: Effect of NP Size and Poly(methacrylic acid) Polymer

Bare gold nanoparticles were used to determine the effect that poly(methyacrylic acid) polymer has on the interaction between 2nm, 5nm and 10nm nanoparticles and SLBs. Results are a continuation of experiments conducted by an MQP group with the polymer last year. The MQP group completed experiments for 2nm, 5nm and 10nm nanoparticles with poly(methyacrylic acid) polymer. Experiments conducted this year were used to establish a baseline of comparision so that the effects of poly(methyacrylic acid) polymer on 2nm, 5nm and 10nm nanoparticles could be determined.

5 nm Nanoparticles

A positive change in frequency of about 0.7 Hz at each overtone was observed for the 5 nm bare gold nanoparticles indicating that the SLB was broken as positive changes in frequency correspond to decreases in mass. Changes in frequency ≥0.1 Hz are significant therefore, it can be concluded that the 5 nm bare gold nanoparticles disrupted cell membrane integrity. All QCM-D plots for 5 nm bare gold experimental replicates can be seen in Appendix H.

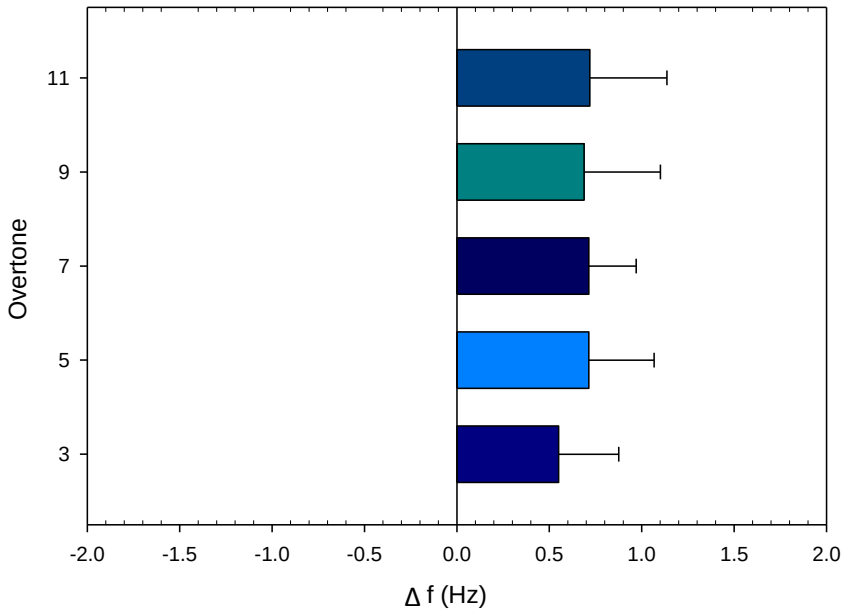

Figure 25: Analysis of the frequency change at each overtone for the interaction of 5 nm bare gold NPs with the PC lipid bilayer. Frequency change is a result of nanoparticle introduction. The plots represent the average frequency change at each overtone for 4 replicates. The concentration of the nanoparticles was held constant for all replicates to determine if the mechanism of interaction for nanoparticles with membranes is dependent on size.

Poly(methyacrylic acid) polymer significantly increases the interaction of 5 nm bare gold nanoparticles with SLBs which is illustrated in Figure 26. The change in frequency when polymer was present was around -0.8 Hz as opposed to 0.7 Hz when polymer was not present.

Therefore, the decrease in frequency when the polymer was present was approximately double the increase in frequency when no polymer was present. This indicates that the polymer increased interaction by a factor of about 2 supporting the conclusion that polymer amplifies the interaction of 5 nm bare gold nanoparticles with SLBs. The increased interaction of the nanoparticles and the cell membranes is likely a result of the characteristic nature of the polymer.

Additionally, the polymer affected the mechanism of nanoparticle and SLB interaction. The frequency change was negative when polymer was present, which correlates to an increase in mass on the membrane and suggests that nanoparticles were adsorbed onto the membrane. Conversely, the frequency change was positive when polymer was not present, suggesting that the membrane was broken, as positive changes in frequency correlate to a decrease in membrane mass. Both mechanisms, nanoparticle adsorption and membrane fracturing, can disrupt cell membrane integrity. If the extent of cell membrane integrity disruption is great enough, cell membrane destabilization will ultimately occur.

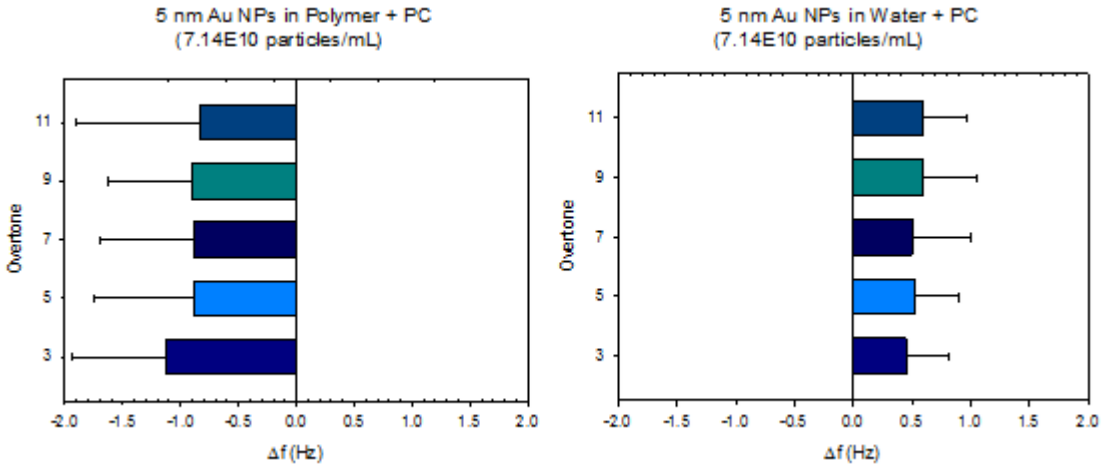

Figure 26: Comparison of bare 5 nm gold NPs in water to 5 nm gold NPs in poly(methacrylic acid) polymer. Frequency change at each overtone for the interaction of gold nanoparticles with the PC lipid bilayer without and without the presence of polymer is illustrated. The frequency charge is the average of 10 replicates in water and 11 replicates in polymer. The concentration of NPs was the same for all experiments so differences in frequency between the two plots are a result of the presence of the polymer. The plots show that the presence of poly(methacrylic acid) polymer increases interaction at all overtone for 5 nm bare gold NPs.

10 nm Nanoparticles

A positive change in frequency was also observed at every overtone for the 10 nm bare gold nanoparticles indicating that the membrane was fractured as positive changes in frequency correlate to decreased membrane mass. Additionally, the change in frequency for the 10 nm bare gold nanoparticles was smaller than the change in frequency for the 5 nm bare gold nanoparticles

by a factor of about 1.5 indicating that the 10 nm bare gold nanoparticles disrupted cell membrane integrity to a lesser extent than the 5 nm. The frequency changes for 10 nm bare gold nanoparticles are summarized in Figure 27 and the corresponding QCM-D plots can be seen in Appendix I.

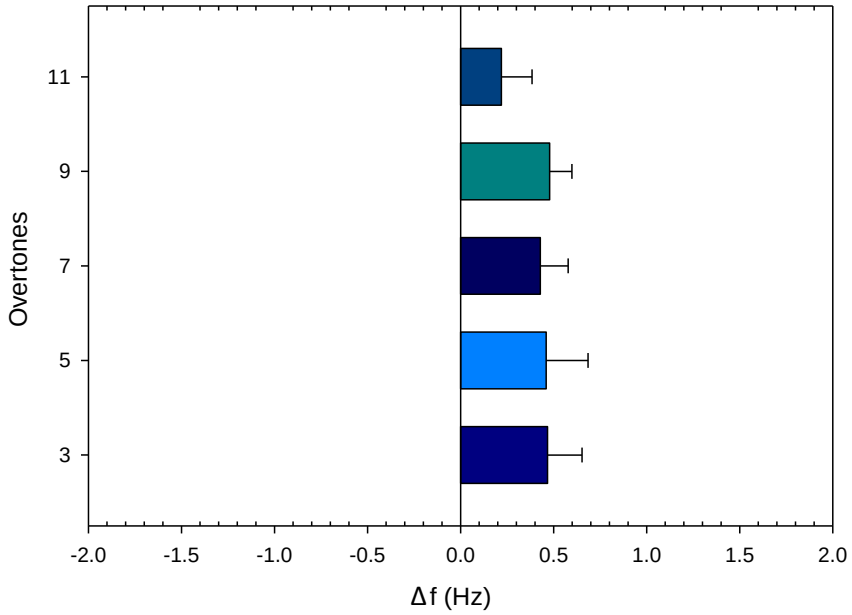

Figure 27: Analysis of the frequency change at each overtone for the interaction of 10 nm bare gold NPs with the PC lipid bilayer. Frequency change is a result of nanoparticle introduction. The plots represent the average frequency change at each overtone for 4 replicates. The concentration of the nanoparticles was held constant for all replicates to determine if the mechanism of interaction for nanoparticles with membranes is dependent on size.

Poly(methyacrylic acid) polymer did not affect the magnitude of the interaction between 10 nm bare gold nanoparticles and SLBs. As seen in Figure 28, the frequency change was not altered by the polymer as the positive change in frequency (~ 0.5 Hz) at each overtone were very similar for experiments with and without polymer. Additionally, the frequency change was positive in both experiments with and without polymer, indicating that the mechanism of interaction was not affected by the polymer. Membrane mass decreased, breaking the membrane and disrupting its integrity regardless of whether polymer was present.

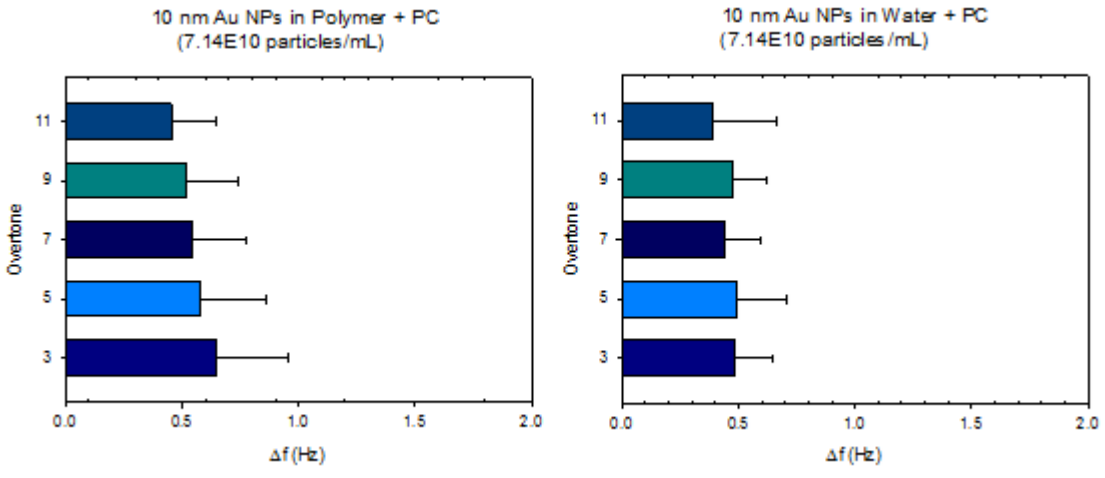

Figure 28: Comparison of bare 10 nm gold NPs to 10 nm gold NPs in poly(methacrylic acid) polymer. Frequency change at each overtone for the interaction of gold nanoparticles with the PC lipid bilayer without and without the presence of polymer is illustrated. The frequency charge is the average of 9 replicates in water and 9 replicates in polymer. The concentration of NPs was the same for all experiments so differences in frequency between the two plots are a result of the presence of the polymer. The plots show that the presence of poly(methacrylic acid) polymer does not affect interaction for 10 nm bare gold NPs.

Influence of Polymer and Size

Polymer amplified the interaction between 5 nm gold nanoparticles and SLBs, but did not affect the interaction for 10 nm nanoparticles. This can likely be attributed to the availability of a surface area for the polymer to interact with which is greater for the 5 nm nanoparticles than the 10 nm nanoparticles. Although our experimentation was not focused on 2 nm nanoparticles the same trend was also observed. The polymer increased interaction at all overtones by at least a factor of three, which is greater than the increased interaction of the 5 nm nanoparticles. This is expected as the cumulative surface area of the 2 nm nanoparticle is even greater than that of the 5 nm. 2 nm experimental data can be seen in Figure 29 below.

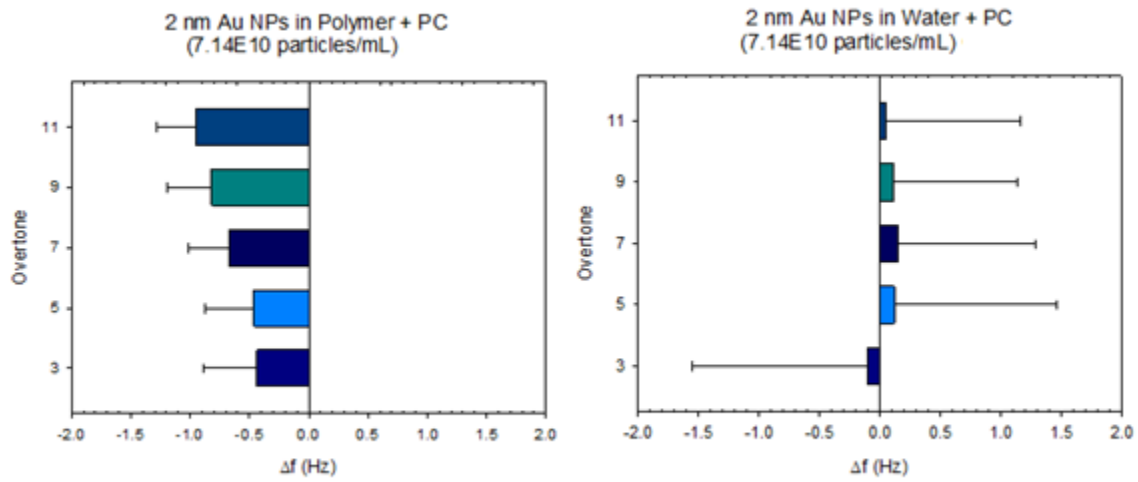

Figure 29: Comparison of bare 2 nm gold NPs in water to 2 nm Au NPs in poly(methacrylic acid) polymer. Frequency change at each overtone for the interaction of gold nanoparticles with the PC lipid bilayer without and without the presence of polymer is illustrated. The frequency charge is the average of 6 replicates in water and 3 replicates in polymer. The concentration of NPs was the same for all experiments so differences in frequency between the two plots are a result of the presence of the polymer. The plots show that the presence of poly(methacrylic acid) polymer increases interaction at all overtone for 2nm bare gold NPs.

Broader Scope

Other research studies have also concluded that nanoparticles are likely to interact with cell membranes and are therefore potentially cytotoxic to humans and the environment. Previous studies have shown that nanoparticles can kill cells by disrupting cell membrane integrity,

damaging cells by the generation of oxygen reactive species, damaging DNA, effecting the functionality of cellular proteins and enzymes, triggering inflammation and damaging mitochondria [1-3]. Research has attempted to determine how engineered nanoparticles interact with biological cells to determine if nanomaterials are cytotoxic to humans, microbial organisms and aquatic organisms. Assessing nanomaterial toxicity is challenging as literature suggests that several properties have the potential to influence toxicity. These properties include: chemical composition, size, shape, concentration, stabilizing coating agents, physiochemical properties, surface functionalization and surface charge [1]. Our research focused primarily on surface functionalization and surface charge. The effect of size was also examined.

Size

Previous research suggests that gold nanoparticles ≤5 nm in diameter induce toxicity by binding to DNA as the smaller the nanoparticle the more likely it is to penetrate the nuclear compartment[1]. This is consistent with our research which concluded that the smaller the nanoparticle the more likely it is to disrupt cell membrane integrity. When cell membrane integrity is disrupted to a great enough extent, cytotoxicity results. Other studies support this conclusion attributing smaller nanoparticles ability to induce toxicity to their ability accumulate and aggregate [51]. Particle accumulation likely results in reduced colloidal stability, raising particle activity thus increasing the likelihood of particle-induced toxicity. These research studies have focused specifically on the interaction between nanoparticles and cell membranes. Numerous other research studies that focused on the interaction between nanoparticles and entire organisms contradict these conclusions suggesting that larger nanoparticles are more toxic than smaller nanoparticles. Several recent studies have determined that larger nanoparticles are more effective in decreasing larva and pupa viability [52]. Other literature explains this conclusion stating that although smaller nanoparticles accumulate more effectively than larger nanoparticles, larger nanoparticles have the ability to distribute better throughout an organism[51]. In summary, literature suggests that small nanoparticles are toxic to cells and other micro-sized organisms, whereas large nanoparticles are more toxic to larger eukaryotic organisms.

Surface Charge

Literature suggests that a nanoparticles surface coating significantly influences its bioactivity. Furthermore, literature agrees with our research suggesting that properties such as surface charge and chemical functionality influence the interaction between nanoparticles and cell membranes. Several research studies recognize the importance of chemical functionality and surface change including a study done by Hardman which highlights the importance of the physiochemical characteristics of quantum dots in governing decay and degradation rates in the environment [31]. Research has also focused on differentiating between the effects of cationic and anionic particles, which was one of the objectives of our research. A study done by Dobrovolskaia et al demonstrated that charged nanoparticles, cationic or anionic, are more likely to disrupt cell membrane integrity than neutral nanoparticles[3]. Research conducted by Lewinski et al supported this conclusion and determined that cationic nanoparticles are more toxic then anionic

nanoparticles[29]. Several other research studies have also suggested that cationic nanoparticle are more toxic then anionic nanoparticles as they are more likely to interact with biological components [31]. Literature suggests that reducing the number of positive charges on a nanoparticles surface decreases cellular uptake efficiency thus decreasing cytotoxicity. Soenen et al. correlated toxicity to nanoparticle stability concluding that cationic nanoparticles are typically less stable than anionic nanoparticles and as a result are more toxic [1]. Our research also demonstrated that cationic nanoparticles are more toxic than anionic nanoparticles as 2-aminoethanethiol, a cationic capping agent, disrupted cell membrane integrity to a greater extent than 3-mercaptopropionic acid, an anionic capping agent. Although literature suggests that cationic nanoparticles are more toxic than anionic nanoparticles it recognizes that both anionic and cationic nanoparticles have the potential to be cytotoxic which is also consistent with our results [4, 29]. All nanoparticles used in our research disrupted cell membrane integrity to some extent.

Environment

Both literature and our research suggests that nanoparticles have a high likelihood of interacting with the environment. This is concerning as the potential commercial applications make environmental exposure inevitable. Studies have shown that nanoparticles can hinder the growth of eukaryotic organisms, such as larvae [52], as well as the growth of some plants such as cabbages and carrots [22]. Additionally, research has demonstrated that nanoparticles can even render soil immobile [22]. Furthermore, some studies suggest that nanoparticles can inhibit the wastewater treatment process. Nanoparticle inhibition can adversely affect the microbes used in many wastewater treatment techniques. Additionally, nanoparticle functionalization can interfere in the reactive treatment and disinfection process [19]. In concurrence with several other sources our research highlights the importance of conducting future research to determine if nanoparticles are cytotoxic in attempt to prevent adverse environmental effects in the future.

Conclusions and Recommendations

All nanoparticles used disrupted cell membrane integrity to some extent, indicating that chemical functionalization and surface charge are likely properties that influence nanoparticle toxicity. Cell membrane integrity was disrupted by two mechanisms, membrane fracture and nanoparticle adsorption to the membrane. Significant disruption of cell membrane integrity leads to cell membrane destabilization, thus resulting in cytotoxicity. Although all nanoparticles used disrupted cell membrane integrity to some extent, the magnitude of the frequency changes were not significant enough to conclude that cell membrane destabilization or cell membrane lyse had occurred. Therefore, it was not possible to determine if the nanoparticles used were cytotoxic, only that cell membrane integrity was disrupted.

Both anionic (bare gold and 3-mercaptopropionic acid) and cationic nanoparticles (2-aminoethanethiol) nanoparticles disrupted cell membrane integrity. However, it was difficult to differentiate the effects of surface charge on nanoparticle cell membrane interaction as cell membrane integrity was disrupted to similar extents for both anionic and cationic nanoparticles. It was expected that the anionic and cationic nanoparticle's zeta potentials would reflect their opposite surface charge, however the manufacturer's zeta potential was extremely similar for all nanoparticles. As zeta potential reflects colloidal stability and surface charge, the similarity in zeta potentials of all nanoparticles used may explain why the nanoparticles behaved similarly. It is recommended that future studies be conducted using a cationic capping agent whose zeta potential reflects its positive charge. It is also recommended that future studies include a nonionic control. Although the bare gold nanoparticles used in this experiment were expected to be nonionic, they were stabilized using citrate during manufacture to prevent aggregation causing them to behave anionically.

Overall, the QCM-D is an effective method to monitor changes in membrane mass and rigidity, which can be correlated to disruptions in cell membrane integrity. It can therefore provide insight on the mechanism of interaction between nanoparticles and cell membranes. The QCM-D is capable of detecting very small changes in frequency and dissipation, therefore some noise in frequency and dissipation overtones occurs that is not a result of nanoparticle interaction. This noise contributes to frequency changes, possibly raising the deviation. As all interactions measured were relatively small, this noise could also explain why it was difficult to determine the effects of surface charge from experimental results. For future studies, testing nanoparticles that elicit a more significant change in frequency and dissipation is recommended.

Humic acid, a laboratory model used to simulate natural organic matter found in the environment, significantly affected the interaction between the cell membrane and all nanoparticles used. It decreased interaction for 2-aminoethanethiol functionalized GNPs and the bare gold nanoparticles

and altered the mechanism of interaction for 3-mercaptopropionic acid functionalized GNPs. As both the anionic and cationic nanoparticles interacted with the humic acid, they are likely to interact with cell membranes of microorganisms in the environment. It is possible that humic acid binds to nanoparticles, thus hindering their ability to interact with cell membranes. It is recommended that future research focus on the mechanism of interaction between humic acid and nanoparticles, as it is essential to fully understanding the interaction between nanoparticles and the environment and whether these interactions are harmful to cells.

The interaction of nanoparticles and the environment is particularly concerning as the potential commercial applications for nanoparticle make environmental exposure inevitable. Nanoparticles are introduced to the environment through inadequate treatment of sewage, industrial and pharmaceutical wastewater discharge. It is essential that further research focus on the interaction between the nanoparticles and the cell membranes to determine if nanoparticles are cytotoxic to microorganisms in the environment. A more complete understanding of the cytotoxicity of nanoparticles is necessary to prevent adverse environmental effects in the future.

References

1. **Soenen SJ, Rivera-Gil P, Montenegro J-M, Parak WJ, De Smedt SC, Braeckmans K. Cellular toxicity of inorganic nanoparticles: Common aspects and guidelines for improved nanotoxicity evaluation. *nanotoday* 2011,6:446-465.**
2. **Kang S, Herzberg M, Rodrigues DF, Elimelech M. Antibacterial Effects of Carbon Nanotubes: Size Does Matter! *Langmuir* 2008:6409-6413.**
3. **Dobrovolskaia MA, McNeil SE. Immunological Properties of Engineered Nanoparticles. *Nature Publishing Group* 2007,2:469-478.**
4. **Luciani N, Gazeau F, Wilhelm C. Reactivity of the monocyte/macrophage system to superparamagnetic anionic nanoparticles. *Journal of Materials Chemistry* 2009,19:6373-6380.**
5. **Railsback JG, Singh A, Pearce RC, McNight TE, Collazo R, Sitar Z, *et al.* Weakly Charged Cationic Nanoparticles Induce DNA Bending and Strand Separation. *Advanced Materials* 2012,24:4261-4265.**
6. **Abu-Lail L, Liu Y, Atabek A, Camesano T. Quantifying the Adhesion and Interaction Forces Between *Pseudomonas aeruginosa* and Natural Organic Matter. *Enviromental Science and Technology* 2007,41:8031-8037.**
7. **Barenholz Y, D. G, B.J. L, J. G, T.E. T, D. CF. A simple method for the preparation of homogeneous phospholipid vesicles. *Biochemistry* 1977,16:2806-2810.**
8. **Richter RP, Brisson AR. Following the Formation of Supported Lipid Bilayers on Mica: A Study Combining AFM, QCM-D, and Ellipsometry. *Biophysical Journal* 2005:3422–3433.**
9. **Dimitrievski K. Influence of Lipid-Bilayer-Associated Molecules on Lipid-Vesicle Adsorption. *Langmuir* 2010,26:5706-5714.**
10. **Solon J, Streicher P, Richter R, Brochard-Wyart F, Bassereau P. Vesicles surfing on a lipid bilayer: Self-inducedhaptotactic motion. *PNAS* 2006:12382–12387.**
11. **Edwards DA, Schneck F, Zhang I, Davis AMJ, Chen H, Langer R. Spontaneous Vesicle Formation at Lipid Bilayer Membranes. *Biophysical Journal* 1996,71:1208-1214.**
12. **Keller CA, Glasmästar K, Zhdanov VP, Kasemo B. Formation of Supported Membranes from Vesicles. *Physical Review Letters* 2000:5443-5446.**
13. **Sperling RA, Rivera Gil P, Zhang F, Zanella M, Parak WJ. Biological Applications of Gold Nanoparticles. *Chemical Society Reviews* 2008:1896-1908.**
14. **Li Y, Schluesener HJ, Xu S. Gold nanoparticle-based biosensors. *Gold Bulletin* 2010:29-41.**
15. **Utekhina AY, Sergeev BG. Organic Nanoparticles. *Russian Chemical Reviews* 2011:219-233.**
16. **Zhang S, Li J, Lykotrafitis G, G. B, Suresh S. Size-Dependant Endocytosis of Nanoparticles. *Advanced Materials* 2009:419-424.**
17. **Deserno M, Bickel T. Wrapping of a spherical colloid by a fluid membrane. *Europhysics Letters* 2003:767-773.**
18. **García A, Delgadoa L, Toràa JA, Casalsb E, Gonzálezb E, Puntesb V, *et al.* Effect of cerium dioxide, titanium dioxide, silver, and gold nanoparticles on the activity of microbial communities intended in wastewater treatment. *Journal of Hazardous Materials* 2012:64-72.**
19. **Brar SK, Verma M, Surampalli R, Tyagi R. Engineered nanoparticles in wastewater and wastewater sludge – Evidence. *Science Direct* 2010:504-520.**
20. **Rezic I. Determination of engineered nanoparticles on textiles and in textile wastewaters. *Trends in Analytical Chemistry* 2011:1159-1167.**
21. **Tan WF, Koopal LK, Weng LP, wan Riemsdijk WH, Norde W. Humic acid protein complexation. *Geochimica et Cosmochimica Acta* 2008:2090-2099.**

22. **Pallem VL, Stretz HA, Wells MJM. Evaluating Aggregation of Gold Nanoparticles and Humic Substances Using Fluorescence Spectroscopy. *Environ. Sci. Technol.* 2009,43:7531-7535.**
23. **Stankus DP, Lohse SE, Hutchison JE, Nason JA. Interactions between Natural organic Matter and Gold Nanoparticles Stabilized with Different Organic Capping Agents. *Environ. Sci. Technol.* 2011,45:3238-3244.**
24. **Nason J, McDowell S, Callahan T. Effeccts of natural organic matter type and concentration on the aggregation of citrate-stabilized gold nanoparticles. *Journal of Enviromental Monitoring* 2012,14:1885-1892.**
25. **Johnson WP, Martin MJ, Gross MJ, Logan BE. Facilitation of bacterial transport through porous media by changes in solution and surface properties. *Colloids and Surfaces* 1996,107:263-271.**
26. **Dong H, Onstott TC, Deflaun MF, Fuller ME, Scheibe TD, Streger SH, *et al.* Relative dominance of Physical versus Chemical Effects on the Transport of Adhesion-Deficient Bacteria in Intact Cores from South Oyster, Virginia. *Environ. Sci. Technol.* 2002,36:891-900.**
27. **Lahlou M, Harms H, Springael D, Ortega-Calvo J-J. Influence of Soil Components on the Transport of Polycyclic Aromatic Hydrocarbon-Degrading Bacteria through Saturated Porous Media. *Environ. Sci. Technol.* 2000,34:3649-3656.**
28. **Wang S, Lawson R, Ray PC, Yu H. Toxic effects of gold nanoparticles on Salmonella typhimurium bacteria. *Toxicity and Industrial Health* 2011:547-554.**
29. **Lewinski N, Colvin V, Drezek R. Cytotoxicity of Nanoparticles. *Small* 2008:26-49.**
30. **Dunphy Guzman KA, Taylor MR, Banfield JF. Environmental Risks of Nanotechnology: National Nanotechnology Initiative Funding, 2000-2004. *Environmental Science and Technology* 2006:1401-1407.**
31. **Hardman R. A Toxicologic Review of Quantum Dots: Toxicity Depends on Physicochemical and Environmental Factors. *Environmental Health Perspect* 2006,114:165-172.**
32. **Limbach LK, Wick P, Manser P, Grass R, Bruinink A, Stark W. Exposure of Engineered Nanoparticles to Human Lung Epithelial Cells: Influence of Chemical Composition and Catalytic Activity on Oxidative Stress. *Environmental Science and Technology* 2007.**
33. **Braydich-Stolle L, Hussain S, Schlager JJ, Hofmann M-C. In Vitro Cytotoxicity of Nanoparticles in Mammalian Germline Stem Cells. *Toxicological Sciences* 2008,2:412-419.**
34. **Brayner R. The toxicological impact of nanoparticles. *nanotoday* 2008:40-55.**
35. **Wilhelm C, Gazeau F. Universal cell labelling with anionic magnetic nanoparticles. *Biomaterials* 2008,29:3161-3174.**
36. **Rutkaite R, Bendoraitiene J, Klimaviciute R, Zemaitaitis A. Cationic starch nanoparticles based on polyelectrolyte complexes. *International Journal of Biological Macromolecules* 2012,50.**
37. **Paillusson F, Dahirel V, Jardat M, Victor J-M, Barbo M. Effective interaction between charged nanoparticles and DNA. *Phys. Chem. Chem. Phys.* 2011,13:12603-12613.**
38. **Poulos AS, Constantin D, Davidson P, Imperor-Clerc M, Pansu B, Rouziere S. The interaction of charged nanoparticles at interfaces. *A Letters Journal Exploring* 2012,100.**
39. **Xiao Y, Wiesner MR. Characterization of surface hydropbicity of engineered nanoparticles. *Journal of Hazardous Materials* 2012,215-216:146-151.**
40. **Doktorovova S, Shegokar R, Martins-Lopes P, Silva AM, Lopes CM, Miller RH, *et al.* Modified Rose Bengal assay for surface hydrophobicity evaluation of cationic solid lipid nanoparticles.**
41. **Yang S, Pelton R. Nanoparticle Flotation Collectors II: The Role of Nanoparticle Hydrophobicity. *Langmuir* 2011,27:11409-11415.**
42. **Gessner A, Waicz R, Lieske A, Pauke B-R, Mader K, Muller RH. Nanoparticles with decreasing surface hydrophobicities: influence on plasma protein adsorption. *International Journal of Pharmaceutics* 2000,196:245-249.**

43. Yuce MY, Demirel AL. The effect of nanoparticles on the surface hydrophobicity of polystyrene. *The European Physical Journal B* 2008,64:493-497.
44. Childs K, Dirk S, Howell S, Simonson RJ, Wheeler D. Functionalized Nanoparticles for Sensor. In. Albuquerque: Sandia National Laboratories; 2005.
45. Schulz-Dobrick M, Sarathy V, Jansen M. Surfactant-Free Synthesis and Functionalization of Gold Nanoparticles. *Journal of the American Chemical Society* 2005:12816-12817.
46. Torres-Chavolla E, Ranasinghe RJ, Alocilja EC. Characterization and Functionalization of Biogenic. *Ieee Transactions On Nanotechnology* 2010:533-538.
47. Shenoy D, Fu W, Li J, Crasto C, Jones G, Dimarzio C, *et al.* Surface-Functionalized Gold Nanoparticles. In. Boston: Northeastern University; 2005.
48. Bain CD, Troughton EB, Tao YT, Evall J, Whitesides GM, Nuzzo RG. Formation of monolayer films by the spontaneous assembly of organic thiols from solution onto gold. *Journal of the American Chemical Society* 1989,111:321-335.
49. Malem F, Mandler D. Self-Assembled Monolayers in Electroanalytical Chemistry: Application of w-Mercapto Carboxylic Acid Monolayers for the Electrochemical Detection of Dopamine in the Presence of aHigh Concentration of Ascorbic Acid. *Analytical Chemistry* 1993,65:37-41.
50. nanoComposix. Zeta Potential Analysis of Nanoparticles. In. SAN DIEGO, CA; 2012.
51. Zhang X-D, Wu D, Shen X, Liu P-X, Yang N, Zhao B, *et al.* Size-dependent in vivo toxicity of PEG-coated gold nanoparticles. *International Journal of Nanomedicine* 2011,6:2071-2081.
52. Gorth DJ, Rand DM, Webster TJ. Silver nanoparticle toxicity in Drosophila: size does matter. 2011,6:343-350.

Appendices

Appendix A.1: 12 nm Bare AuNP Control PC Bilayer QCM-D Plots

1/11/2013 Chamber 1

12nm Bare Au NPs Control PC Bilayer Tris NaCl

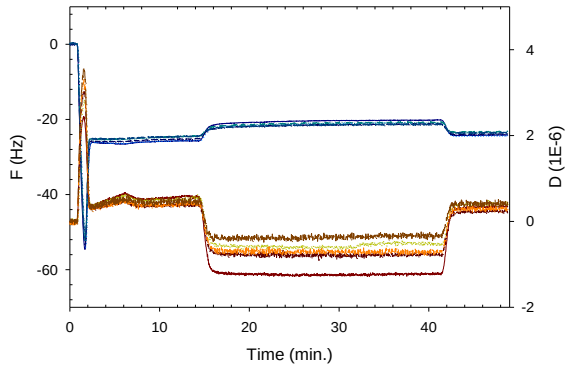

1/11/2013 Chamber 2

12nm Bare Au NPs Control PC Bilayer Tris NaCl

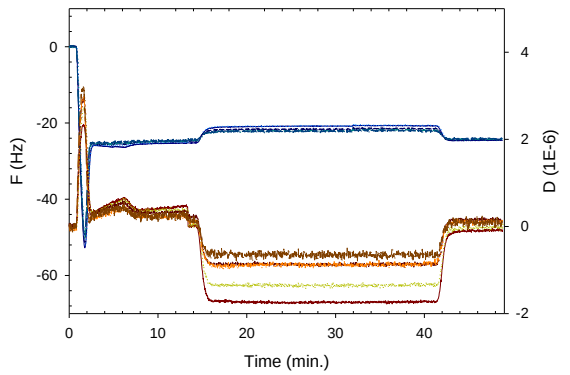

1/11/2013 Chamber 3

12nm Bare Au NPs Control PC Bilayer Tris NaCl

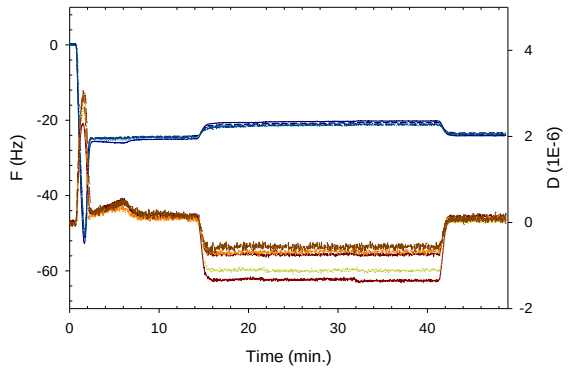

1/13/2013 Chamber 1

12nm Bare Au NPs Control PC Bilayer Tris NaCl

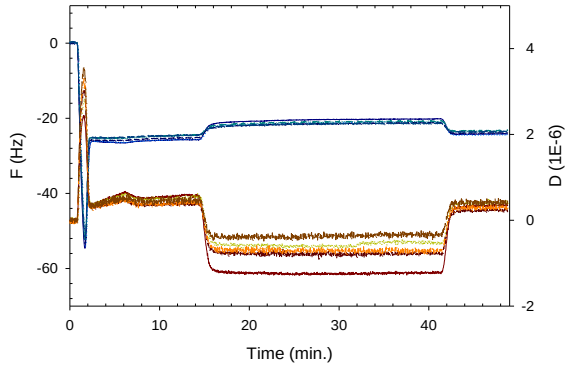

11/13/2013 Chamber 2

12nm Bare Au NPs Control PC Bilayer Tris NaCl

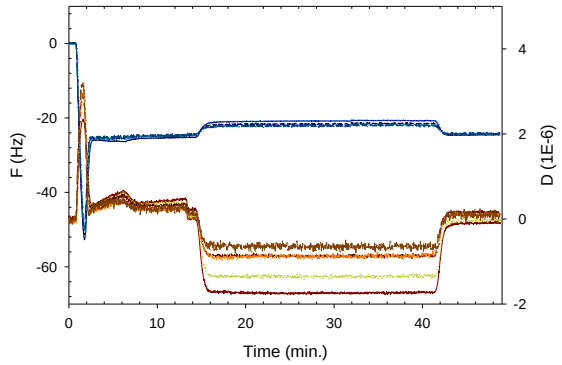

11/13/2013 Chamber 3

12nm Bare Au NPs Control PC Bilayer Tris NaCl

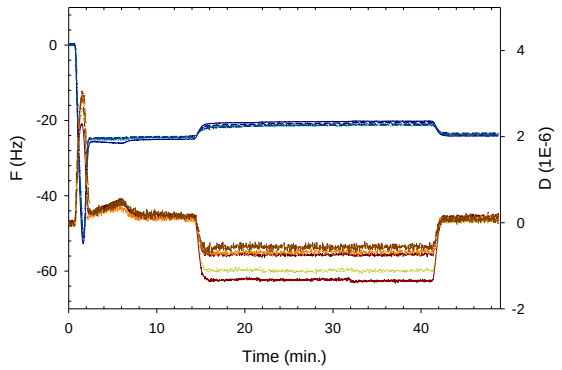

Appendix A.2: 12 nm Bare AuNP Control Frequency Data

	Overtone 3	Overtone 5	Overtone 7	Overtone 9	Overtone 11
Average Δf	0.429883	0.452017	0.450917	0.377117	0.33655
Error Bar Value	0.158404	0.211391	0.124769	0.118149	0.175222

Appendix B.1: 3-Mercaptopropionic Acid PC Bilayer QCM-D Plots

1/18/2013 Chamber 2

12nm Mercaptopropionic Acid Au NPs PC Bilayer Tris NaCl

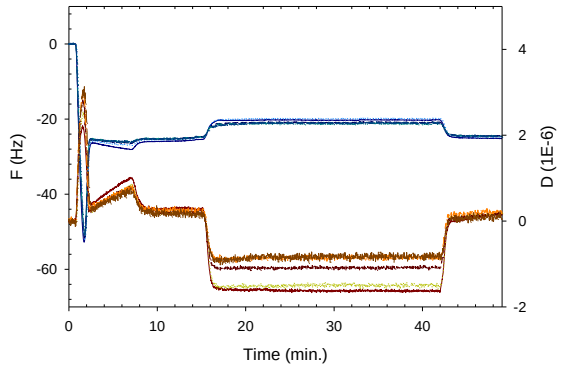

1/18/2013 Chamber 3

12nm Mercaptopropionic Acid AU NPs PC Bilayer Tris NaCl

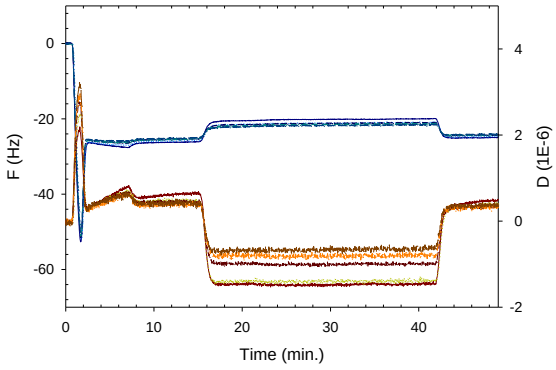

1/20/2013 Chamber 2

12nm Mercaptopropionic Acid Au NPs Control PC Bilayer Tris NaCl

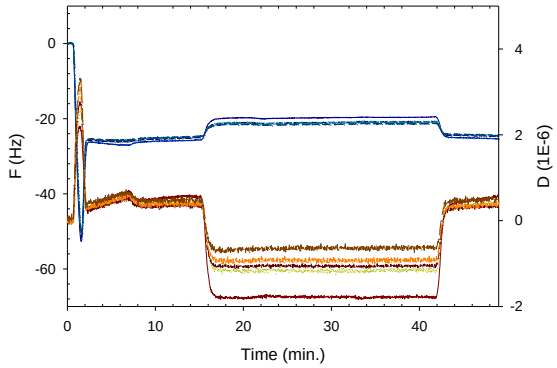

1/20/2013 Chamber 3

12nm Mercaptopropionic Acid AU NPs PC Bilayer Tris NaCl

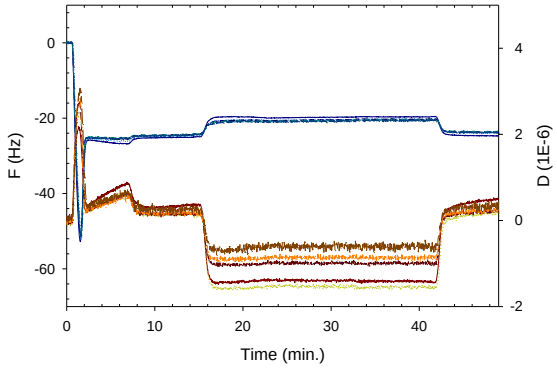

1/25/2013 Chamber 3

12nm Mercaptopropionic Acid AU NPs PC Bilayer Tris NaCl

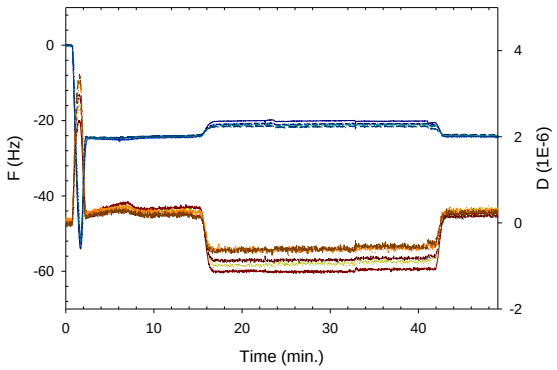

2/7/2013 Chamber 1

12nm Mercaptopropionic Acid Au NPs PC Bilayer Tris NaCl

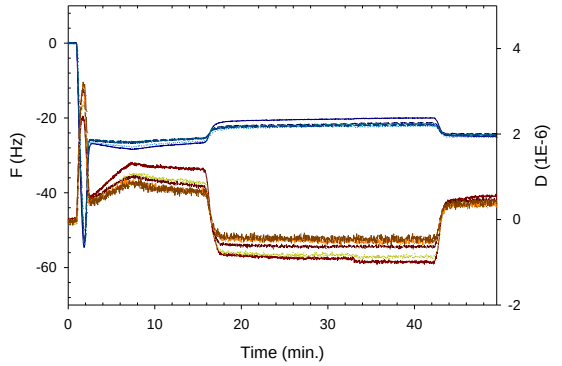

2/7/2013 Chamber 2

12nm Mercaptopropionic Acid Au NPs PC Bilayer Tris NaCl

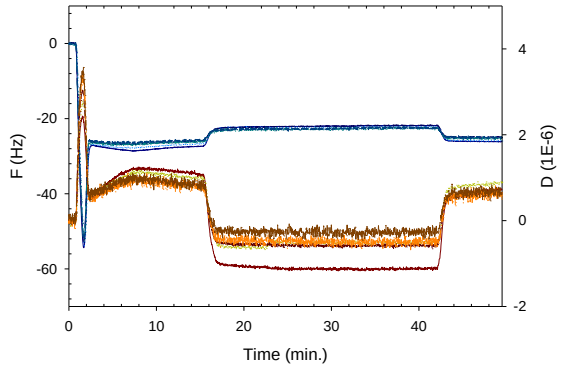

2/7/2013 Chamber 3

12nm Mercaptopropionic Acid AU NPs PC Bilayer Tris NaCl

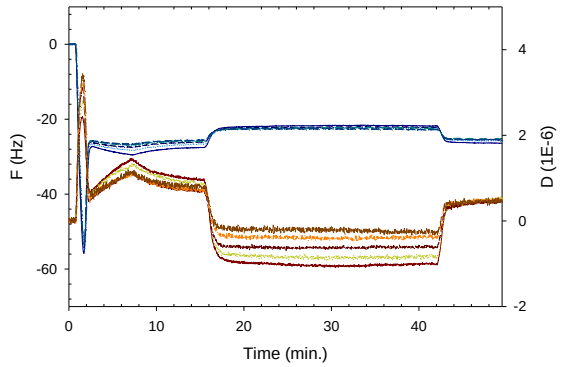

Appendix B.2: 3-Mercaptopropionic Acid Frequency Data

	Overtone 3	Overtone 5	Overtone 7	Overtone 9	Overtone 11
Average Δf	0.201687	0.161333	0.233029	0.277575	0.100275
Error Bar Value	0.227771	0.247688	0.241535	0.312091	0.33148

Appendix C.1: 2-Aminoethanethiol PC Bilayer QCM-D Plots

1/27/2013 Chamber 1

12nm 2-Aminoethanethiol Au NPs PC Bilayer Tris NaCl

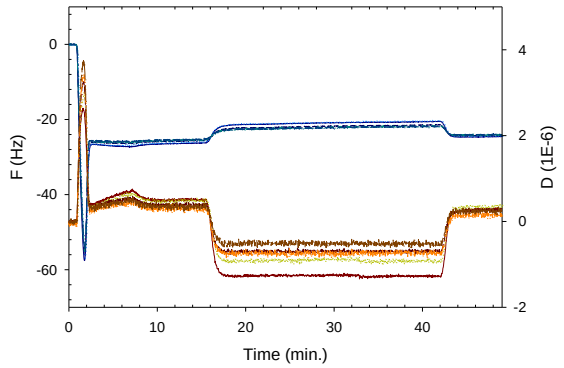

1/27/2013 Chamber 2

12nm 2-Aminoethanethiol Au NPs PC Bilayer Tris NaCl

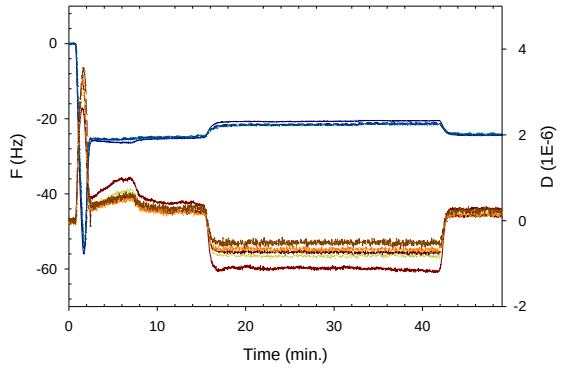

1/27/2013 Chamber 3

12nm 2-Aminoethanethiol AU NPs PC Bilayer Tris NaCl

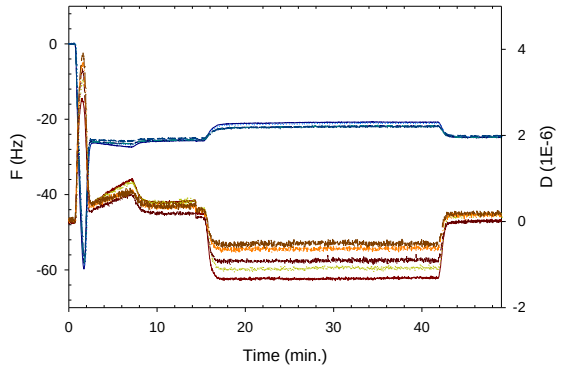

2/1/2013 Chamber 1

12nm 2-Aminoethanethiol Au NPs PC Bilayer Tris NaCl

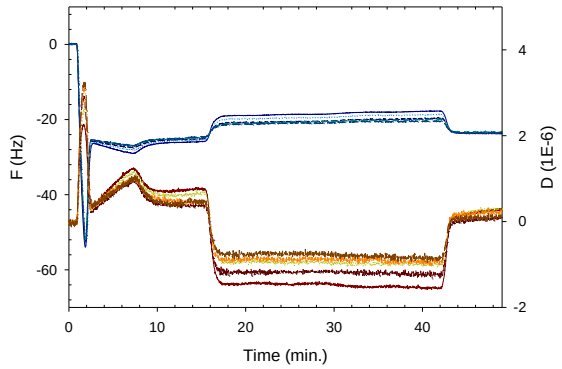

2/1/2013 Chamber 2

12nm 2-Aminoethanethiol Au NPs PC Bilayer Tris NaCl

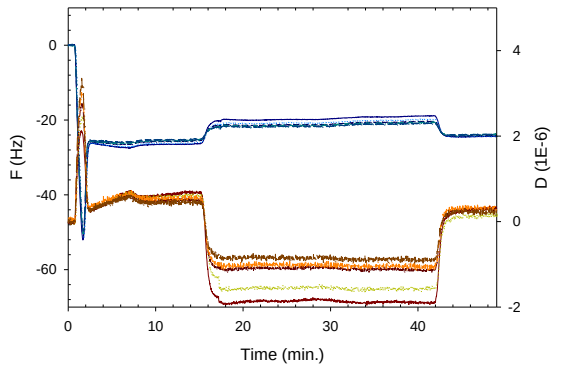

2/3/2013 Chamber 1

12nm 2-Aminoethanethiol Au NPs PC Bilayer Tris NaCl

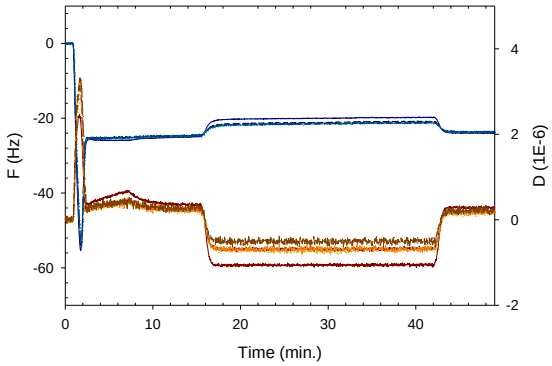

2/3/2013 Chamber 2

12nm 2-Aminoethanethiol Au NPs PC Bilayer Tris NaCl

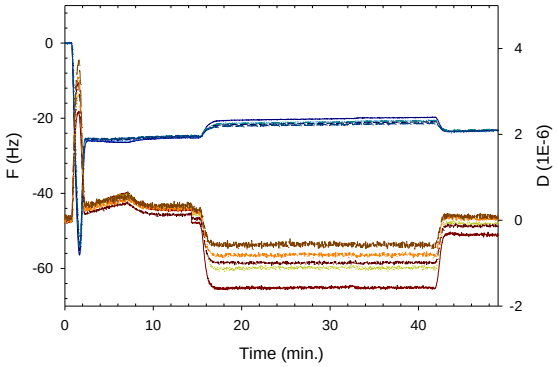

2/3/2013 Chamber 3

12nm 2-Aminoethanethiol AU NPs PC Bilayer Tris NaCl

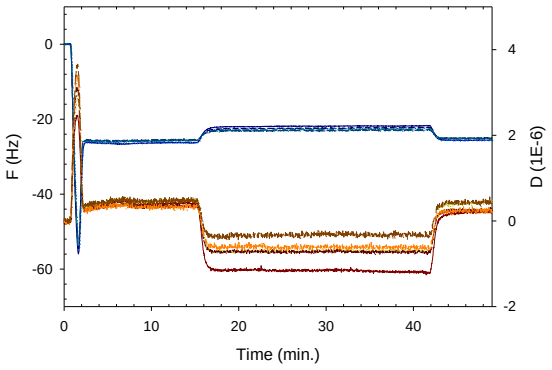

Appendix C.2: 2-Aminoethanethiol Frequency Data

	Overtone 3	Overtone 5	Overtone 7	Overtone 9	Overtone 11
Average Δf	0.562188	0.564275	0.626075	0.594738	0.457263
Error Bar Value	0.403758	0.374385	0.329625	0.341317	0.289788

Appendix D.1: 12 nm Bare Au NPs in Humic Acid Control QCM-D Plots

1/29/2013 Chamber 1

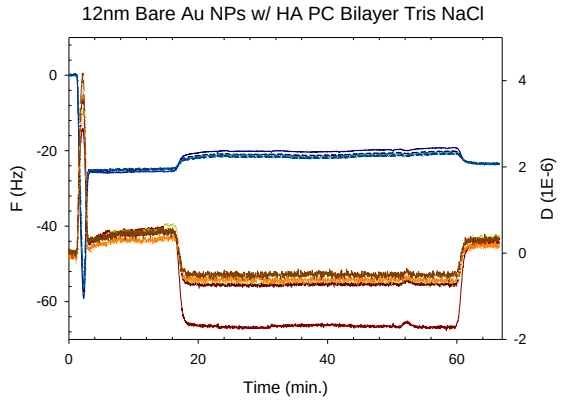

1/29/2013 Chamber 2

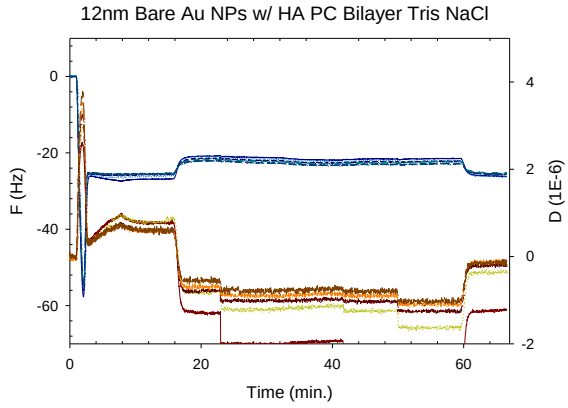

1/29/2013 Chamber 3

12nm Bare Au NPs w/ HA PC Bilayer Tris NaCl

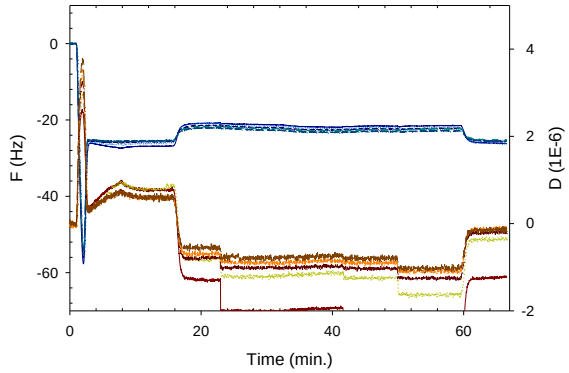

2/1/2013 Chamber 2

12nm Bare Au NPs HA Control PC Bilayer Tris NaCl

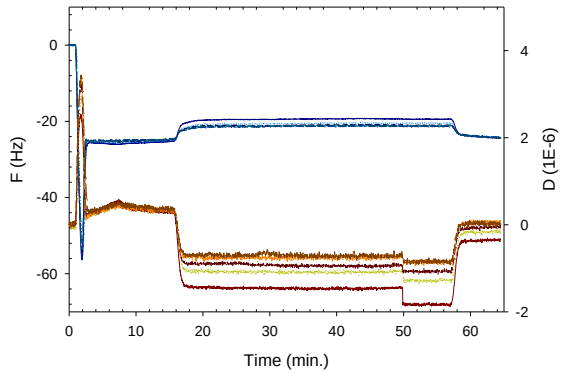

2/1/2013 Chamber 3

12nm Bare Au NPs HA Control PC Bilayer Tris NaCl

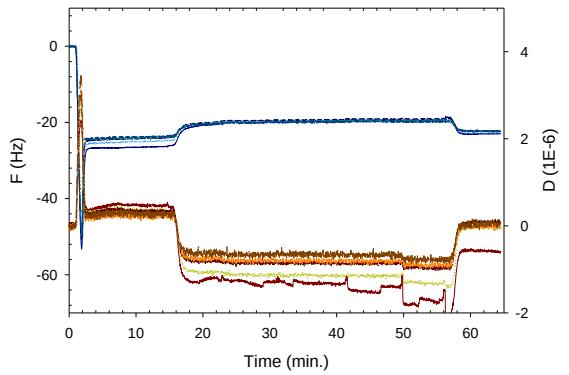

Appendix D.2: 12 nm Bare Au NPs in Humic Acid Control Frequency Data

	Overtone 3	Overtone 5	Overtone 7	Overtone 9	Overtone 11
Average Δf	0.066380	0.108900	0.043540	-0.012580	-0.030440
Error Bar Value	0.342864	0.342052	0.329036	0.230519	0.266244

Appendix E.1: 3-Mercaptopropionic Acid With Humic Acid Polymer PC Bilayer QCM-D Plots

2/11/2013 Chamber 1

12nm Mercaptopropionic Acid AU NPs in Humic Acid + PC Bilayer Tris NaCl

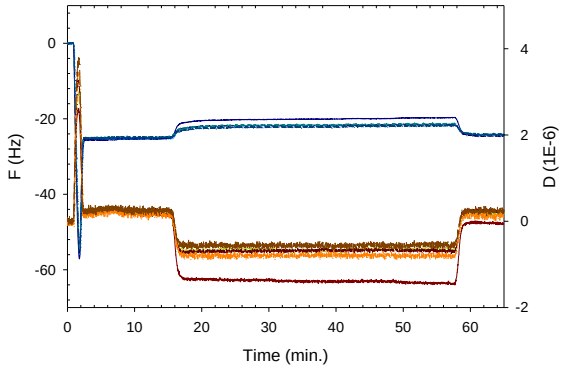

2/11/2013 Chamber 3

12nm Mercaptopropionic Acid AU NPs in Humic Acid + PC Bilayer Tris NaCl

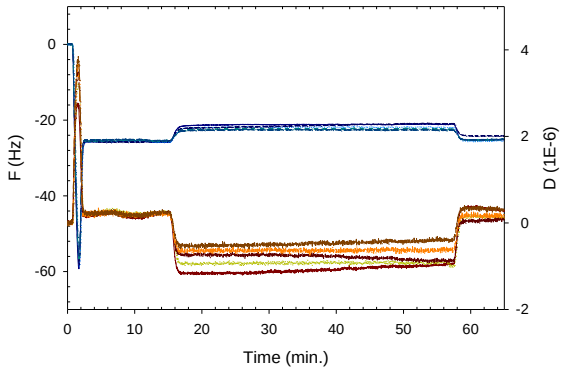

2/22/2013 Chamber 1

12nm Mercaptopropionic Acid AU NPs in Humic Acid + PC Bilayer Tris NaCl

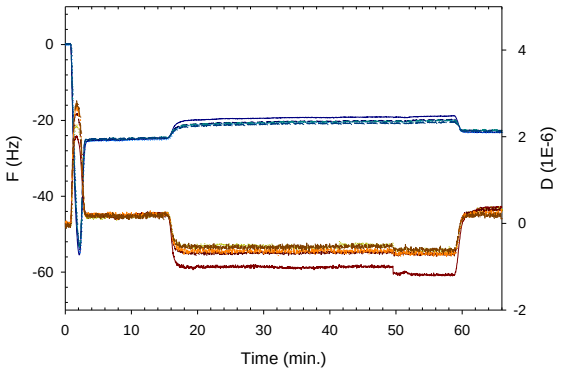

2/22/2013 Chamber 2

12nm Mercaptopropionic Acid AU NPs in Humic Acid + PC Bilayer Tris NaCl

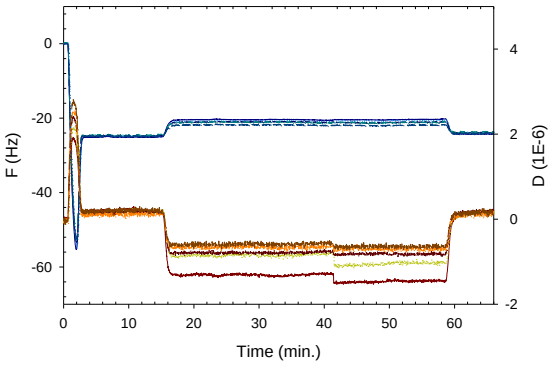

2/22/2013 Chamber 4

12nm Mercaptopropionic Acid AU NPs in Humic Acid + PC Bilayer Tris NaCl

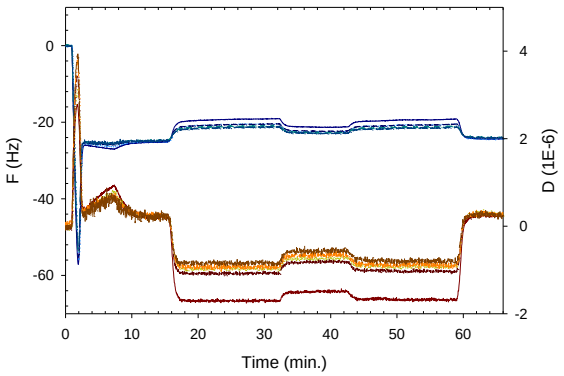

3/1/2013 Chamber 1

12nm Mercaptopropionic Acid AU NPs in Humic Acid + PC Bilayer Tris NaCl

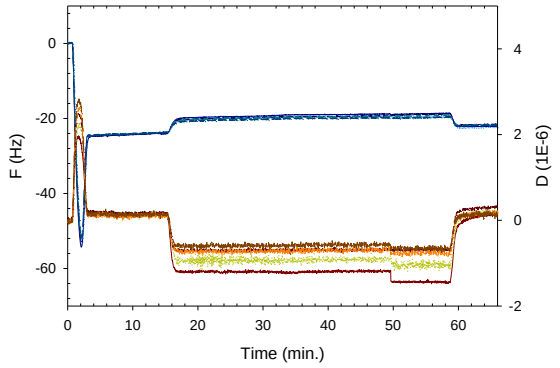

3/1/2013 Chamber 2

12nm Mercaptopropionic Acid AU NPs in Humic Acid + PC Bilayer Tris NaCl

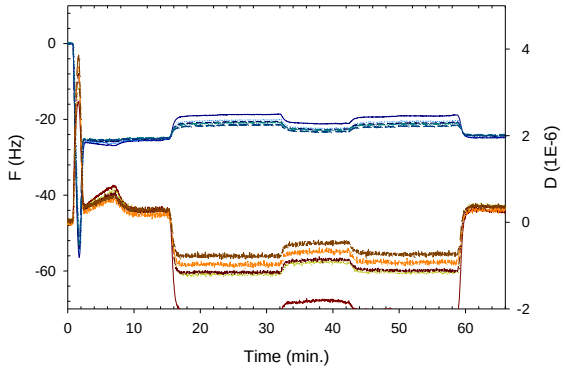

3/1/2013 Chamber 3

12nm Mercaptopropionic Acid AU NPs in Humic Acid + PC Bilayer Tris NaCl

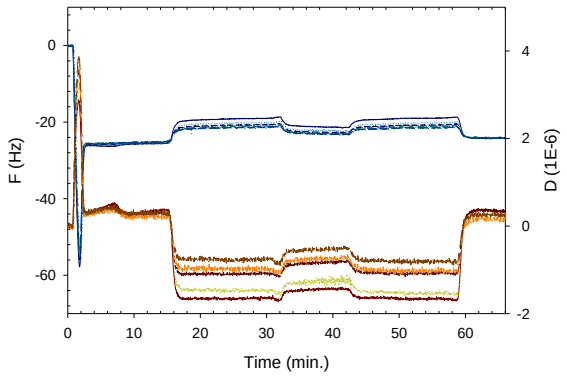

3/1/2013 Chamber 4

.2nm Mercaptopropionic Acid AU NPs in Humic Acid + PC Bilayer Tris NaC

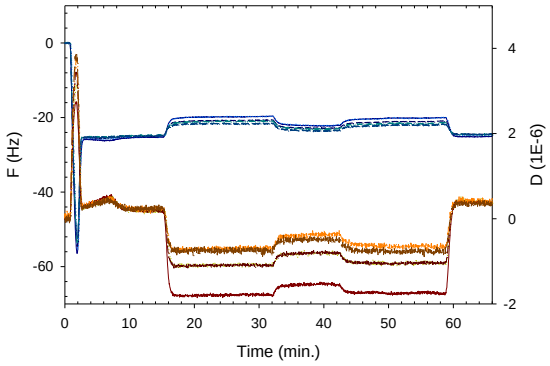

3/2/2103 Chamber 1

12nm Mercaptopropionic Acid AU NPs in Humic Acid + PC Bilayer Tris NaCl

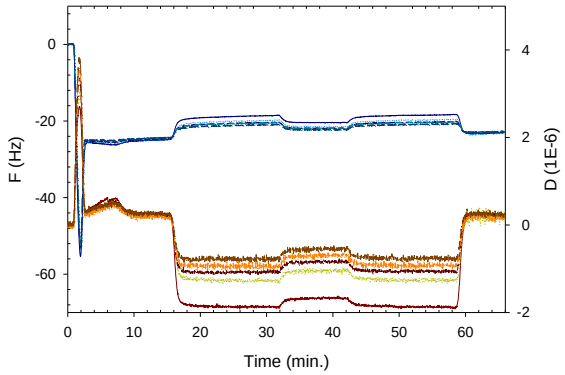

3/2/2013 Chamber 2

12nm Mercaptopropionic Acid AU NPs in Humic Acid + PC Bilayer Tris NaCl

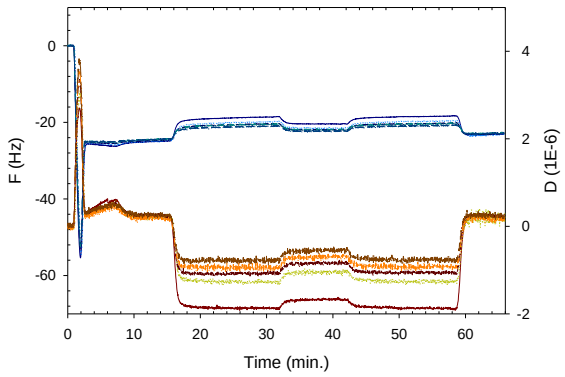

3/2/2013 Chamber 4

.2nm Mercaptopropionic Acid AU NPs in Humic Acid + PC Bilayer Tris NaC

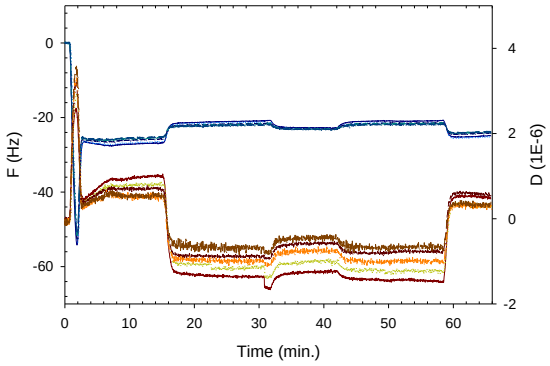

3/12/2013 Chamber 1

12nm Mercaptopropionic Acid AU NPs in Humic Acid + PC Bilayer Tris NaCl

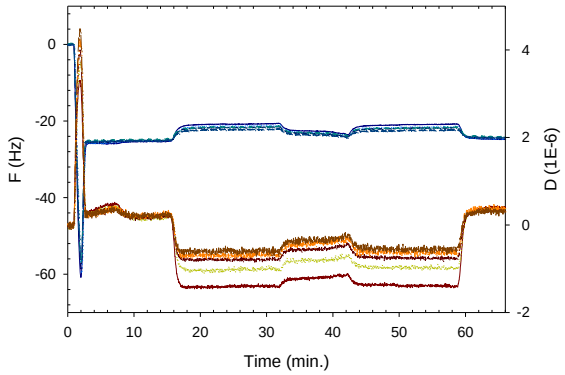

3/12/2013 Chamber 4

.2nm Mercaptopropionic Acid AU NPs in Humic Acid + PC Bilayer Tris NaC

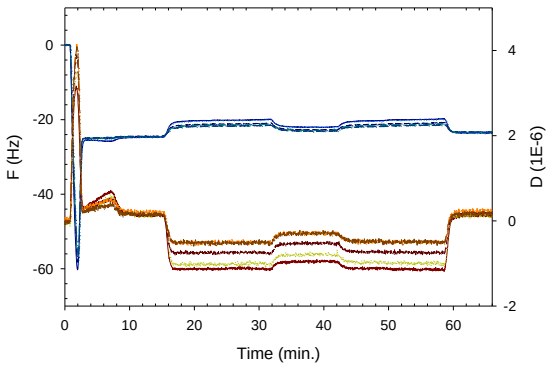

Appendix E.2: 3-Mercaptopropionic Acid With Humic Acid Polymer Frequency Data

	Overtone 3	Overtone 5	Overtone 7	Overtone 9	Overtone 11
Average Δf	-0.087692	-0.118071	-0.113839	-0.171071	-0.168038
Error Bar Value	0.327911	0.382155	0.365418	0.367159	0.316332

Appendix F.1: 2-Aminoethanethiol With Humic Acid Polymer PC Bilayer QCM-D Plots

2/24/2013 Chamber 1

12 nm Aminoethanethiol Au NPs in Humic Acid + PC Bilayer

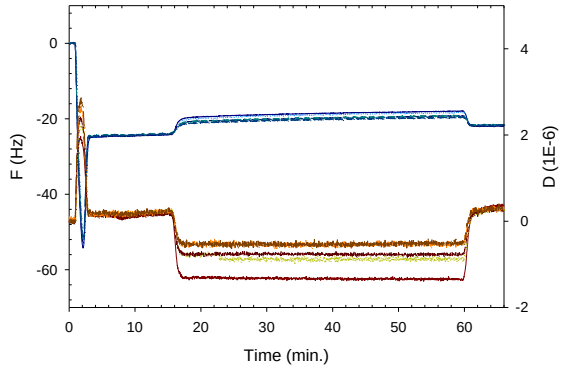

2/24/2013 Chamber 2

12 nm Aminoethanethiol Au NPs in Humic Acid + PC Bilayer

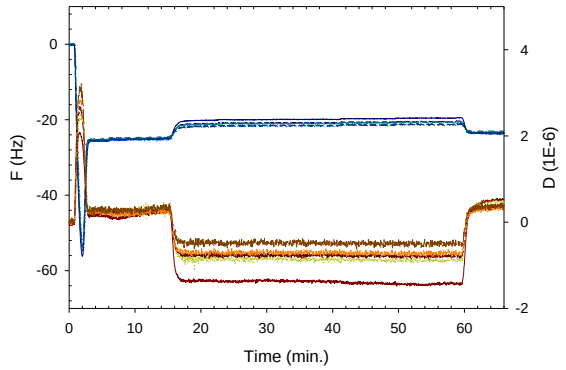

2/24/2013 Chamber 3

12 nm Aminoethanethiol Au NPs in Humic Acid + PC Bilayer

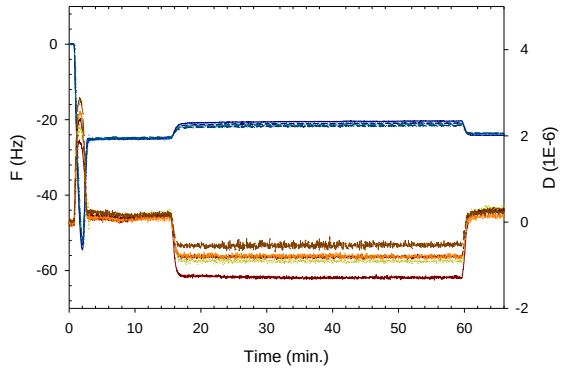

2/24/2013 Chamber 4

12 nm Aminoethanethiol Au NPs in Humic Acid + PC Bilayer

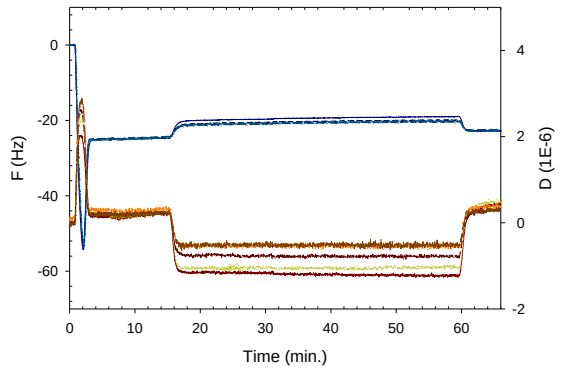

1/25/2013 Chamber 1

12 nm Aminoethanethiol Au NPs in Humic Acid + PC Bilayer

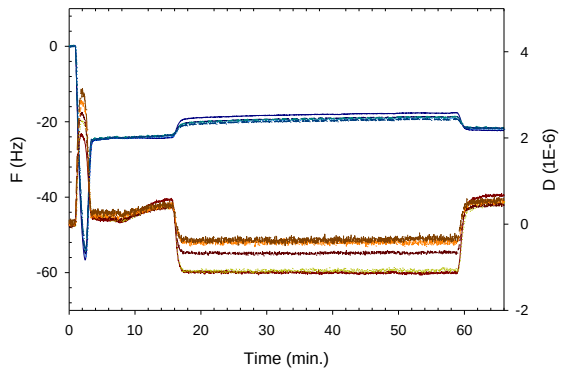

1/25/2013 Chamber 2

12 nm Aminoethanethiol Au NPs in Humic Acid + PC Bilayer

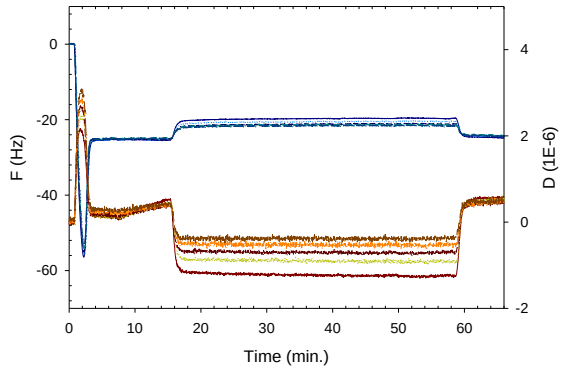

2/25/2013 Chamber 3

12 nm Aminoethanethiol Au NPs in Humic Acid + PC Bilayer

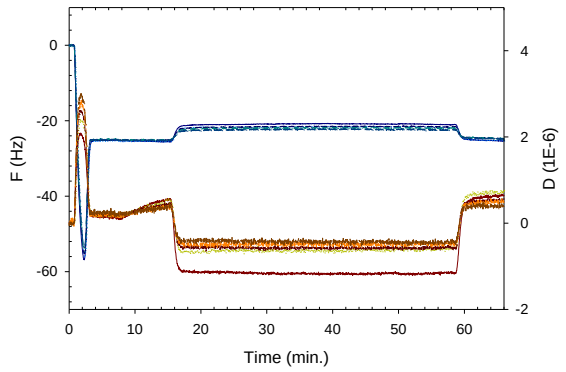

2/25/2013 Chamber 4

12 nm Aminoethanethiol Au NPs in Humic Acid + PC Bilayer

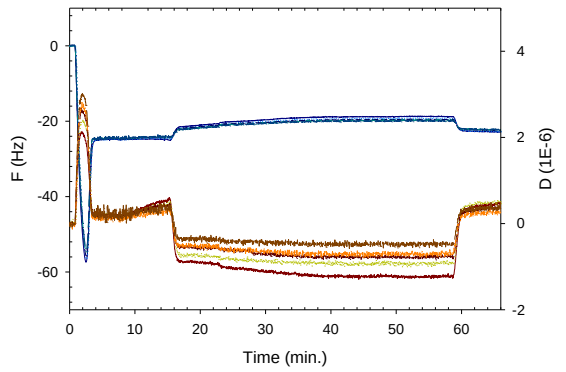

Appendix F.2: 2-Aminoethanethiol With Humic Acid Polymer Frequency Data

	Overtone 3	Overtone 5	Overtone 7	Overtone 9	Overtone 11
Average Δf	0.359000	0.352700	0.379725	0.338175	0.303325
Error Bar Value	0.306214	0.306937	0.291294	0.294317	0.223238

Appendix G.1:5.7 nm Ag NPs

9/6/2012 Chamber 1

Hydrophobic 5.7nm Ag NP 4:1 PC: LGP+ PG in HEPES+ CaCl2

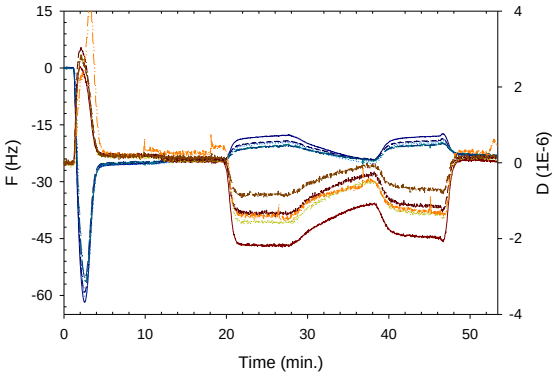

9/6/2012 Chamber 2

Hydrophobic 5.7nm Ag NP 4:1 PC: LGP+ PG in HEPES+ CaCl2

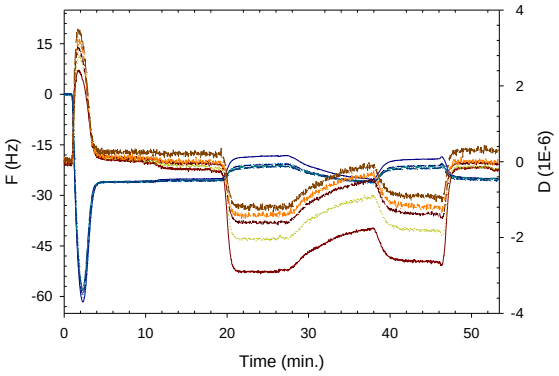

9/6/2012 Chamber 3

Hydrophobic 5.7nm Ag NP 4:1 PC: LGP+ PG in HEPES+ CaCl2

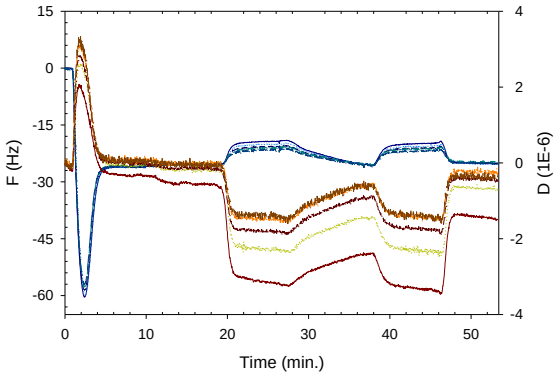

9/6/2012 Chamber 4

Hydrophobic 5.7nm Ag NP 4:1 PC: LGP+ PG in HEPES+ CaCl2

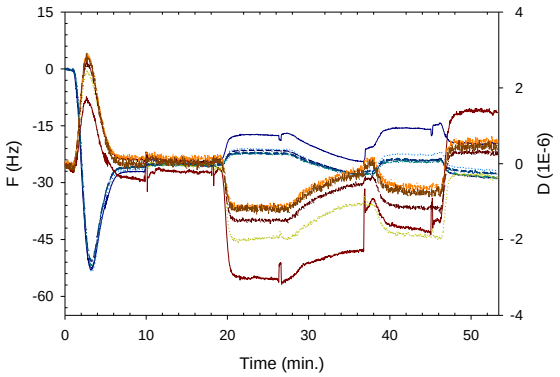

Appendix G.2:5.7 nm Ag NPs Frequency Data

	Overtone 3	Overtone 5	Overtone 7	Overtone 9	Overtone 11
Average Δf	-5.539025	-5.466900	-5.170300	-4.586925	-4.149925
Error Bar Value	1.846176	0.269215	0.642553	0.664069	0.675133

Appendix H.1: 5 nm Bare Au NPs Control PC Bilayer QCM-D Plots

11/7/2012 Chamber 2:

5nm Bare Au NPs Control PC Bilayer Tris NaCl

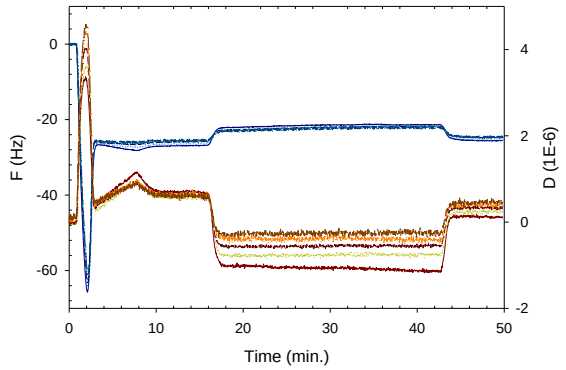

11/7/2012 Chamber 3:

5nm Bare Au NPs Control PC Bilayer Tris NaCl

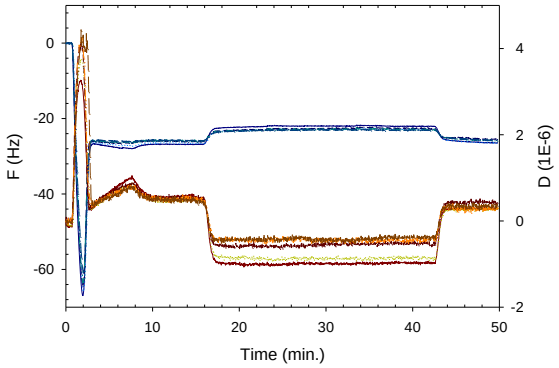

11/12/2012 Chamber 1

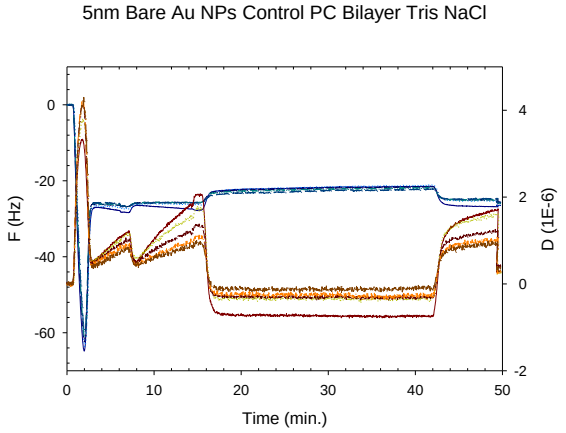

11/12/2012 Chamber 3

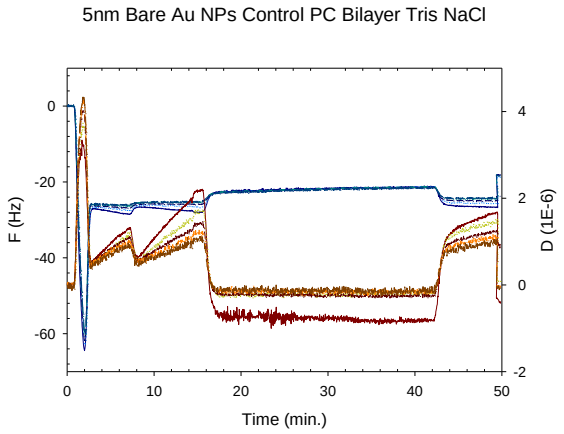

Appendix H.2: 5 nm Frequency Data

	Overtone 3	Overtone 5	Overtone 7	Overtone 9	Overtone 11
Average Δf	0.550100	0.714100	0.797975	0.688450	0.719525
Error Bar Value	0.325901	0.353241	0.255983	0.412299	0.417204

Appendix I.1: 10 nm Bare Au NPs Control PC Bilayer QCM-D Plots

11/28/2012 Chamber 1

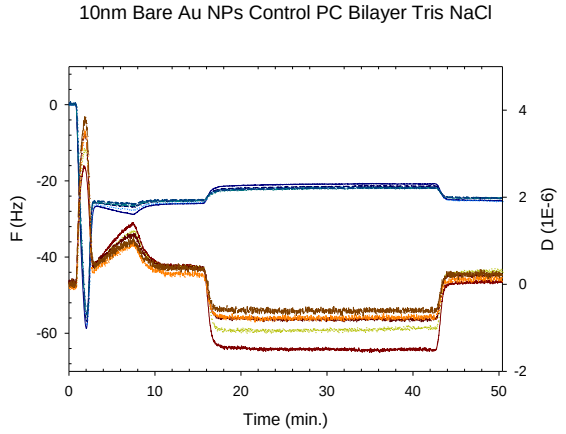

12/3/2012 Chamber 1

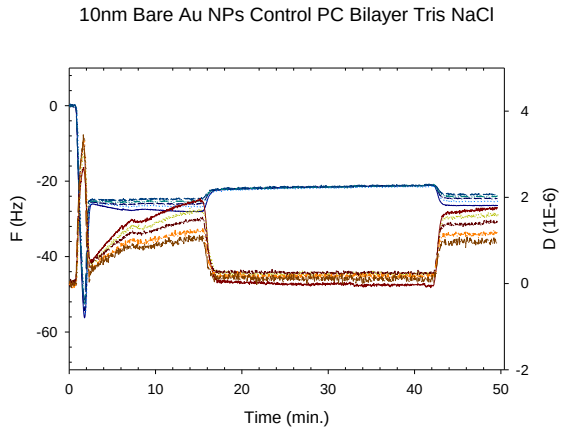

12/3/2012 Chamber 2

10nm Bare Au NPs Control PC Bilayer Tris NaCl

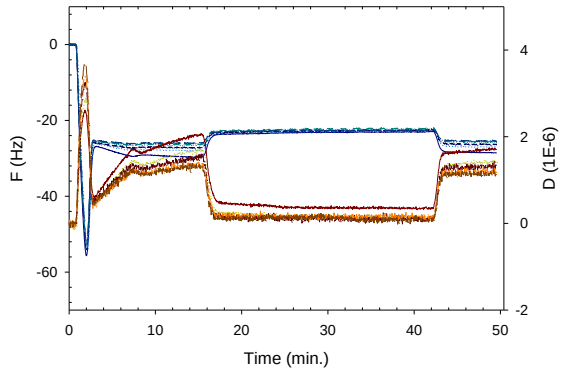

12/3/2012 Chamber 3

10nm Bare Au NPs Control PC Bilayer Tris NaCl

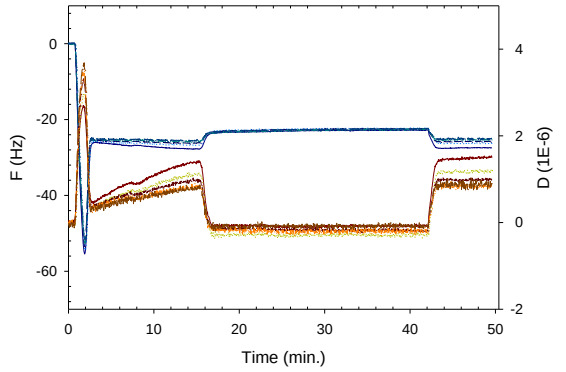

Appendix I.2: 10 nm Frequency Data

	Overtone 3	Overtone 5	Overtone 7	Overtone 9	Overtone 11
Average Δf	0.467325	0.460000	0.428200	0.478900	0.219625
Error Bar Value	0.185621	0.225300	0.129979	0.119285	0.164554

Appendix J: Plots Analyzing Frequency and Dissipation at 7th Overtone

12 nm Bare GNP (1/11/2012 Chamber 1)

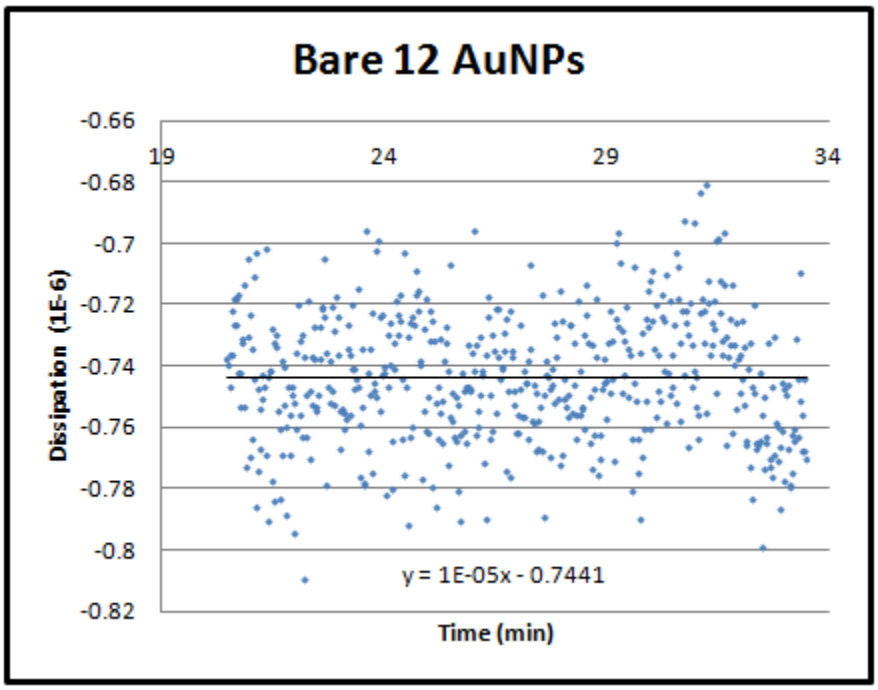

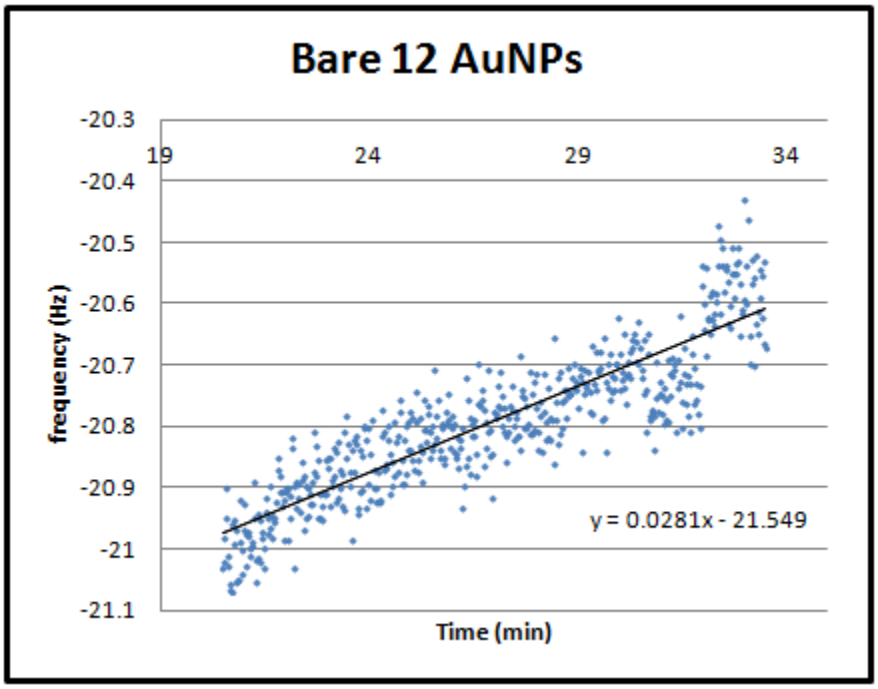

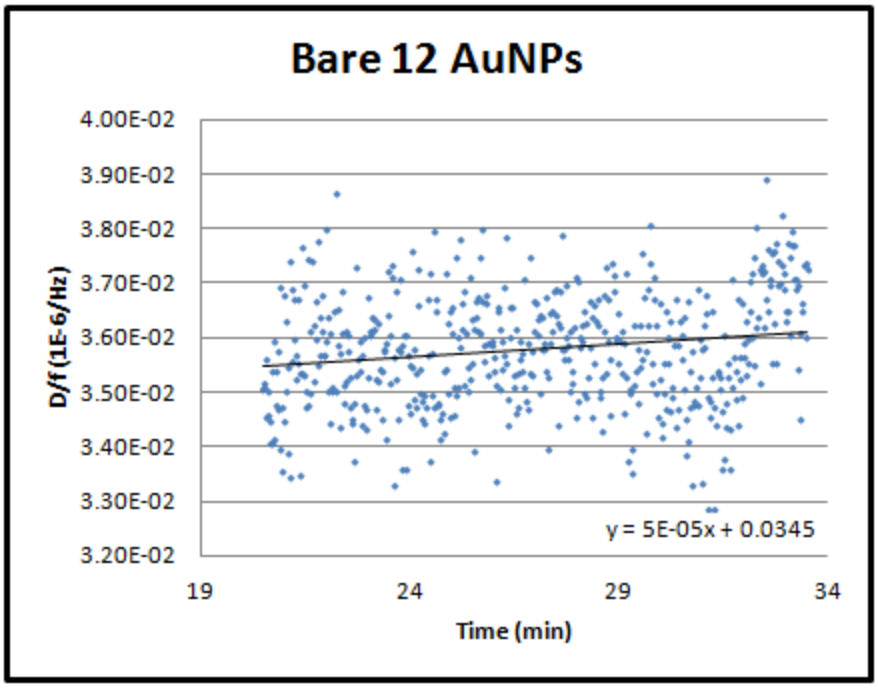
Bare 12 AuNPs
4.00E-02
3.90E-02
3.80E-02
3.70E-02
3.60E-02
3.50E-02
3.40E-02
3.30E-02
3.20E-02
D/f (1E-6/Hz)
y = 5E-05x + 0.0345
19
24
29
34
Time (min)

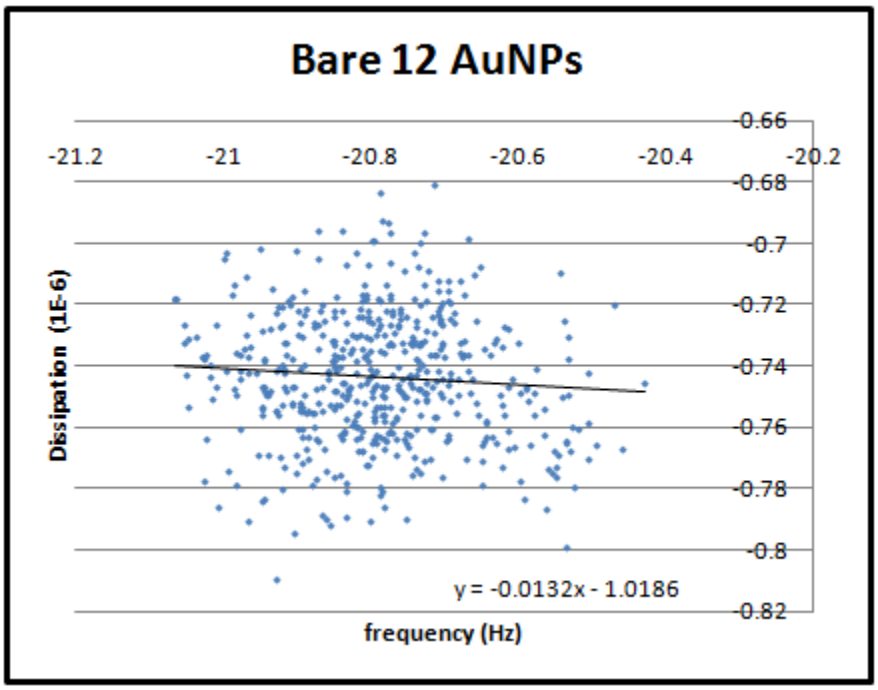
Bare 12 AuNPs
-21.2
-21
-20.8
-20.6
-20.4
-20.2
-0.66
-0.68
-0.7
-0.72
-0.74
-0.76
-0.78
-0.8
-0.82
Dissipation (1E-6)
y = -0.0132x - 1.0186
frequency (Hz)

3-Mercaptopropionic Acid (1/20/2013 Chamber 3)

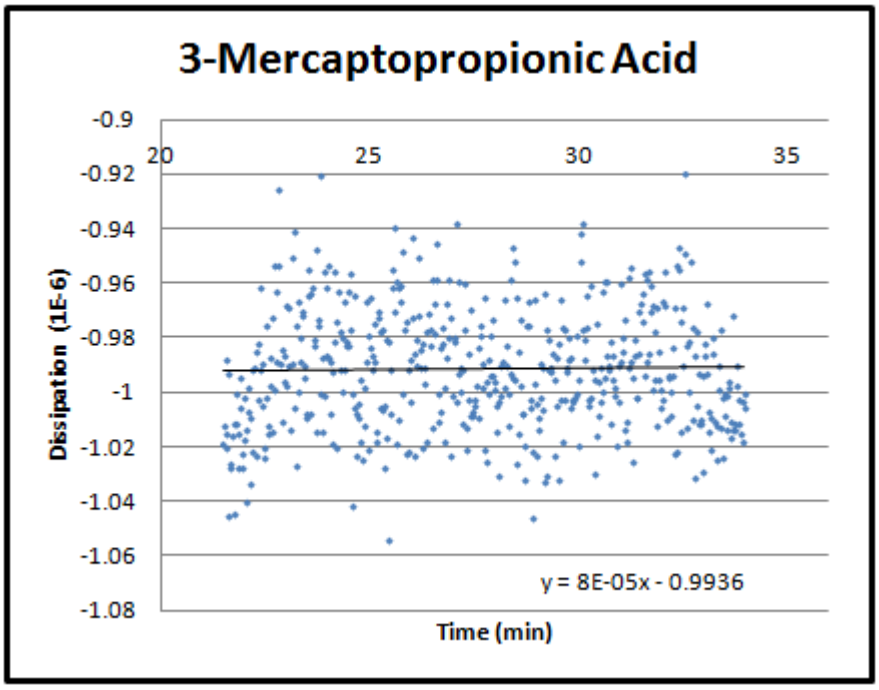

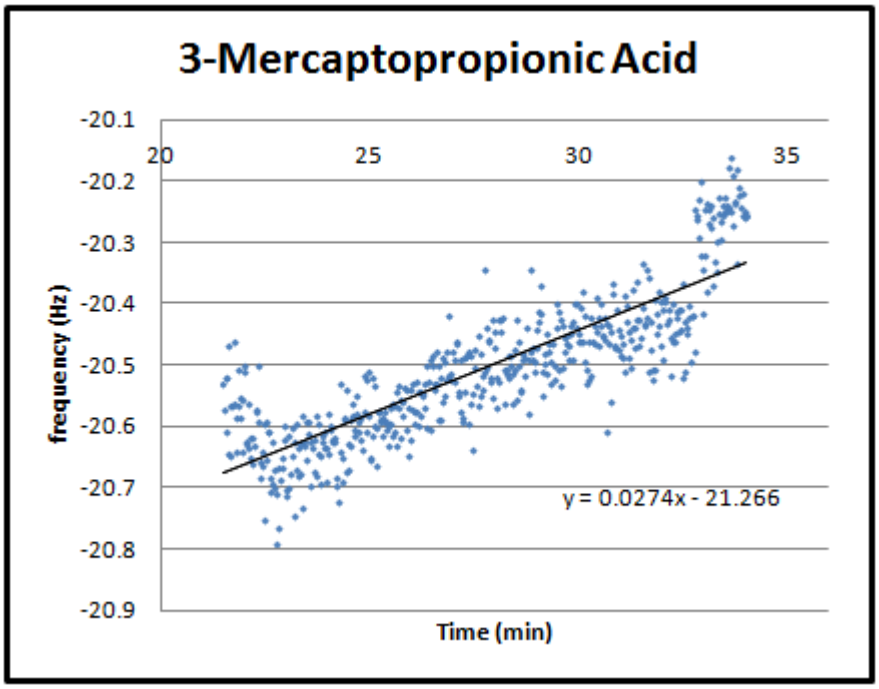

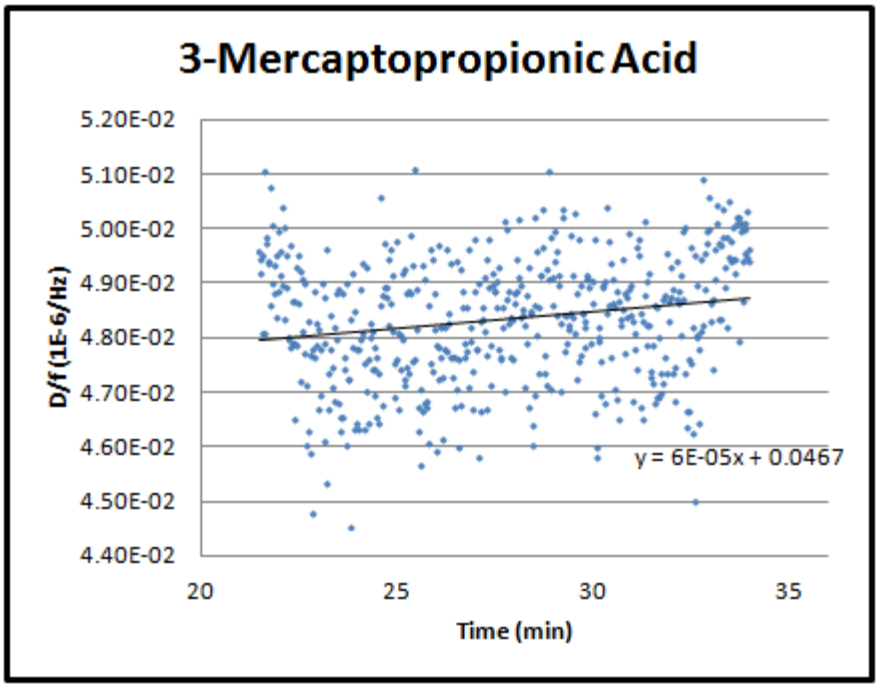
3-Mercaptopropionic Acid
5.20E-02
5.10E-02
5.00E-02
4.90E-02
4.80E-02
4.70E-02
4.60E-02
4.50E-02
4.40E-02
D/f (1E-6/Hz)
y = 6E-05x + 0.0467
20
25
30
35
Time (min)

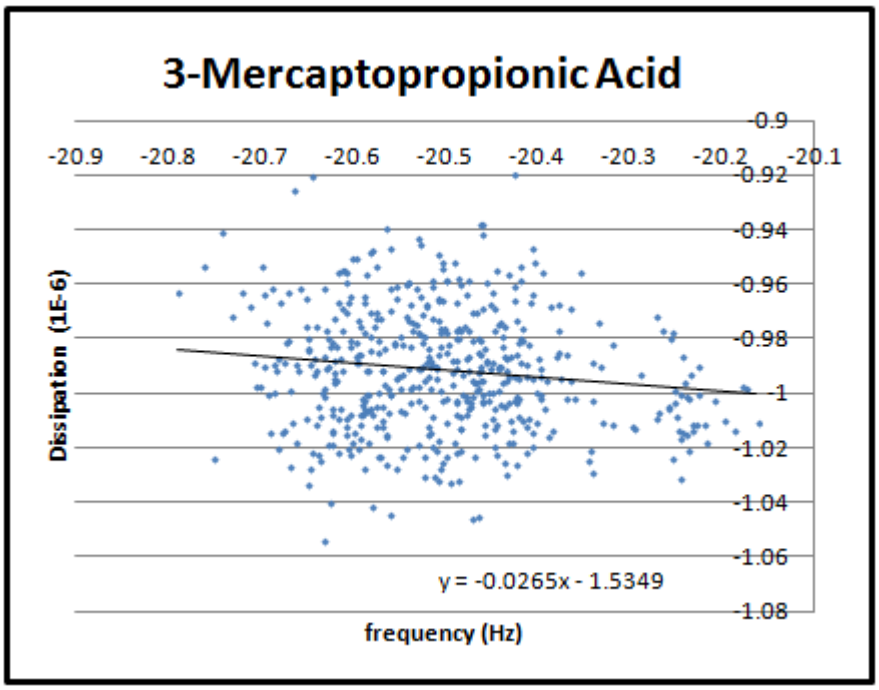
3-Mercaptopropionic Acid
-20.9
-20.8
-20.7
-20.6
-20.5
-20.4
-20.3
-20.2
-20.1
-0.9
-0.92
-0.94
-0.96
-0.98
-1
-1.02
-1.04
-1.06
-1.08
Dissipation (1E-6)
y = -0.0265x - 1.5349
frequency (Hz)

2 Aminoethanethiol (2/3/2013 Chamber 3)

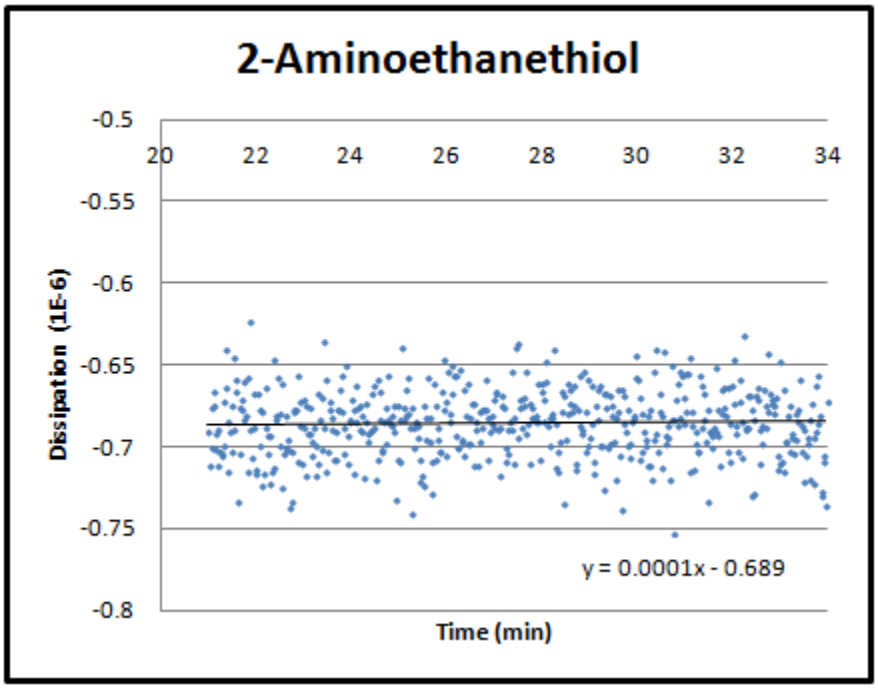

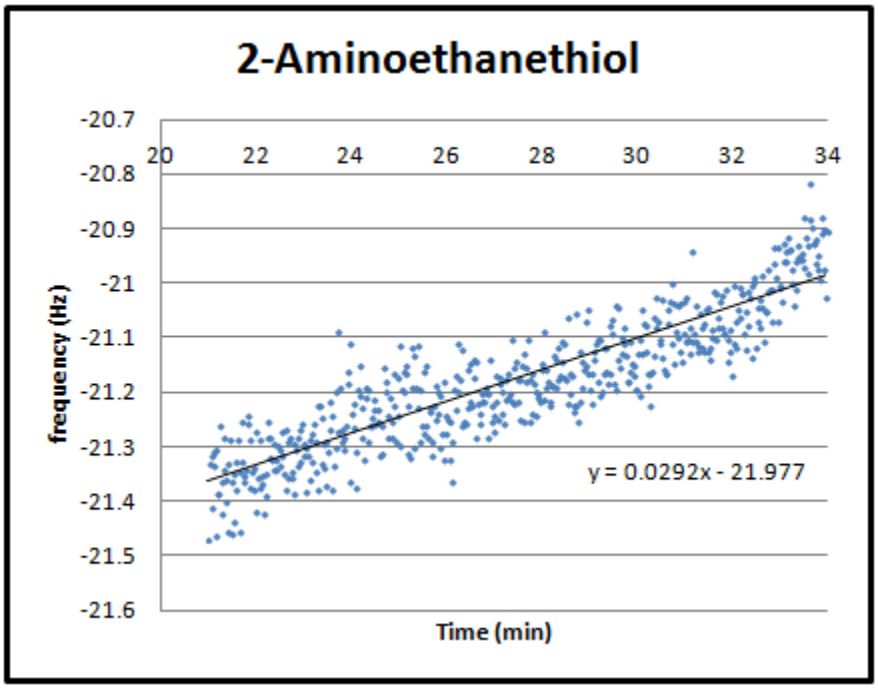

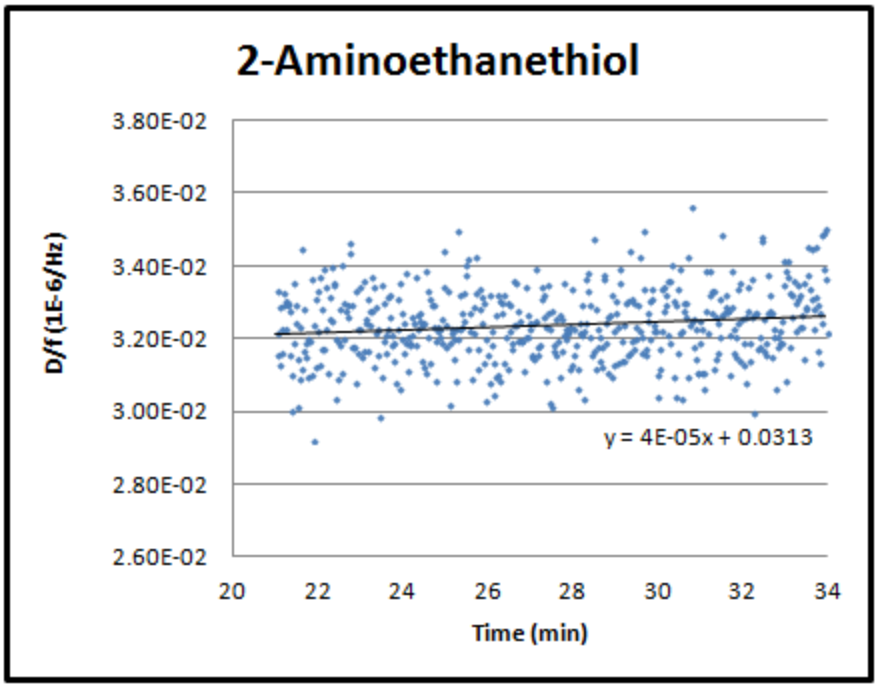
2-Aminoethanethiol
3.80E-02
3.60E-02
3.40E-02
3.20E-02
3.00E-02
2.80E-02
2.60E-02
D/f (1E-6/Hz)
y = 4E-05x + 0.0313
20
22
24
26
28
30
32
34
Time (min)

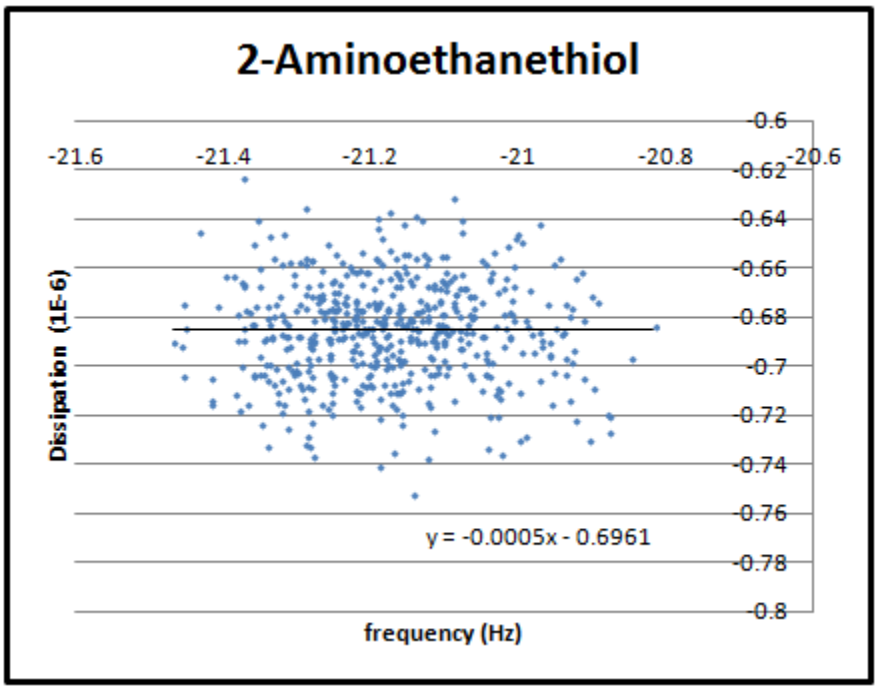
2-Aminoethanethiol
-21.6
-21.4
-21.2
-21
-20.8
-20.6
-0.6
-0.62
-0.64
-0.66
-0.68
-0.7
-0.72
-0.74
-0.76
-0.78
-0.8
Dissipation (1E-6)
y = -0.0005x - 0.6961
frequency (Hz)

12 nm Bare AuNPs with Humic Acid (1/29/2013 Chamber 1)

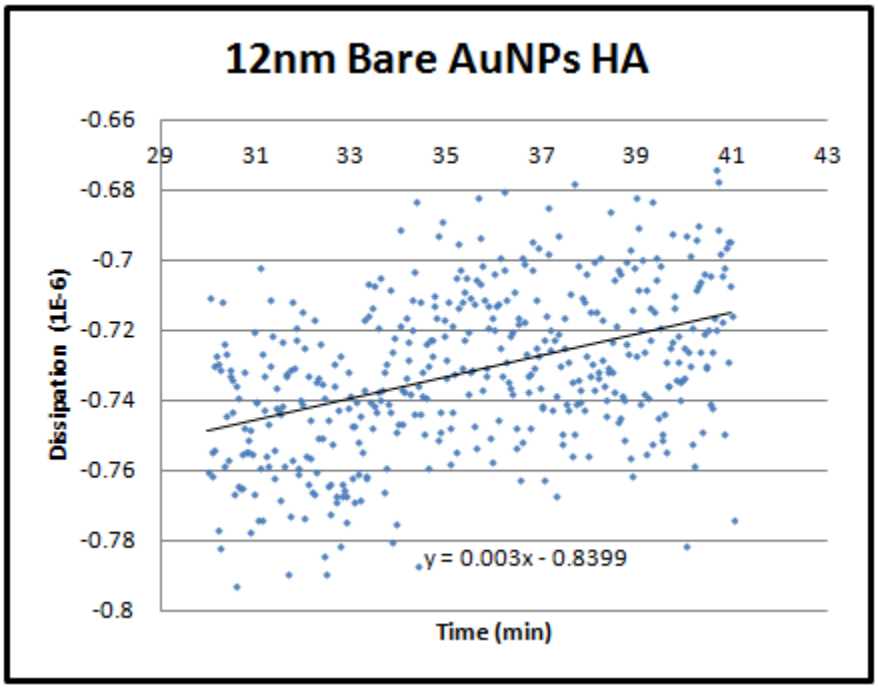

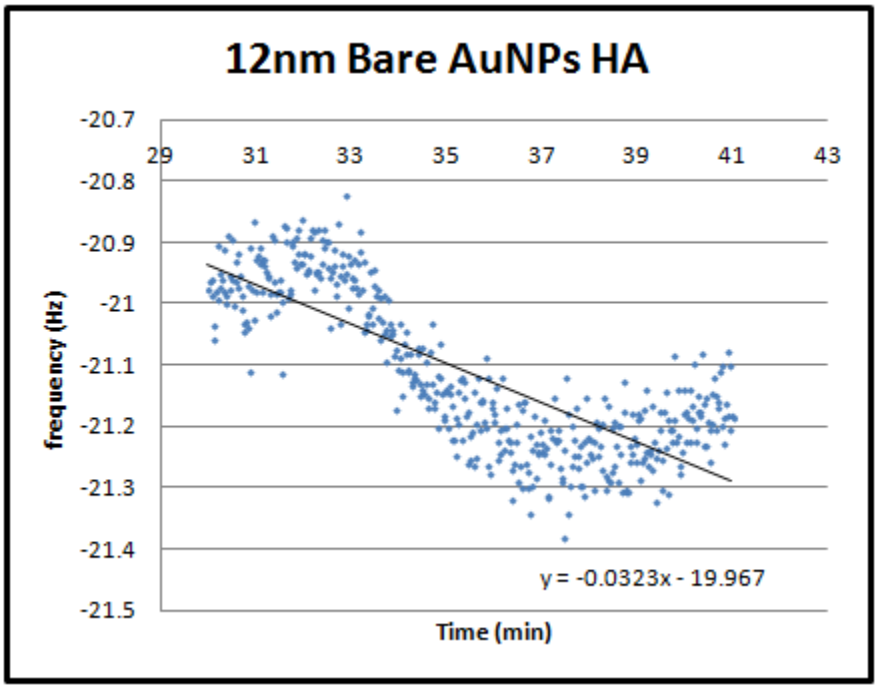

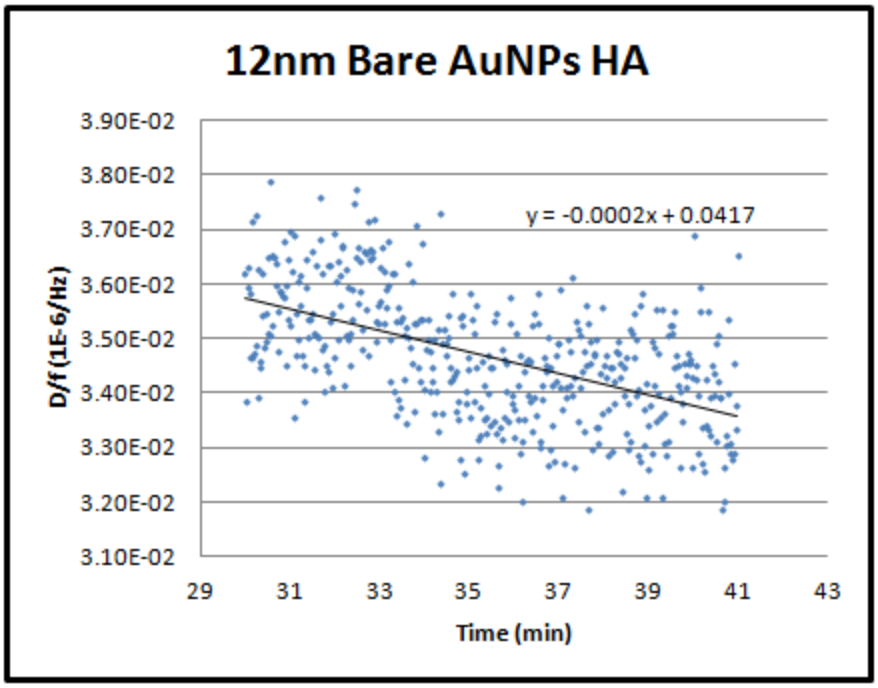
12nm Bare AuNPs HA
3.90E-02
3.80E-02
3.70E-02
3.60E-02
3.50E-02
3.40E-02
3.30E-02
3.20E-02
3.10E-02
D/f (1E-6/Hz)
y = -0.0002x + 0.0417
29
31
33
35
37
39
41
43
Time (min)

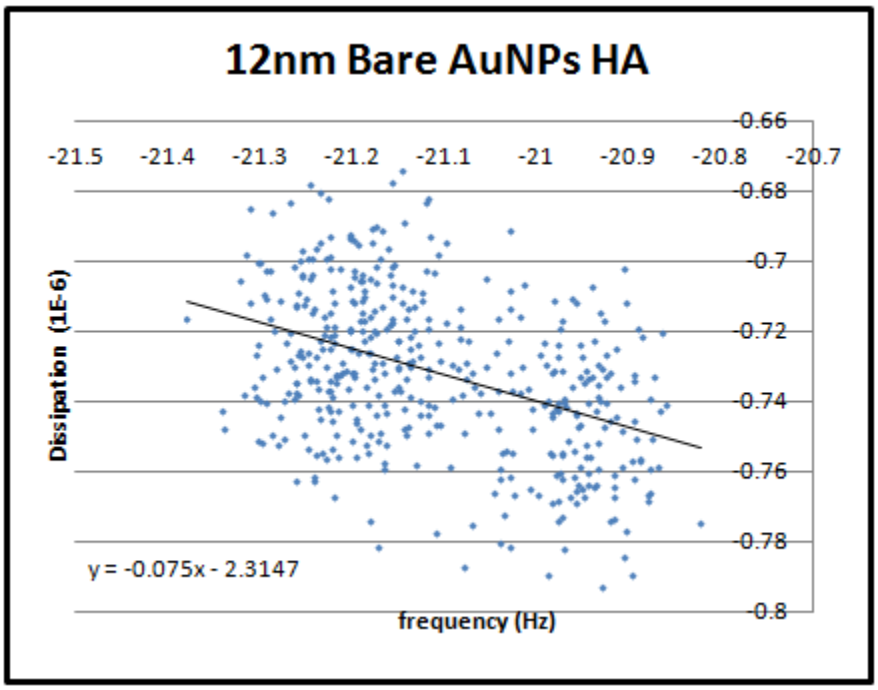
12nm Bare AuNPs HA
-21.5
-21.4
-21.3
-21.2
-21.1
-21
-20.9
-20.8
-20.7
0.66
0.68
0.7
0.72
0.74
0.76
0.78
0.8
Dissipation (1E-6)
y = -0.075x - 2.3147
frequency (Hz)

3-Mercaptopropionic Acid with Humic Acid (2/22/2013 Chamber 1)

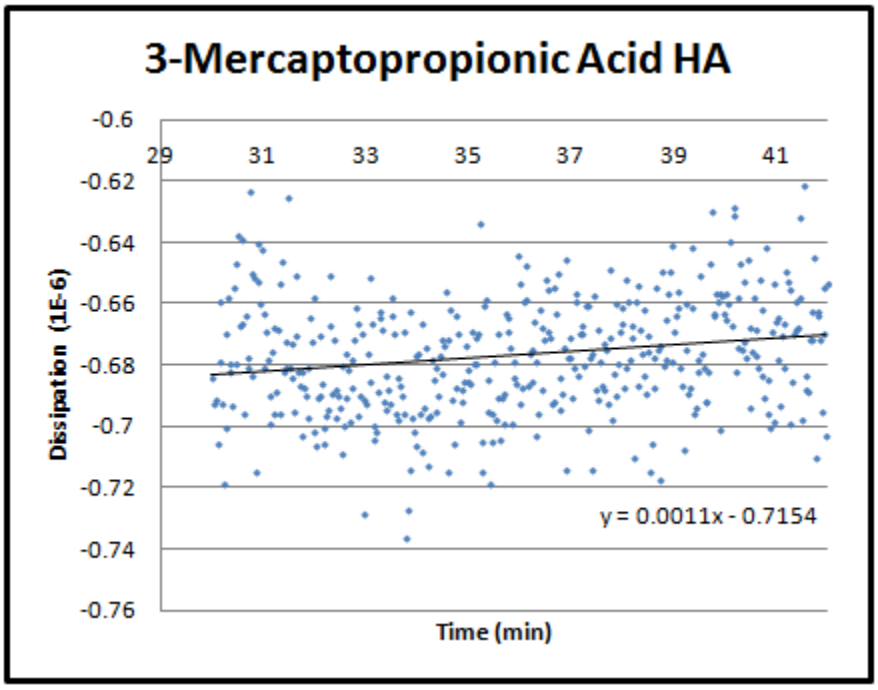

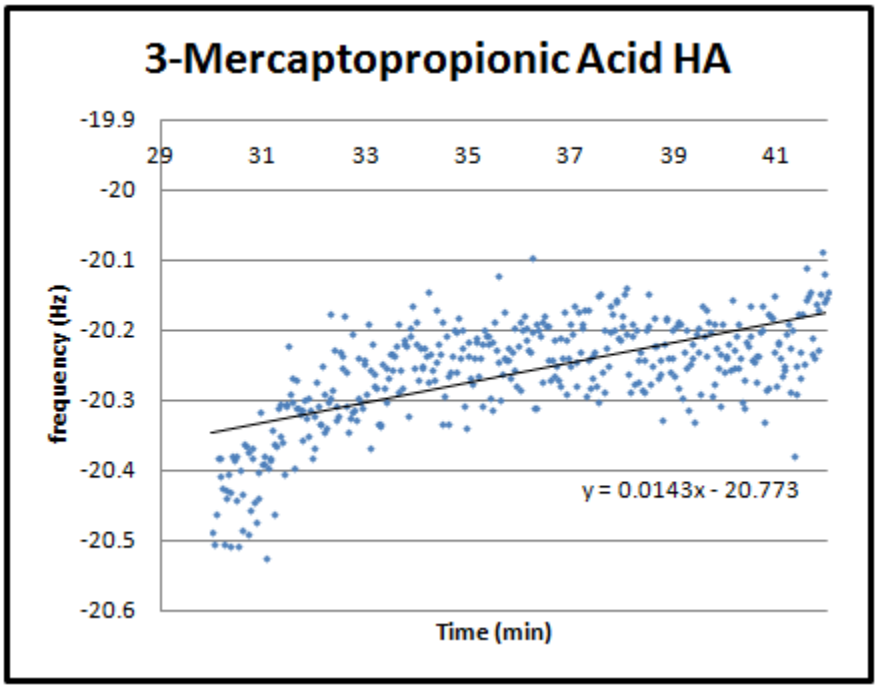

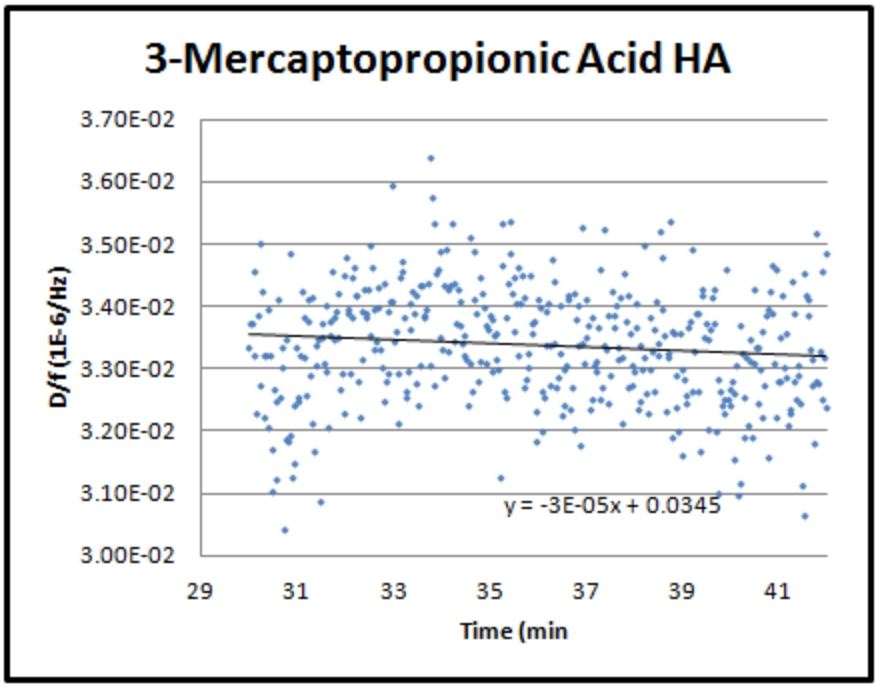
3-Mercaptopropionic Acid HA
3.70E-02
3.60E-02
3.50E-02
3.40E-02
3.30E-02
3.20E-02
3.10E-02
3.00E-02
D/f (1E-6/Hz)
y = -3E-05x + 0.0345
29
31
33
35
37
39
41
Time (min

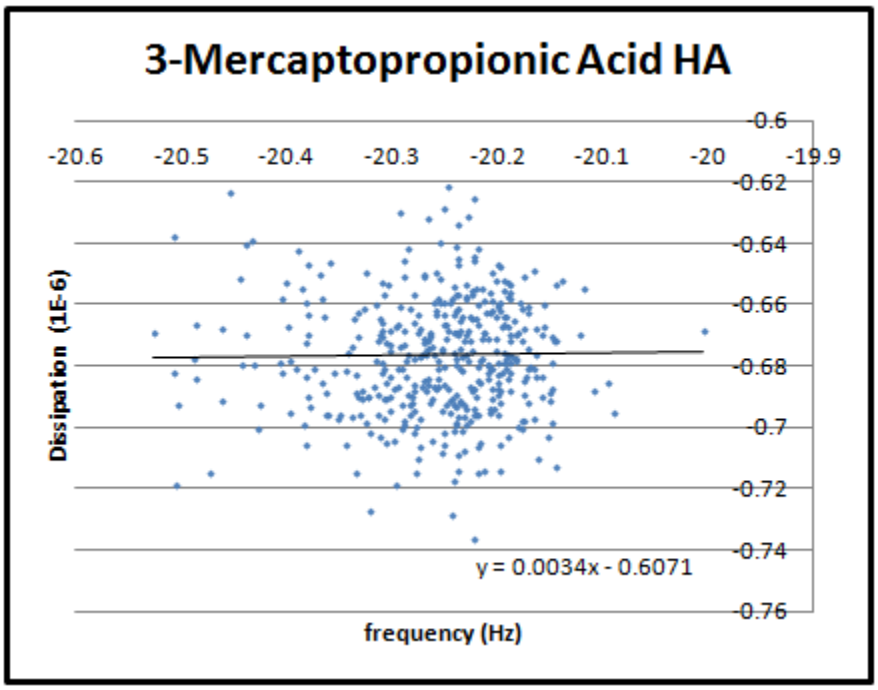
3-Mercaptopropionic Acid HA
-20.6
-20.5
-20.4
-20.3
-20.2
-20.1
-20
-19.9
-0.6
-0.62
-0.64
-0.66
-0.68
-0.7
-0.72
-0.74
-0.76
Dissipation (1E-6)
y = 0.0034x - 0.6071
frequency (Hz)

2-Aminoethanethiol with Humic Acid (2/24/13 Chamber 4)

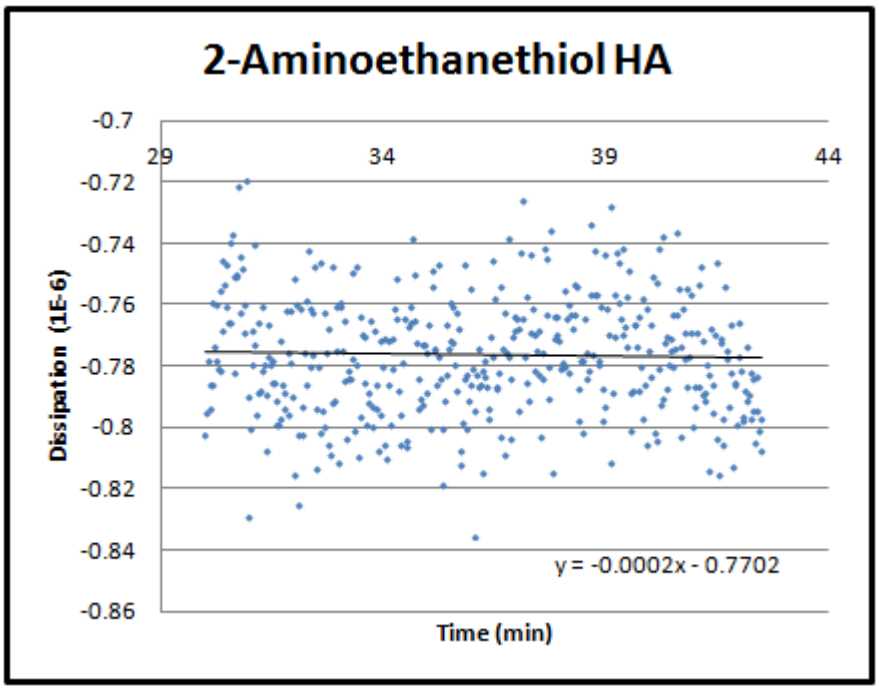

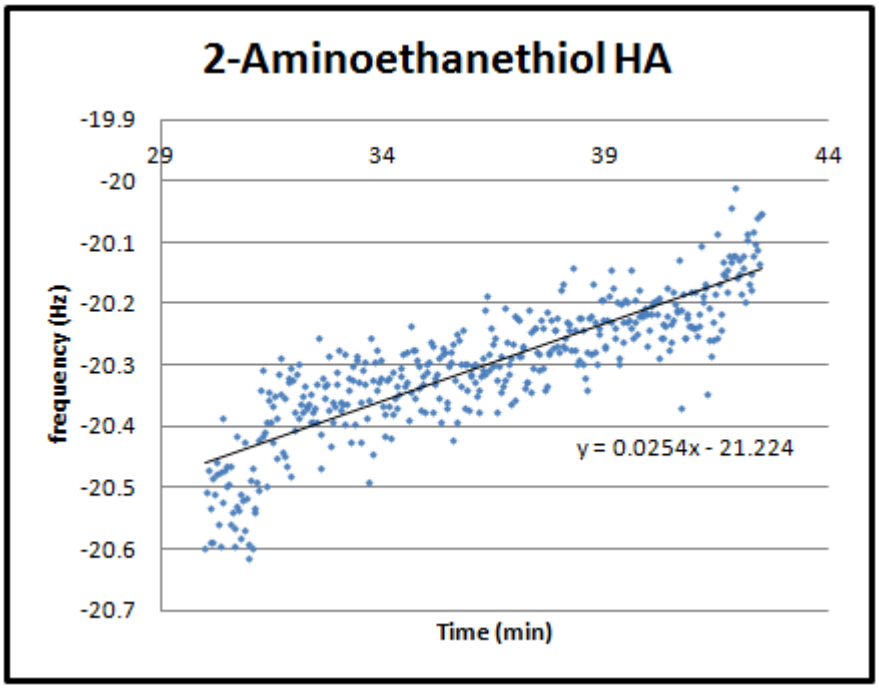

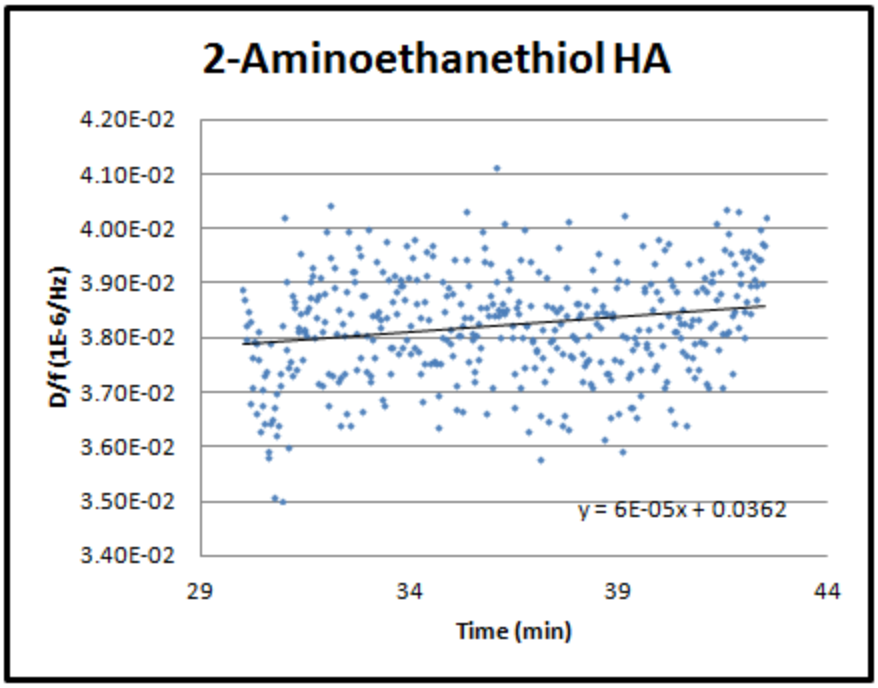
2-Aminoethanethiol HA
4.20E-02
4.10E-02
4.00E-02
3.90E-02
3.80E-02
3.70E-02
3.60E-02
3.50E-02
3.40E-02
D/f (1E-6/Hz)
y = 6E-05x + 0.0362
29
34
39
44
Time (min)

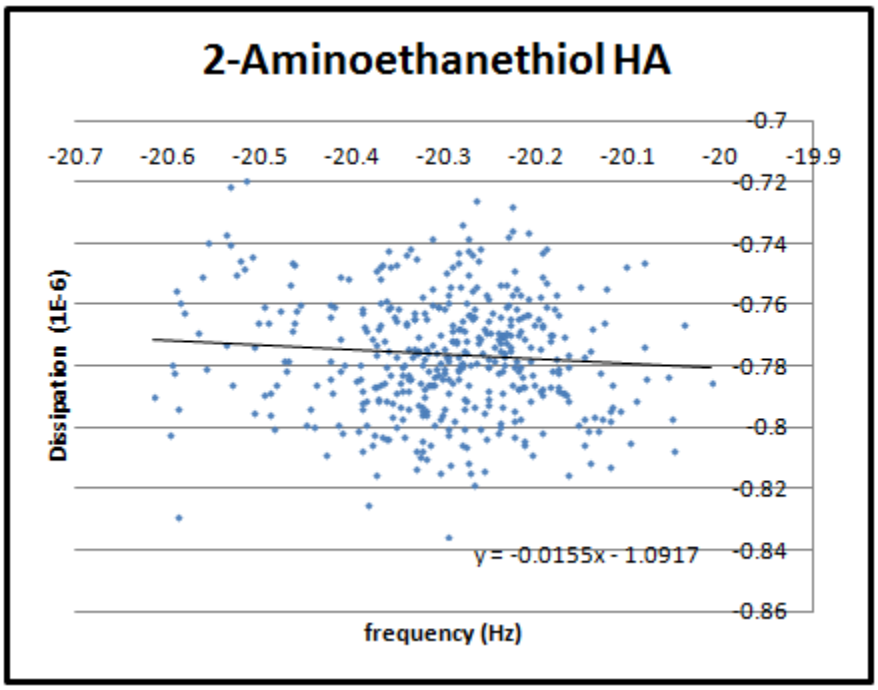
2-Aminoethanethiol HA
-20.7
-20.6
-20.5
-20.4
-20.3
-20.2
-20.1
-20
-19.9
-0.7
-0.72
-0.74
-0.76
-0.78
-0.8
-0.82
-0.84
-0.86
Dissipation (1E-6)
y = -0.0155x - 1.0917
frequency (Hz)

4.7 nm Hydrophobic AgNPs (9/6/2012 Chamber 1)